CHLOROPHYLL DISTRIBUTION AND PRIMARY PRODUCTION ON THE GRAND BANKS OF NEWFOUNDLAND INVESTIGATED BY REMOTE SENSING

KOTA SIVARAMAKRISHNA PRASAD

CHLOROPHYLL DISTRIBUTION AND PRIMARY PRODUCTION ON THE GRAND BANKS OF NEWFOUNDLAND INVESTIGATED BY REMOTE SENSING

BY

© KOTA SIVARAMAKRISHNA PRASAD, M.Sc.

A thesis submitted to the School of Graduate
Studies in partial fulfillment of the
requirements of the degree of
Doctor of Philosophy

Department of Biology
Memorial University of Newfoundland
February 1993

St. John's Newfoundland

ISBN 0-315-82630-4

AGREEMENT

This is an agreement between the author (s) and Xerox University Microfilms, Ann Arbor, Michigan, providing for the publication of an abstract of not more than 600 words of the dissertation (d) in *Dissertation Abstracts International*, which is distributed on a subscription basis. If more than 600 words are contained in the abstract, publication is delayed. *Mathematical formulas, diagrams, and other illustrative materials are not recommended for the printed abstract.*

SUBJECT CATEGORIES

Dissertation Abstracts International is arranged by broad, general subject categories. Choose the *one* listed below (capital letters) which most nearly describes the general content of your dissertation. If major subject category has sub-fields under it, and *only* if it does, please choose *one* (small letters). (Ex.: ECONOMICS, Theory). Enter subject category on Item 9 of Agreement Form.

ACCOUNTING
AEROSPACE STUDIES
AGRICULTURE
- General
- Animal Culture
- Animal Pathology
- Forestry & Wildlife
- Plant Culture
- Plant Pathology
- Plant Physiology
- Range Management
- Wood Technology

AGRONOMY
ANATOMY
ANTHROPOLOGY
ARCHITECTURE
ASTRONOMY
ASTROPHYSICS
AUDIOLOGY
BACTERIOLOGY
BANKING
BIOLOGY
BIOPHYSICS
- General
- Medical

BIOSTATISTICS
BOTANY
BUSINESS ADMINISTRATION
CHEMISTRY
- General
- Analytical
- Biological
- Inorganic
- Nuclear
- Organic
- Pharmaceutical
- Physical
- Polymer
- Radiation

CINEMA
COMPUTER SCIENCE
ECOLOGY
ECONOMICS
- General
- Agricultural
- Commerce-Business
- Finance (includes Public Finance)
- History
- Theory

EDUCATION
- General
- Administration
- Adult
- Business
- Curriculum Development
- Elementary
- Guidance and Counseling
- Health
- Higher
- History
- Industrial
- Music
- Physical
- Preschool
- Psychology
- Religion
- Sciences
- Secondary
- Social Sciences
- Special
- Teacher Training
- Theory and Practice
- Vocational

ENGINEERING
- General
- Aeronautical
- Agricultural
- Automotive
- Biomedical
- Chemical (includes ceramics and fuel)
- Civil
- Electrical
- Heat
- Hydraulic
- Industrial
- Marine
- Materials Science
- Mechanical
- Metallurgy
- Mining
- Nuclear
- Petroleum
- Sanitary and Municipal
- System Science
- Thermodynamics

ENGINEERING MECHANICS
ENTOMOLOGY
ENVIRONMENTAL SCIENCES
FINE ARTS
FOLKLORE
FOOD TECHNOLOGY
GENETICS
GEOCHEMISTRY
GEODESY
GEOGRAPHY
GEOLOGY
GEOPHYSICS
HEALTH SCIENCES
- General
- Chemotherapy
- Dentistry
- Hearing
- Hospital Management
- Human Development
- Hygiene
- Immunology
- Medicine & Surgery
- Nursing
- Nutrition
- Pathology
- Pharmacy
- Public Health
- Radiology
- Recreation

HISTORY
- General
- Ancient
- Archaeology
- Medieval
- Modern

HISTORY OF SCIENCE
HOME ECONOMICS
HYDROLOGY
INFORMATION SCIENCE
JOURNALISM
LANGUAGE AND LITERATURE
- General
- Classical
- Linguistics
- Modern

LAW
LIBRARY SCIENCE
LIMNOLOGY
MASS COMMUNICATIONS
MATHEMATICS
MICROBIOLOGY
MINERALOGY
MUSIC
OCEANOGRAPHY
OPERATIONS RESEARCH
PALEONTOLOGY
PALEOZOOLOGY
PHARMACOLOGY
PHILOSOPHY
PHYSICS
- General
- Acoustics
- Atomic
- Electronics and Electricity
- Elementary Particles
- High Energy
- Meteorology
- Molecular
- Nuclear
- Optics
- Plasma
- Radiation
- Solid State

PHYSIOLOGY
PLASTICS TECHNOLOGY
POLITICAL SCIENCE
- General
- International Law and Relations
- Physiological
- Public Administration

PSYCHOLOGY
- General
- Clinical
- Experimental
- Industrial
- Social

PUBLIC RELATIONS
RADIATION BIOLOGY
RECREATION
RELIGION
SOCIAL WORK
SOCIOLOGY
- General
- Criminology
- Demography
- Family
- Labor Relations
- Public Welfare
- Race Question
- Socialism, Communism, Anarchism

SPEECH
SPEECH PATHOLOGY
STATISTICS
TEXTILE TECHNOLOGY
THEATER
TRANSPORTATION
URBAN AND REGIONAL PLANNING
VETERINARY SCIENCE
WATER CHEMISTRY
ZOOLOGY

REPRINTS

Upon request, Xerox University Microfilms will furnish reprints of the abstract in multiples of 100. The cost is $12.00 (U.S.) for the first 100, $1.25 (U.S.) for additional hundreds. Fill in Item 10 overleaf if you wish reprints.

" The Ocean being full of unfathomable water does not require any more; likewise a Yogi being full of infinite bliss does not require any worldly enjoyment "

- The Bhagavad Geeta

ABSTRACT

A sequence of surface pigment images of the 1980 phytoplankton spring bloom on the Grand Bank of Newfoundland was derived from the Nimbus-7 Coastal Zone Color Scanner (CZCS). This data set is augmented with *in situ* observations of physical and biological data to examine spatial and temporal variability of the surface pigment fields. The satellite imagery suggests considerable temporal and spatial variability in surface chlorophyll concentrations across the period of investigation. Patterns in near-surface pigment concentrations were associated with the evolution of the spring bloom.

A semi-empirical model, which is in part physiologically based, is presented which utilizes integral chlorophyll (IC), photosynthetically available radiation (PAR) and light absorption by chlorophyll to predict integral production (IP). A preliminary assessment of the relationship between sea-surface temperature (SST), water column stability (VS), integral chlorophyll (IC), and remote sensing optical depth (1/K490) allows the development of another model based on secondary variables to predict integral production (IP). Simultaneous assimilation of sea surface temperature and optical depth into one model for predicting integral chlorophyll demonstrates the usefulness and need for a thermal channel in future ocean color sensors.

Water column light utilization index, ψ, varies seasonally over the Grand Banks and cannot be treated as a constant in primary production models. Mean values of ϕ_C showed a twofold to sixfold variation from spring through summer. A shift in distribution of normalized quantum yield (i.e. ϕ_C/ϕ_{max}) towards lower values in the upper 20m suggested frequent occurrence of light saturation.

Chlorophyll determined from satellite imagery is used to calculate the depth-

integrated pigment content of the euphotic zone. This value, along with a computed value of chlorophyll-specific cross section and computed values of quantum yield, are used in an algorithm developed to predict annual production on the Grand Banks of Newfoundland. Adjustment of the phytoplankton physiological parameters was necessary to take seasonal variation into account. Mean primary production computed from the algorithm was 194 g C m^{-2} yr^{-1} which compared well with the mean shipboard measured value of 186 g C m^{-2} yr^{-1}.

The work presented in this thesis represents a significant advance for the synoptic description of oceanography in the Newfoundland area and provides baseline information, for mid-latitude cold oceans, of use in pigment retrieval and production estimation from the proposed ocean color sensor (SeaWiFS) when it becomes available in 1993. The study gives CZCS-derived production estimates which are similar and reasonable in comparison to the few other such studies which have been carried out in the Pacific and Atlantic oceans.

ACKNOWLEDGEMENTS

I thank Dr. R.L. Haedrich, my Graduate supervisor for his keen interest and financial support during the study period. His able guidance has helped me think and write more coherently.

I am grateful to Dr. J.T. Hollibaugh, San Francisco State University, for making the shipboard data from the Hibernia environmental impact study surveys available, without which this work would have been impossible.

I am thankful to Drs. D.C. Schneider and D. Deibel for their role as members of my supervisory committee. I am also thankful to Dr. D.C. Schneider for selection of Nimbus-7 Coastal Zone Color Scanner Satellite data and for his guidance during the initial period of this study. I am also grateful to Dr. Don Deibel for suggesting Dr. Hollibaugh as a source to obtain the shipboard data.

I thank Drs. B. Topliss and L. Payzant, Bedford Institute of Oceanography, for their help during my visit. I am grateful to them for allowing me to use the MIAMI image processing software and allotting time on their micro-vax computer for the CZCS data analyses. I also thank Mr. J. Lane of the Hibernia Management Co., for providing me with phytoplankton species composition data for the Grand Banks.

I would like to thank all my friends in St. John's who helped and supported me in many ways during my study. In particular, I would like to thank S. Jayaram, S. Bhoominathan, S. Dhanakoti, J. Horne, H. Raghuram and K.A. Prasad, the people who made my stay in St. John's memorable.

Finally, I would like to thank all the members of my family, for their patience, understanding, and support during my study period and stay abroad.

Financial support for this study was provided by NSERC (Canada) grants awarded to Dr. R.L. Haedrich and through teaching assistantships from the Department of Biology.

Table of Contents

LIST OF FIGURES AND TABLES

Page

List of Symbols and Notations used in the algorithm

Symbol	Definition	Units	First appears in page
SST	Sea-surface temperature	°C	5
K490	Diffuse attenuation coefficient at irradiance wavelength 490	nm m^{-1}	11
SDC	Satellite detectable chlorophyll	mg m^{-3}	26
ψ	Light utilization index	mg C (mg Chla)$^{-1}$ m^2 Ein^{-1}	26
I_o	Total incident radiation	Ein m^{-2} day^{-1}	30
Z_e	Layer above 1% light depth	m	30
D_E	Euphotic depth	m	30
IC	Integral chlorophyll	mg m^{-2}	31
IP	Integral production	mg C m^{-2} day^{-1}	31
k	Mean diffuse attenuation coefficient	m^{-1}	32
PAR'	Photosynthetically Available Radiation from equation 2.6	Ein m^{-2} day^{-1}	33
1/K490	Remote sensing optical depth	m	34
<C>	Mean euphotic chlorophyll	mg m^{-3}	31
V_z	Light absorption by phytoplankton at depth z	Ein m^{-3} day^{-1}	44

Symbol	Definition	Units	First appears in page
K_c	Chlorophyll specific diffuse attenuation coefficient	m^2 (mg chl*a*)$^{-1}$	45
C_z	chlorophyll at depth	mg m^{-3}	45
P_z	Production at depth	mg C m^{-3} day^{-1}	45
K (in Chapter 2)	Quantum yield	mg C (Ein)$^{-1}$	45
ν	Angström coefficient	dimensionless	53
VS	Water colum stability	m^{-1}	70
IP'	Predicted integral production	mg C m^{-2} day^{-1}	73
IC'	Predicted integral chlorophyll	mg m^{-2}	73
ρ	Chl*a* to (chl*a* + phaeo*a*) ratio	dimensionless	74
aph·Chl^{-1}	Specific absorption coefficient for phytoplankton	m^2 (mg Chl*a*)$^{-1}$	82
ϕ_C	Quantum yield for carbon fixation	mol C Ein^{-1}	82
ϕ_{max}	Maximum quantum yield for carbon fixation	mol C Ein^{-1}	83
$\bar{\phi}_C$	Mean quantum yield	mol C Ein^{-1}	84
ψ^*	Cross-section for photosynthesis per unit of areal chlorophyll	m^2 (mg Chl*a*)$^{-1}$	74

Symbol	Definition	Units	First appears in page
$\overline{PAR}$	Photosynthetically Available Radiation	M J m^{-2} day^{-1}	104
kd	Downward diffuse attenuation coefficient	m^{-1}	109
P_m^b	Maximum photosynthesis per unit chlorophyll	gC g chl^{-1} h^{-1}	108
$\overline{PSR}$	Photosynthetically Stored Radiation	M J m^{-2} day^{-1}	104

CHAPTER 1. REMOTE SENSING AS AN OCEANOGRAPHIC TOOL

1.1 The need for remote sensing

Estimation of ocean primary productivity and an increased understanding of the processes controlling marine biogeochemical cycling on regional to global scales have been a major goal of ocean sciences (JGOFS, 1984). Ship-derived oceanographic data sets are insufficient to address questions on processes affecting the distribution of biological and physical properties on regional scales. Optical measurements from satellites provide information at temporal and spatial scales not possible with traditional *in situ* oceanographic campaigns.

Pioneering work on remote sensing of algal pigments (Clarke *et al.*, 1970) provided oceanographers with their first opportunity to make synoptic maps of algal biomass from aircraft. Converting these static measurements of algal biomass to rates of primary production has been the subject of much research that pre-dates chlorophyll remote sensing by more than a decade (Ryther and Yentsch, 1957). With the advent of satellite remote sensing to estimate pigment concentration, the modelling of primary

production over large scales has taken on a renewed interest.

Remotely sensed radiometric data, such as those from the Coastal Zone Color Scanner (CZCS), which operated intermittently during the period 1978-1986, have been used for synoptic mapping of algal pigments within the upper layer (first attenuation length) of the ocean. Future operational sensors such as SeaWiFS (SeaWiFS, 1987) are expected to offer more complete coverage. Archived CZCS data can then be used to validate models for deriving primary production and its associated carbon flux at a global scale (Platt and Sathyendranath, 1988; Kuring *et al.*, 1990).

When phytoplankton are abundant, as in the highly productive coastal zones, their spatial distribution varies greatly. Serious overestimation or underestimation of mean phytoplankton abundance can easily result from shipboard assessment because of complex and rapidly changing spatial patterns. Satellite remote sensing is one of the few tools that allows oceanographers to assess phytoplankton distribution synoptically in regions of high spatial variability (Perry, 1986). Satellite measurements when combined efficiently with *in situ* observations, can help significantly in estimating production on continental shelves and in understanding the processes that control the spatial and temporal distribution of production (Walsh and Dieterle, 1988).

Site-specific algorithms can be used to transform chlorophyll maps obtained from ocean color sensors to maps of primary production (Morel and André, 1991; Prasad *et al.*, 1992). This site specificity is due, among other things, to changes in the species composition of the phytoplankton and in their adaptive state, which result in variation of

physiological responses such as light absorption capability (Bricaud *et al.*, 1988) and maximum quantum yield for growth (Cleveland *et al.*, 1989). The use of any production model rests on parameterization of the essential physiological responses of phytoplankton. This necessitates the adaptation of general production models to the regional or local conditions that apply in different parts of the world ocean (Morel and André, 1991).

1.2 Some potential applications

1.2.1 *Mesoscale processes*

As in the application of AVHRR (Advanced Very High Resolution Radiometer) data for estimating sea surface temperature, CZCS data analysis focused initially on comparison of a few images to field observations. Extensive comparisons between CZCS imagery and *in situ* observation are reported by McClain *et al.* (1984) who used phytoplankton as a passive tracer to study water circulation in the South Atlantic Bight. Similarly sequences of both AVHRR and CZCS data have been used to study circulation patterns and plumes (Arnone and La Violette, 1986; Deuser *et al.*, 1988; Mueller-Karger *et al.*, 1988).

Recently, research on longer time series from the CZCS has increased due to the better availability of these data. The first synoptic views of the evolution of the spring bloom using CZCS on the U.S. east coast were offered by Brown *et al.*, (1985), who also provided an estimate of primary productivity from the CZCS pigment information. CZCS data have been used to estimate characteristic time and space scales in the coastal

ocean (Walsh and Dieterle, 1988). Estimation of patch sizes (Yoder *et al.*, 1987) and correlation of spatial scales within an upwelling region (Abbott and Zion, 1987) are among other studies that receive particular attention. One unusual application of the CZCS has been to study biological and physical processes in Lake Michigan (Mortimer, 1988). Although the study found that the presence of "yellow substances" (humic substances) and suspended sediments interfered with pigment retrieval, it was still possible to obtain useful information on whole-lake dynamics. (The term "retrieval" is used in the remote sensing literature to signify obtaining pigment information from the total signal sensed by the satellite sensor using image processing techniques).

1.2.2 *Large-scale processes*

CZCS data have also been used in observing and quantifying large-scale processes in the ocean. With CZCS data becoming more readily available, the study of large-scale processes has become simpler. Feldman *et al.* (1984) observed dramatic changes in pigment concentration in the eastern tropical Pacific in response to the 1982-1983 El Niño. Longer time series of CZCS data have been used in the North Atlantic to infer productivity rates from temporal changes in phytoplankton abundance (Campbell, 1989). Seasonal progression of pigment in relation to upper ocean forcing is reported by McClain *et al.* (1990). Biological or physical coupling of data has been used to study the phytoplankton response to spring transition. Thomas and Strub (1989) observed considerable interannual variability in phytoplankton abundance, and attributed it to the

nature of nutrient flux induced by wind mixing and/or upwelling.

Several workers have studied the relationships between pigment patterns, bottom topography and recurrent features in selected images (Barale and Wittenburg Fay, 1986; Pelaez and McGowan, 1986). Comparisons with hydrographic data suggest that nutrient patterns and circulation play an important role in maintaining these features.

A relationship between wind forcing and pigment determined using empirical orthogonal functions (EOF) analysis suggested a coupling exists between pigment pattern and forcing by wind stress curl (Abbott and Barksdale, 1991). Similar studies of circulation patterns using ocean color suggests fluctuation in river discharge as the dominant source of pigment variability near the coast (Barale *et al.* 1984; 1986).

Most research efforts with CZCS have focused on phytoplankton pigment, but some studies have exploited the CZCS capability to produce maps of the diffuse attenuation coefficient at 490 nm (K490). Data from the 490 nm channel have mainly been used to characterize optical properties (Barale and Trees, 1987) in the North Atlantic and North Pacific, and for defining bio-optical provinces (Mueller and Lange, 1989) of the Northeast Pacific.

Using the argument that phytoplankton pigment concentration is an indicator of food abundance, CZCS images have been used in several studies of fish distributions. Aggregations of albacore have been indicated by good fish catches near color or SST (sea surface temperature) boundaries (Laurs *et al.*, 1984).

Basin-scale models of processes in the ocean have been developed and compared

to CZCS imagery. A simple, two-dimensional model of mixing, nutrients, phytoplankton, and zooplankton was developed by Wroblewski (1989) to describe the spring bloom in the North Atlantic. The model reproduces some of the gross features seen in the CZCS imagery, although extension of this model to cover the seasonal cycle indicates that the model must include horizontal circulation since many observed features do not appear in the model output.

Programs such as the Joint Global Ocean Flux Study, JGOFS (1988), and the International Geosphere-Biosphere Programme, IGBP (1988), are directed towards the determination of the time-varying flux of carbon (and associated elements) in the world ocean. Year-to-year fluctuations in the primary production of coastal ecosystems are well known, although rarely documented systematically. The principal constraints lie in sampling intensity resulting from spatial, temporal, and economic limitations of using ships, moorings, and drifters.

1.2.3 *Coccolithophore blooms*

Coccolithophores have long been recognised as the principle cause of "white-water" conditions. Availability of satellite imagery in the visible wavebands from LANDSAT (thematic mapper), CZCS, and AVHRR have aided in resolving the scale and frequency of these blooms (Holligan *et al.*, 1983). Coccolithophores contribute to high reflectance (up to 25% of the incident light) in open ocean and coastal waters, a fact which makes their identification easy on satellite images. The main cause of this high

reflectance has been attributed to backscattering by detached coccoliths as opposed to whole cells (Holligan *et al.*, 1983; Bricaud and Morel, 1986; Balch *et al.*, 1989a).

The coccolithophore *Emiliania huxleyi* (Löhm) (Class Prymnesiophyceae) is thought to be the most abundant calcifying organism on earth (Westbroek *et al.*, 1985). The distribution of *E. huxleyi* in surface waters tends to match that in the sediments. The occurrence of bloom-forming *E. huxleyi* has been reported from tropical to sub-arctic regions of the Atlantic. Coccolithophores succeed diatoms over time during increasing stabilization of the water column and depletion of surface nutrients (Margalef, 1978). Apart from ecological interests, recent attention on coccoliths has focused on their role in global biogeochemical cycles. Coccoliths form a major component of the pelagic calcareous sediments in the world oceans, and the determination of their rate of downward flux is a matter of much current attention.

Studies in the Gulf of Maine indicate that coccolithophore blooms can represent a significant perturbation at fairly large scales and can dramatically alter the optical properties of the water column. Therefore, coccoliths induce noise in remote sensing algorithms which depend on the blue to green ratio for pigment retrieval. Optical properties indicate that the most accurate method to estimate coccolith concentration *via* remote sensing is to measure water-leaving radiance in the green wavebands (Balch *et al.*, 1991).

1.3 Precision and accuracy of CZCS Pigment estimates

It is clear that a high-sensitivity sensor such as the CZCS is useful in retrieving the phytoplankton pigment content of the ocean over large scales. Under optimal conditions, precision of the retrieved pigment data is about $\pm$ 30%. The satellite-estimated values are within $\pm$ 0.3 $\log_{10}$ (pigment) under more typical conditions (Gordon *et al.*, 1983a), and the scatter tends to be worse at extremely low and high pigment values (Brown *et al.*, 1985).

The accuracy of pigment retrieval depends on estimates of atmospheric effects which are required for correcting imagery. This is important as 80-90% of the signal detected by the CZCS originates in the atmosphere. The basic CZCS algorithms (Gordon *et al.*, 1983a; Gordon and Morel, 1983) assume that Rayleigh scattering (scattering from the air molecules) can be separated from aerosol scattering (scattering from particles suspended in the air). The Rayleigh component has been easier to estimate than the aerosol component. The latter can vary greatly on small temporal and spatial scales.

After atmospheric correction has been taken care of, the water-leaving radiance must be converted into estimates of phytoplankton pigment concentration through the use of bio-optical algorithms. Complications can result in bio-optical algorithms due to the presence of coccolithophores, although Gordon *et al.* (1988) describe a model that will allow retrieval of pigment concentration in the presence of these organisms.

Further refinement of bio-optical algorithms is described by Morel (1988) and Sathyendranath *et al.* (1989). Their work is extremely relevant to the future design of

sensors with higher spectral resolution. These sensors may be able to separate the effects of various materials that affect the optical properties of the ocean. Therefore, due to the presence of varying amounts of suspended material in the water column and problems associated with latitudinal differences in pigment retrieval (including atmospheric affects), regionally specific algorithms are likely to perform better than algorithms employing constant global parameters for atmospheric correction procedures.

1.4 Need for algorithm development

As more sensitive sensors are launched, it is essential that algorithm development continue. Experience with the CZCS has indicated that a continuing program of thorough calibration is necessary in diverse oceanic situations. The original CZCS bio-optical algorithms were dominated by measurements made in waters around the U.S.; future sensors must have calibration or validation programs that collect bio-optical data from a larger variety of water types and areas (Abbott and Chelton, 1991).

Pigment retrieval at high latitudes has received particular attention; however, algorithms may not work efficiently at large solar zenith angles without including the effects of multiple Rayleigh scattering (Gordon *et al.*, 1983a). Experience from the Bering Sea suggests that a regionally-specific algorithm is likely to be required there for pigment retrieval (Mueller-Karger *et al.*, 1990).

1.4.1 *Empirical versus physiological algorithms*

Primary production models fall into two types: empirical and physiological (Perry, 1986). Empirical models simply form regressions between primary production and various environmental variables. Physiological models, on the other hand, are derived from first principles based on experimental or theoretical understanding of the mechanisms involved. Physiological models may rely on regression techniques at some point to estimate certain parameters, for example nutrient saturation coefficients, but the degree to which various processes are included explicitly in the model *vs* simple parameterization of the process differentiates between a physiological and empirical approach. Semi-empirical algorithms utilize a combination of empirically derived relationships (site-specific) along with physiological parameters to predict primary production (Balch *et al.*, 1989b; Prasad *et al.*, 1992). A balanced approach is necessary to decide if the inclusion of a physiological process improves the model predictions enough to weigh against the utility and comprehension of a simpler model (with fewer variables). A physiological model may not necessarily perform better than an empirical model in predicting production because of seasonal variability in model parameters (Balch *et al.*, 1989b). Therefore, there is no reason to overlook empirical approaches simply because they are less mechanistic.

Empirical relationships to predict primary production have shown considerable scatter both seasonally and regionally (Eppley *et al.*, 1985). Much of the variability in pigment or production relationships appears to be related to light history. Thus, most

physiological models use information on incident light, phytoplankton absorption, and quantum efficiency to estimate growth rates of phytoplankton.

The photosynthetic yield parameter has also been found to be critical in improving production models (Balch *et al.*, 1989c; Campbell and O'Reilly, 1988). Most workers agree on the importance of incident light. They agree that further research is required in the areas of light absorption and utilization by phytoplankton and the effects of vertical variation in phytoplankton concentration.

1.4.2 *Importance of secondary variables*

Initial models to predict primary production relied on pigment, light absorption and incident light in the water column. All three factors are related and focus on the light-harvesting capacity of phytoplankton. Seasonal variability in these factors induced considerable scatter in the relationships used for predicting primary production. Information concerning other variables such as sea surface temperature, when used in certain models (Balch *et al.*, 1989c), resulted in a reduction in the variability. The possibility of using other secondary variables such as the diffuse attenuation coefficient (K490), water column stability, and the depth of the mixed layer in primary production models holds promise. This matter will be examined more fully in Chapter 4.

1.5 Algorithm development and techniques

The sensitivity of the CZCS underwent a complex degradation over time that was dependent on wavelength. The CZCS sensor operated for a much longer period than

expected; therefore, the degradation function had to be reformulated several times (Gordon *et al.*, 1983b; Mueller, 1985). This was important as the algorithms for chlorophyll retrieval improved. Originally only the 443 nm channel was used for basic calibration. Other channels were later included in the calibration function. In-water optical properties were useful for the calibration scheme and could achieve the accuracies necessary in algorithms for pigment retrieval (Gordon, 1987).

Saturation of CZCS sensor amplifiers over bright targets such as land and clouds was yet another problem that corrupted algorithms. This phenomenon was described as "ringing" and a cloud masking correction algorithm was implemented by Mueller (1988).

The most important change in the basic CZCS atmospheric correction algorithm has been the inclusion of multiple Rayleigh scattering (Gordon *et al.*, 1983a). As CZCS atmospheric correction algorithms became further refined, it became necessary to account for the actual values of atmospheric pressure and total ozone concentration, rather than relying on climatological averages (André and Morel, 1989).

Morel (1988) and Sathyendranath *et al.* (1989a) aim at using bio-optical models in Case 2 waters (those waters for which the inorganic and/or organic sediments make an important or dominant contribution to the optical properties: Morel and Prieur (1977), where significant contamination of non-chlorophyllous material may exist. The presence of yellow substance contributes to noise in bio-optical algorithms, necessitating regional knowledge of water properties (Carder *et al.*, 1986; 1989).

Phytoplankton themselves contribute a final complication in respect to bio-optical

algorithms. Accuracy of CZCS pigment retrievals depends strongly on phytoplankton species composition (Balch *et al.*, 1989a). Presence of coccolithophores can cause large errors in pigment estimates (see Section 1.2.3). Dinoflagellates which exhibit vertical migration can also complicate comparisons between *in situ* and satellite data unless the two data sets are coincident.

The CZCS senses the weighted-average of pigment to one attenuation length, which is approximately equal to the 37% light level depth. Sathyendranath and Platt (1989) suggest that the knowledge of vertical profiles of pigment concentrations from a few locations should be sufficient to retrieve pigment concentration for the whole image. Kitchen and Zaneveld (1990) suggest that Sathyendranath and Platt's assumption of a monotonic dependence of backscattering of chlorophyll may not be an appropriate approach.

Although the CZCS data have problems, they are essentially no different than those found in any large, *in situ*, data sets which also have their own calibration and algorithm problems (Abbott and Chelton, 1991). Therefore, regional knowledge of water properties and local calibration for site-specific bio-optical algorithm development is necessary.

1.6 Remote Sensing on the Grand Banks

1.6.1 *The study area and purpose*

The Grand Banks is a cold, mid-latitude region of the northwest Atlantic Ocean

that is plagued by cloud and fog, and where large solar zenith angles complicate satellite data processing. Consequently, very little attention has been devoted to satellite remote sensing in this region. There has been no published scientific literature in this regard for the Grand Banks, despite the fact that there are important questions of oceanography and fisheries (e.g. Helbig *et al.*, 1992) that could be addressed with remote sensing data. Therefore, there has been an immediate need to investigate the use of ocean color remote sensing and to develop site-specific algorithms for estimating primary production in this region.

The purpose of my thesis is to investigate the potential and availability of ocean color data for satellite remote sensing in the Grand Banks region, and in particular to develop approaches and algorithms that might be useful for calculating primary production there. Previous ship-to-satellite bio-optical calibrations have been performed in warm-water low and mid-latitude U.S. coastal regions. Ship-to-satellite calibrations have been very rare in cold ocean regions in general, and there have been no previous attempts to derive these on the Grand Banks. Therefore, a calibration exercise was an important first step to satellite pigment retrieval before algorithms for primary production could be developed.

1.6.2 *Approach and assumptions*

Recognizing the need for synoptic observations of the kind possible from satellites, I have sought to develop some models and relationships for predicting primary

production from satellite detectable chlorophyll, based exclusively on data available for the Grand Banks. In so doing, I have relied on established practices in remote sensing, and have followed in the path of data analyses prescribed for the North Atlantic and other oceanic regions (e.g. Campbell and O'Reilly, 1988; Morel, 1991). For the most part, the thesis has not dealt with theoretical matters, but has dealt directly with questions of broad applicability, for example the assumed constancy of certain parameters in remote sensing algorithms.

Shipboard observations are seldom coincident with satellite observations. However, I was very fortunate to have access to a comprehensive set of shipboard data for use in my satellite data calibration and model development. The shipboard data were collected as a part of an Environmental Impact Statement (EIS) survey done on the Grand Banks during 1980-81 for Mobil Oil Canada Limited as preparation for the Hibernia development. The raw data were collected and collated by Dr. J.T. Hollibaugh, now at San Francisco State University. When Dr. Hollibaugh came to Memorial as a Visiting Scholar, I had the chance to talk to him about my interests, and he subsequently very kindly turned over several hundred sheets of computer printout from the Hibernia EIS for my use.

I have derived a number of original variables for the Grand Banks study area, which I have used in my models. I have compared my parameter estimates and results to the results obtained by other investigators in work on the remote sensing of ocean production. There have been no previous attempts to do this on the Grand Banks. The

study proceeded in a stepwise fashion and, as I began to obtain results, my supervisor and committee encouraged me to write them up for publication in peer-reviewed journals. Therefore, at every stage of my work, I was fortunate to receive comments and suggestions from anonymous reviewers of my research papers. I have used these comments constructively and incorporated them into my thesis whenever appropriate.

1.6.3 *Satellite data and software*

The Coastal Zone Color Scanner (CZCS) raw data on five 9-track (6250 bpi) computer tapes were obtained from NASA Goddard Space Flight Center (GSFC), Maryland, U.S.(Appendix Table A). I had at first planned to analyse the images at NORDCO in St. John's., while their Image analysis system was adequate, NORDCO did not have the suitable image processing software for CZCS data. The nearest place where the software was available was at the Bedford Institute of Oceanography (BIO) in Halifax, and I ended up going there to do the data analyses. I spent eight days (20 - 28 June) in the spring of 1990, learning first to use the BIO micro-vax-based image analysis system and then finally doing all the analyses myself with the MIAMI-DSP software available there. This software package was the most recent version available at the time I did the analyses.

MIAMI is a comprehensive package of image-processing software that performs geometric, radiometric, and atmospheric corrections on raw CZCS data, before applying algorithms to retrieve pigments. It is the fundamental software that all investigators

working with CZCS data must use. MIAMI-DSP software has been used, for example, to produce global ocean color maps (Feldman *et al.*, 1989). The basic ingestion routine is called SAT_DECODE. Subroutines like CALEPS help in the computation of epsilon ratios. SAR (Sectorize, Atmospheric correction, Remap) uses a base map with ground control points to navigate the image, then the atmospheric corrected images are remapped to the original map coordinates. The NASA pigment palette is applied to get the pigment concentration in mg. m^{-3}. MIAMI software was developed for CZCS analyses by the University of Miami, Rosenstiel School of Marine and Atmospheric Science, in collaboration with the NASA/GSFC Laboratory for Oceans in Maryland.

1.6.4 *Organization of the thesis*

Chapter 2 describes the Grand Banks study area and presents a standard primary production model based on shipboard data gathered for the Hibernia Environmental Impact Statement survey during 1980-1981. The shipboard data initially helps to investigate relationships between the surface chlorophyll, mean euphotic chlorophyll, and integral chlorophyll on the Banks. A semi-empirical model based on these relationships is then presented.

Chapter 3 presents a seasonal picture of the spring bloom sequence on the Grand Banks as seen from the ship-based data and CZCS satellite images obtained from the NASA data. This chapter also includes a ship-to-satellite calibration and a model to estimate satellite chlorophyll on the Banks. Spatial and temporal variations in surface

chlorophyll, sea-surface temperature and vertical stability during the evolution of the spring bloom are investigated by integrating satellite and shipboard data. Satellite data provide evidence for the formation of a dinoflagellate bloom offshore during the fall.

Chapter 4 explores the use of secondary variables in the remote sensing of primary production, and offers a second semi-empirical model. Algorithms which include sea surface temperature along with chlorophyll, for example, have been shown to account for the variability in predicted values of production (Balch *et al.*, 1989c). Thus, it seemed worthwhile to investigate the use of variables other than pigment concentration that could be derived from satellites and used to predict primary production. Secondary variables such as the sea-surface temperature, water column stability and the remote sensing optical depth have been investigated for their utility in predicting integral chlorophyll and, from there, primary production.

Chapter 5 examines the variation in the quantum yield of photosynthesis on the Grand Banks and the impact of this variation on physiological factors throughout the year. It is demonstrated that quantum yield is spatially and temporally variable, and that the assumption that it can be treated as a constant in models could lead to twofold to threefold overestimates of production.

Chapter 6 summarizes the results from earlier chapters and applies the relationships derived to calculate primary production on the Grand Banks. Estimated production from the model reveals that the Banks are heterogenous seasonally and the Tail of the Banks supports more average algal biomass and carbon fixation annually than

the northern Grand Banks.

Finally, Chapter 7 adds a brief summary of the thesis, including some comments on the relation of this work to the next generation of satellites as represented by SeaWiFS. The chapter concludes with a comparison of the Grand Banks results to those of the few other studies of ocean production based on CZCS data.

CHAPTER 2. THE STUDY AREA AND A PRODUCTION ALGORITHM

2.1 The Grand Banks

The Grand Banks of Newfoundland is one of the largest fishing banks in the world and is of particular importance to the ecology and economy of the northwest Atlantic Ocean. Despite its importance to commercial fisheries, dating from the 16th century, little is known of its physical and biological oceanography, or its true potential for biological production (Anderson and Gardner, 1986).

Biological components of the Grand Banks ecosystem show strong pulses in abundance and reproduction. Many seasonal pulses are strongly linked to the abundance and availability of phytoplankton, the basic food source. Hollibaugh and Booth (1981) suggest that over 40 percent of the annual production of phytoplankton on the Grand Banks occurs during the spring bloom. This burst of production is tracked by planktonic herbivores such as copepods, and ultimately by fish. Most animals characteristic of the Grand Banks reproduce during the period of the spring bloom.

Phytoplankton distribution on the Grand Banks is affected by current flow. Currents can form large gyres over the continental shelf, and these play a role in the

ecosystem of the Grand Banks. Plankton, including fish eggs and larvae, can be retained there by such current patterns (Helbig *et al.*, 1992). On an even larger scale, offshore eddies and rings have an important influence on the circulation patterns, such as interactions between the Labrador Current and eddies of the North Atlantic Current system (Petrie and Anderson, 1983; Greenberg and Petrie, 1988).

The principle physical oceanographic features at work on the Grand Banks are the Labrador Current (Petrie and Anderson, 1983) and the North Atlantic Current (Clarke *et al.*, 1980). To understand the physical causes which underlie the patterns observed in the phytoplankton, these currents must be taken into account.

Other major currents of the region are the Slope Water Current, and, to the south, the Gulf Stream. The North Atlantic current forms where these and the Labrador Current interact. The intrusion of the Slope Water Current and Gulf Stream from offshore can have a profound effect on the local biota of the Grand Banks. This effect can be attributed to increasing bottom water temperatures, usually decreasing nutrient concentrations, and the transport of slope water communities onto continental shelf areas (Bainbridge, 1961; Wroblewski, 1989).

Prolific phytoplankton growth is typical of oceanic front boundaries. Zooplankton populations on the Grand Banks are often different on either side of a front (Gardner and Howell, 1983), reflecting differences in water temperature, salinity, and food availability in the water types that occur there.

The spring bloom of phytoplankton on the Grand Banks has long been recognized

as an extremely important and dramatic aspect of the ecology of this part of the Western North Atlantic. Shipboard sampling may not be adequate to study and monitor its rapid evolution. Although satellite coverage of the Grand Banks is generally poor, it has been possible to describe the spatial and temporal patterns of phytoplankton pigment distribution by augmenting the data with a complementary and comprehensive set of ship-derived ground truth data. Ground truth data is an important component of satellite data analyses. It allows local calibration and validation which are vital in models.

The Grand Banks of Newfoundland are difficult to study by remote sensing. This mid-latitude region is plagued by cloud and fog; therefore, a very small number of relatively cloud-free images are available for analysis in any given year. Another problem is the large solar zenith angle, which complicates data processing. Satellite bio-optical algorithms of Gordon *et al.* (1983a) apparently will not work in such cases without including the effects of multiple Rayleigh scattering. Seasonal variability in the physical and biological factors also results in considerable scatter in relationships that attempt to relate biomass to production. To gain useful information in this situation requires a ship-to-satellite calibration exercise and a systematic study of the factors that affect the physiological properties of phytoplankton. As a first step, I will look into the effects of selected of local, physical and biological factors on phytoplankton.

2.2 Variation in physical and biological factors

Soule *et al.*(1951) used over eight years of temperature and salinity data collected

over the Grand Banks to identify three different water masses clearly: the Labrador Current (salinity 34.3‰, temperature 0 - 1.0°C), the Atlantic Current water (salinity 34.7 - 35.1‰, temperature 8.0 - 10.0°C) and mixed water (salinity 34.1 - 34.5‰, temperature 4.0 - 6.0°C). However, more recent data, collected by the United States Coast Guard during ice patrol surveys, have indicated that the sea surface temperature can range from -1.0 to 14°C on the Grand Banks (Hayes and Robe, 1978). The ice patrol surveys during June and July 1973 clearly indicate the infiltration of the Labrador Current onto the Grand Banks.

The northern part of the Grand Banks is influenced by the Labrador Current flowing out of the Arctics, whereas waters of subtropical origin may penetrate the southern and southwestern parts of the Bank. Therefore, the Banks' waters experience seasonal fluctuations of physical properties which in turn influence the biological properties. Intense vertical mixing in the central region of the Grand Banks disrupts the vertical temperature gradient in winter, so that temperatures are uniform and around +1°C from surface to bottom (Buzdalin and Elizarov, 1962).

Sectional plots of the physical characteristics (temperature and salinity) of the Grand Banks (Mobil Oil Canada, 1981) suggest that:

1) Water column stratification is mainly determined by temperature.
2) The Labrador Current has an inshore and an offshore branch, resulting in the presence of cold water on both the eastern and western sides of the Grand Banks.
3) A frontal zone is a permanent feature along the eastern edge of the Banks, where it

is associated with the southerly flow of the offshore branch of the Labrador Current.

Study of the seasonal variability of the physical and biological processes is important in determining production. Principally, seasonality can induce a large variance in primary production models which relate biomass to production. This variance is expected because phytoplankton biomass and primary production rates can be regulated differentially by the availability of nutrients and radiant energy in the ocean, which in turn are determined by the physical, biological, and optical properties of the water column. Temporal and spatial distribution of phytoplankton on the Grand Banks is influenced by both physical and biological processes. Physical properties such as sea surface temperature and water column stability play an important role in the evolution of the spring bloom on the Grand Banks.

Identification of physical processes which could induce variability in the primary production estimates on the Grand Banks is a preliminary step in algorithm development. Algorithm development further requires a comprehensive set of physical and biological data collected over both spatial and temporal scales. Comparison of ship and satellite data requires that the sea-truth data be synchronous to satellite overpasses. However, due to cloud cover and other logistic constraints in the Grand Banks region, such synchronous data are available only on a highly opportunistic basis.

2.3 Ship data required for algorithm development

Satellite remote sensing offers the potential of circumventing the problem of undersampling inherent in shipbased measurements (Esaias, 1980; Smith *et al.*, 1982; Feldman, 1986). Ocean basin-scale maps of phytoplankton abundance (Esaias *et al.*, 1986) mapped with the aid of spectral radiometers (Gordon *et al.*, 1980; Gordon *et al.*, 1982; Gordon *et al.*, 1983a; Smith and Baker, 1982), may contribute directly to a better understanding of patterns and processes in oceanic primary production.

To transform maps of chlorophyll into primary production maps, algorithms need to be developed. Such algorithms are basically light-production models, and are sometimes used in conjunction with information on the integrated pigment content and its vertical distribution. Ship-based data for this purpose should ideally include measurements of integrated pigment content of the water column, its vertical distribution, primary production, and the photosynthetically available radiation (PAR) and its vertical attenuation.

Spectral models use information on changes in the spectral composition of light with depth and the photosynthetic action spectrum to estimate phytoplankton growth (e.g. Bidigare *et al.*, 1987; Smith *et al.*, 1989). Knowledge of the euphotic depth (the thickness of the water column above the 1% light level) is also needed to compute integral production and chlorophyll biomass. Therefore, an algorithm for determining the total PAR extinction coefficient in the water column is required.

Some investigators have developed models based on known relationships between

production and chlorophyll, and factors such as light, nutrients, photoadaptive state, and the depth of the mixed layer (Collins *et al.*, 1986; Platt, 1986). To do so requires measurements of nutrient availability and phytoplankton physiological factors. But for any model, a satellite algorithm can depend only on those variables that are derivable from remote sensing, together with those that can be modeled from theory or empirical observations (Campbell and O'Reilly, 1988).

My investigation, aimed at developing a production algorithm for the Grand Banks, suggested that satellite-derived chlorophyll could be employed to predict total chlorophyll concentration (water column integrated chlorophyll), and from there integral production. During development of a first model, these questions were addressed:

1) How is satellite detectable chlorophyll (SDC) related to total euphotic zone chlorophyll and mean euphotic zone chlorophyll?
2) How is integral production related to total chlorophyll in the euphotic zone?
3) Is the biomass-specific production a linear function of incident radiation in cold oceans?
4) Is the water column light utilization index (ψ) relatively constant within cruises and over seasons in cold oceans?

2.4 Methods for measured and estimated variables

A total of 200 pigment and 80 production stations were sampled in 1980-1981 in four seasons. The data come from a comprehensive environmental impact study funded

by Mobil Oil Canada Limited and partners for the Hibernia oil drilling site, off Newfoundland. Data for the phytoplankton species composition and abundance during the study period were provided by Mr. John Lane of Hibernia Management Co., St. John's. Figure 1 shows the positions of the sampling sites on the Grand Banks. Water samples were collected at depths of 0, 5, 10, 15, 20, 30 and 50 m at each station with Niskin bottles on a rosette sampler.

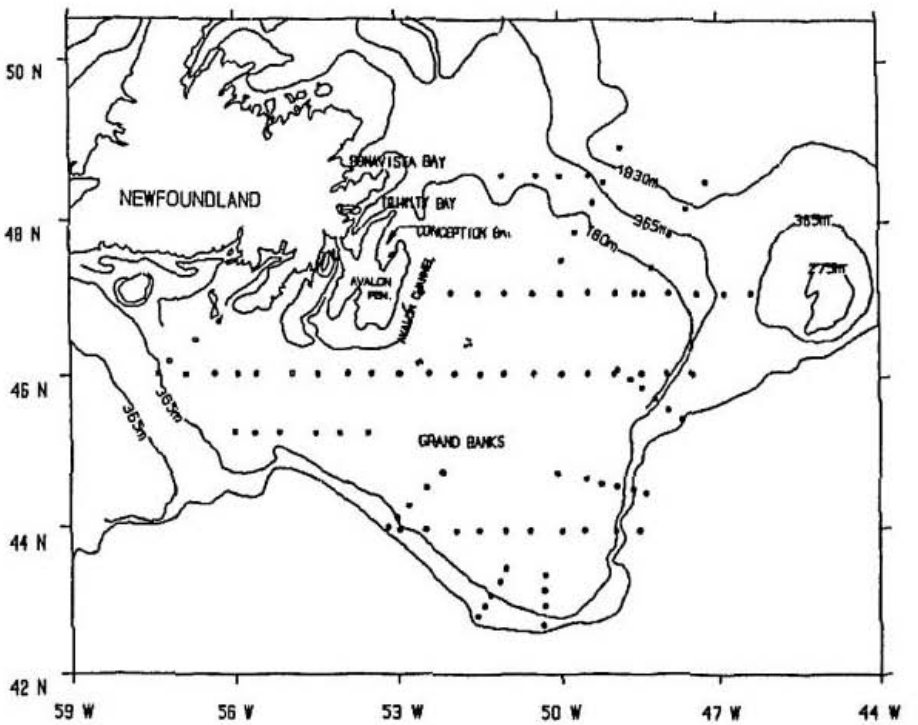

Figure 1. Grand Banks study area with Hibernia EIS survey station locations indicated.

Chlorophyll and phaeopigment concentrations were determined by fluorometry. Primary production was determined by the ^{14}C method. Samples were placed in 125ml narrowmouth, screwcap, borosilicate glass bottles which were inoculated with approximately 5 μCi of $NaH^{14}CO_3$ solution (New England Nuclear brand) that had been filtered through a 0.45μm nominal pore-size membrane filter (Whatman brand) prior to use. The activity of the bicarbonate solution used was determined by radioassaying subsamples of the solutions (Hollibaugh and Booth, 1981).

Inoculated bottles of water from each depth were placed in deck-mounted incubation chambers, cooled by surface seawater. The light reaching the bottles was attenuated to 100, 50, 30, 14.5, 3.5, and 1% of the incident radiation by layers of screen incorporated into the incubation chamber walls. The incubation conditions simulated *in situ* conditions with the *caveat* that samples were taken from fixed depths and incubated at fixed light levels. Actual light attenuation at the fixed depths, however, was usually similar to the imposed attenuation, so that this probably does not introduce a major source of error into production estimates.

Bottles were incubated for 24 h, after which the particulate matter contained in them was collected on 0.45μm nominal pore-size 25mm-diameter membrane filters (Whatman brand). Filters were frozen at -20°C in a desiccator and returned to the laboratory for further processing. Data were converted from counts per minute to disintegrations per minute using the external standard channels ratio which was calibrated against actual samples to which ^{14}C toluene internal standard was added after the sample

had been counted once.

Phytoplankton cells were enumerated with inverted microscopy by Utermöhl's technique. A calibrated counting grid was used to estimate dimensions of phytoplankton cells. Data on phytoplankton cell size and the species composition were needed for interpreting the variation observed in light absorption and utilization. These matters will be discussed in detail in Chapter 5.

Key data needed for the model are the integrated pigment content, primary production measurements within the euphotic layer, and the photosynthetically available radiation, PAR, integrated over 400-700 nm and measured just beneath the sea surface with a quantum sensor.

Chlorophyll*a*, phaeopigments, and ^{14}C uptake rate measurements should represent the three phytoplankton size classes; netplankton (retained by 20μm filter), and nanoplankton and picoplankton (retained by 0.45μm filter) fractions. Recent evaluation of the efficiency of the 0.45μm pore-size filter indicates that some picoplankton may not be retained during filtration in the ^{14}C technique, and this may lead to underestimation of production in oligotrophic waters (Li, 1986). Therefore, the total daily rate of primary production from the measurements made as above would be the sum of netplankton, nanoplankton, and, if present, any extracellular material. Such measurements allow integration of chlorophyll and production over the euphotic depth.

2.4.1 *Euphotic depth*

The euphotic depth is defined by convention as the layer above the 1% light depth, Z_e. Therefore, the average diffuse attenuation coefficient for PAR, K_T, can be defined as

$$K_T = (- \log_e (I_{(Ze)}/I_o)) / Z_e \qquad (2.1)$$

where I_o and $I_{(Ze)}$ are the irradiances at the sea surface and euphotic depth respectively. Thus K_T can be computed from measurements of Z_e (Campbell and O'Reilly, 1988) according to $K_T = 4.6/Z_e$.

If Secchi disc values are available, then the euphotic depth D_E can be estimated following Strickland (1958) as

$$D_E = 4.605\ D_S / C_K \qquad (2.2)$$

where D_S is the Secchi disc depth in metres and C_K is a Secchi disc calibration factor calculated from vertical extinction coefficients measured with a light meter. Equation 2.2 was used for estimating the euphotic depth in the Grand Banks data. Preisendorfer (1986) has recently proposed another relationship for estimating the euphotic depth from Secchi disc measurements (he uses Z_{SD} in his equation),

$$Z_{eu} = 1.79\ Z_{SD} \qquad (2.3)$$

where Z_{SD} is the Secchi disc depth in metres. (Please note that $Z_{eu} = D_n$).

2.4.2 *Computation of integral chlorophyll, primary production, and mean euphotic chlorophyll*

Vertically integrated primary production, IP, can be computed from n determinations of production (P_i, mg m^{-3} day^{-1}) at depth z_i (m) by

$$IP = \sum_{i=0}^{n-1} \frac{1}{2} (P_i + P_{i+1}) (z_{i+1} - z_i) \qquad (2.4)$$

Similarly, integral chlorophyll, IC (mg chl*a* m^{-2}), the sum of total chlorophyll *a* and phaeopigment concentrations, is computed from n determinations of chl*a* at depth i (C_i, mg m^{-3}) at depth z_i (m) by

$$IC = \sum_{i=0}^{n-1} \frac{1}{2} (C_i + C_{i+1}) (z_{i+1} - z_i) \qquad (2.5)$$

Mean euphotic chlorophyll, $<C>$, is computed by dividing IC by Z_e, the euphotic depth (Campbell and O'Reilly, 1988).

2.4.3 *Satellite detectable chlorophyll*

Satellite detectable chlorophyll, SDC, is computed as the weighted average of chlorophyll *a* and phaeophytin to a depth of one attenuation length (i.e., $Z_K = 1/K_T$), which corresponds approximately to the top 37% light depth (Campbell and O'Reilly, 1988). This method of weighing accounts for the light attenuation at depth. Light is attenuated by a factor of exp(-2kz), where k is the mean light attenuation coefficient.

The value of k depends on the amount of chlorophyll present and its light attenuation. Feldman (1986) has estimated the attenuation length in the Peru Upwelling of the equatorial Pacific, and his values correspond to approximately the top 22% of the euphotic depth. However, his estimates of primary production from this very productive part of the equatorial Pacific are higher than the value of production estimated for the Georges Bank region (2.77 *vs* 1.13 g C m^{-2} d^{-1}) (Kuring *et al.*, 1990). The attenuation length and phytoplankton concentration are inversely related; therefore, the presence of more phytoplankton biomass in the water column would correspondingly reduce the attenuation length.

2.4.4 *Estimation of PAR*

Photosynthetically available radiation (Ein m^{-2}, integrated over wavelengths between 400 to 700 nm) is normally measured by a quantum sensor on a ship or on the land. When direct measurements are not available, PAR must be estimated.

On the Grand Banks, PAR values for the sampling dates were estimated from a

regression equation relating measured PAR to total incident radiation, I_o. PAR was measured at a coastal location at Kelligrews (47°30' N 53°01'W). I_o was measured by Atmospheric and Environment Service (AES) Canada at St.John's (47°32'N 52°47'W). These are simultaneous measurements although at different locations. The regression equation obtained was

$$PAR' = 0.382\ I_o - 2.263 \quad (r^2 = 0.96,\ n = 36) \qquad (2.6)$$

Equation 2.6 takes into account the effects of fog and cloud on PAR because of this local calibration. Values calculated from this equation are denoted hereafter as PAR'. The daily total incident radiation data (Ein $m^{-2}\ d^{-1}$) and PAR' data (Ein $m^{-2}\ d^{-1}$) for 1980 are reported in Appendix Table B. The PAR' data in Table B were calculated from equation 2.6.

2.4.5 *Estimation of K490*

The diffuse light attenuation coefficient at 490nm wavelength (K490) was calculated using a statistical relationship presented by Morel (1988). His model predicts attenuation of solar radiation as a function of phytoplankton pigment concentration

$$K490 = 0.0217 + 0.0690\ Chl^{0.702} \qquad (2.7)$$

where Chl is a mean pigment (chlorophyll + phaeopigment) concentration (mg m^{-3}) within the euphotic zone regardless of the vertical pigment distribution. Remote sensing optical depth has been estimated as 1/K490.

This statistical relationship of Morel (1988) was recently used by Wroblewski (1989) to develop a model of the spring phytoplankton bloom in the North Atlantic and determine its effect on light attenuation in the water column.

2.4.6 *Computation of* ψ

If a stable relationship exists between integral primary production, chlorophyll and light, then the slope in a single parameter linear regression of IP/IC ratio *vs* incident light is an appropriate estimate of the water column light utilization index, ψ (Falkowski, 1981).

ψ has been considered a relatively "stable" parameter in the estimation of primary production from remote sensing measurements (Platt *et al.*, 1988). However, for a global application of any model, more research into the causes of variation in the photosynthetic-irradiance (P-I) parameters, which are often assumed to be constant, is required (Balch *et al.*, 1989b; Campbell and O'Reilly, 1988).

IP and IC, along with total incident radiation, I_o, on the Grand Banks, were used to compute ψ for each station according to the formula of Falkowski (1981),

$$\psi = IP / (IC\ I_o). \qquad (2.8)$$

2.5 Satellite detectable, mean euphotic, and total chlorophyll

Information regarding the vertical distribution of pigment in the water column is not available to satellite sensors. Therefore, attempts have been made by investigators to determine the column-integrated pigment content from knowledge of the pigment concentration in that upper layer which is sensed by a satellite.

The upper layer is one optical depth, which is about 10 to 15m on the Grand Banks (see 2.4.3). The CZCS detects the weighted average of pigment within this optical depth, which corresponds approximately to the 37% light depth.

Chlorophyll concentrations measured on shipboard can be used to compute the concentration presumably "seen" by a remote sensor, referred to herein as satellite detectable chlorophyll, SDC. SDC is a useful variable for predicting the column-integrated pigment content, IC, from empirical relationships. Normally, the predicted IC value accounts for the existence of a chlorophyll maximum. For inferring the biomass profile in stratified waters it may be necessary to categorize the pigment profiles according to their trophic status (Morel and Berthon, 1989). However, these authors caution that the use of such parameterization should be restricted to the range of SDC from 0.02 to 10 mg chl*a* m^{-3}.

Initially, simple empirical relationships between integral chlorophyll (IC) and integral production (IP) were studied for predicting production. However, empirical relationships based on integral chlorophyll may not give reliable predictions because the

relation between IP and IC depends strongly on date and location, as indicated by an analysis of covariance (Prasad *et al.*, 1992).

To test the strength of the several relationships possible, a number of hypotheses were investigated with the data and a series of covariance analyses were performed. The statistical design was such that the effects of the class variables were controlled by the analysis of covariance. Cruise and station were treated as class variables in the GLM procedure (SAS, 1985). Table 1 outlines the hypotheses, along with the variance, probability, and the degrees of freedom values in each test. Predicted values from each model were plotted against residuals to see whether patterns existed. None were apparent, and therefore the underlying assumptions of independence in the test are not violated.

The outcomes of the tests in Table 1 allowed a choice of those variables that might be expected to give the best results in developing an algorithm. Therefore, the semi-empirical approach developed here uses integral chlorophyll (IC), light absorption by phytoplankton, and incident PAR to predict integral production. This approach takes into account the chlorophyll-specific, PAR absorption in the study area. Further, it is in part physiologically based, taking into account differences in photosynthetic efficiency of the phytoplankton. The semi-empirical algorithm utilizes a combination of derived as well as measured variables to predict integral production.

The first step in algorithm development was to determine whether total euphotic chlorophyll, IC, and mean euphotic chlorophyll, $<C>$, in the water column were

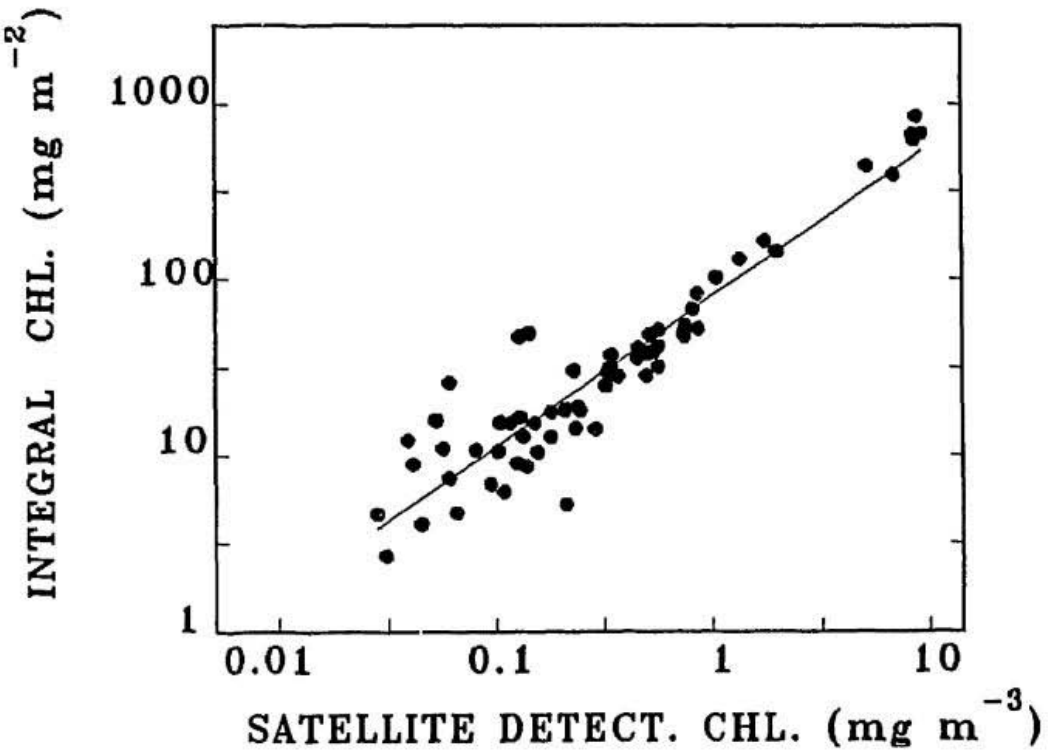

Figure 2. Log Integral chlorophyll (IC) versus Log Satellite detectable chlorophyll (SDC).

related to SDC. IC, SDC, and <C> were normalized by a logarithmic transformation and IC was regressed against SDC. The resulting linear relationship,

$$\log_e IC = 3.822 + 0.8408 \log_e SDC, \qquad (2.9)$$

was found to have an excellent fit, with a high explained variance ($r^2 = 0.88$, $n = 54$)(Figure 2). The data used for this relationship appear in Appendix Table C.

The high r^2 of equation 2.9 could be due, in part, to the fact that IC includes SDC, leading to a part-whole correlation. To check whether or not this was so, SDC was regressed against the remaining chlorophyll below the SDC. Surface and sub-surface chlorophyll were highly correlated with each other ($r^2 = 0.88$), indicating that the relation of IC to SDC was not just a statistical artifact. Only a fraction of the chlorophyll present is actually "seen" by the satellite, so it was very encouraging to find that IC and chlorophyll below one attenuation length could be estimated reliably from SDC. Figure 3 shows the monthly mean variation of SDC for the Grand Banks during 1980.

2.5.1 *Total chlorophyll and integral production*

Integral production was regressed against integral chlorophyll. Although the relationship had a high r^2 (=0.81), statistical analysis revealed a strong dependence on date and location (Table 1, Hypothesis B and C). The least squares regression between IP and IC was

$$IP = 73.20 + 11.33\ IC \qquad (2.10)$$

Some of the dependence of the relationship between IP and IC on date and location may be attributed to spatial or temporal variation in the availability of light. Therefore, PAR was included in the relationship between IP and IC. The relationship between IP, IC, and PAR was dependent on date and location (Table 1, Hypotheses E and F). IP was normalized by dividing IP by IC. Biomass-normalized production was then used for

further analyses. The relationship between biomass-normalized production (IP/IC) and PAR was significant (Table 1, Hypothesis G); however, it was again found dependent on date but not on location (Table 1, Hypotheses H and I).

2.5.2 *Variation in* ψ

The water column light utilization index, ψ (Falkowski, 1981), is the ratio of integral production to integral chlorophyll and incident light. ψ is calculated with equation 2.8, as discussed in section 2.4.6. Platt (1986) suggested that the biomass-normalized production (IP/IC) is proportional to the incident light, and that this relationship could be used in remote sensing models to estimate water column production. Platt *et al.* (1988) proposed the basic model and suggested that further information on the detailed vertical distribution of phytoplankton will be needed, rather than a series of surface observations on a horizontal spatial scale. This matter will be considered in Chapter 5.

Despite the good performance of the Platt *et al.* (1988) model for a limited data set, the observations of Balch *et al.* (1989b), Balch *et al.* (1989c) and Campbell and O'Reilly (1988) suggest that the application of such a model on a global basis would be extremely difficult without additional research into the cause of variation of the Photosynthesis-Irradiance (P-I) parameter. ψ varied remarkably little in the studies by Platt (1986), with values ranging from 0.31 to 0.66 gC $(gChl)^{-1}$ $(Ein\ m^{-2})^{-1}$. Higher values, however, have been reported (Yoder *et al.*, 1985; Campbell and O'Reilly, 1988;

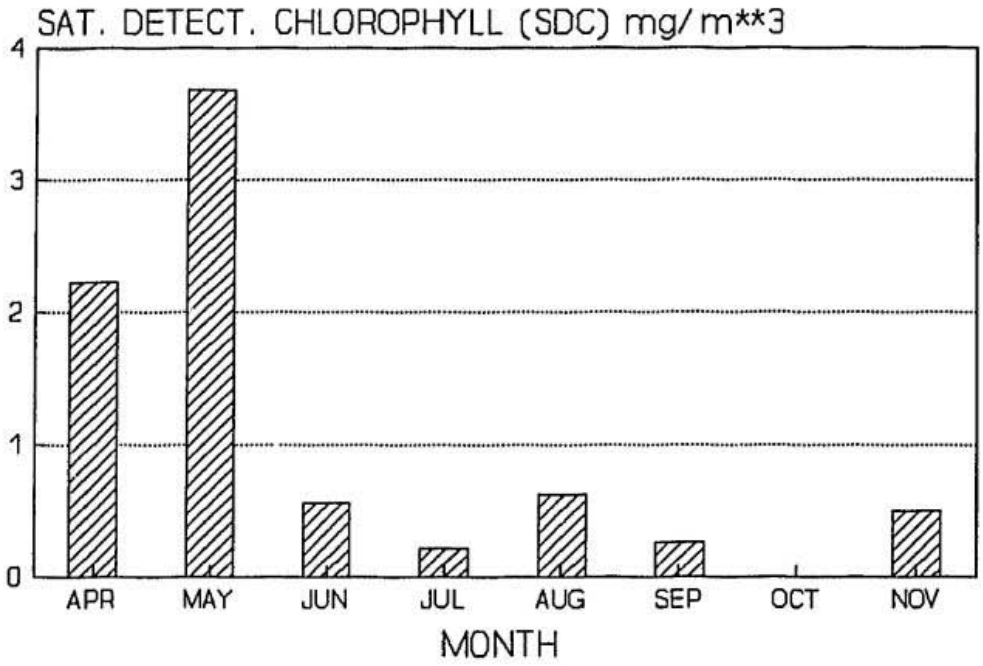

Figure 3. Mean monthly variations in Satellite Detectable Chlorophyll (SDC, mg m^{-3}) on the Grand Banks for the year 1980.

Prasad *et al.*, 1992). Hypotheses J and K (Table, 2) clearly indicate that ψ is variable within cruises. There was a significant association between the biomass-normalized production and incident radiation (Table 1, Hypotheses H and I) on the Grand Banks. However, the level of explained variance was low (r^2 = 0.08, Figure 4) and the relationship changed with time of year.

Table 1. Results of statistical tests for hypotheses studied. Multiplication sign $X_1 \times X_2$ indicates interaction of X_1 and X_2 in a two-way design. Vertical line | X_1 indicates that effects of X_1 have been controlled by linear regression in an analysis of covariance. † indicates significant relationship. F is the variance. P is probability.

Hypotheses	F(n1,n2)	P
A. IP = IC	569.45 (1,68)	0.0001†
B. IP = IC × cruise | IC	3.18 (6,62)	0.008†
C. IP = IC × station | IC	2.54 (15,53)	0.006†
D. IP = IC PAR′	572.95 (1,65)	0.0001†
E. IP = IC PAR′ × cruise | IC PAR′	1.18 (6,59)	0.33
F. IP = IC PAR′ × station | IC PAR′	0.46 (15,50)	0.94
G. (IP/IC) = PAR′	6.43 (1,66)	0.013†
H. (IP/IC) = PAR′ × cruise | PAR′	7.01 (7,67)	0.0001†
I. (IP/IC) = PAR′ × station | PAR′	0.93 (16,51)	0.54
J. ψ = cruise	3.14 (6,61)	0.009†
K. ψ = station	0.71 (15,52)	0.76

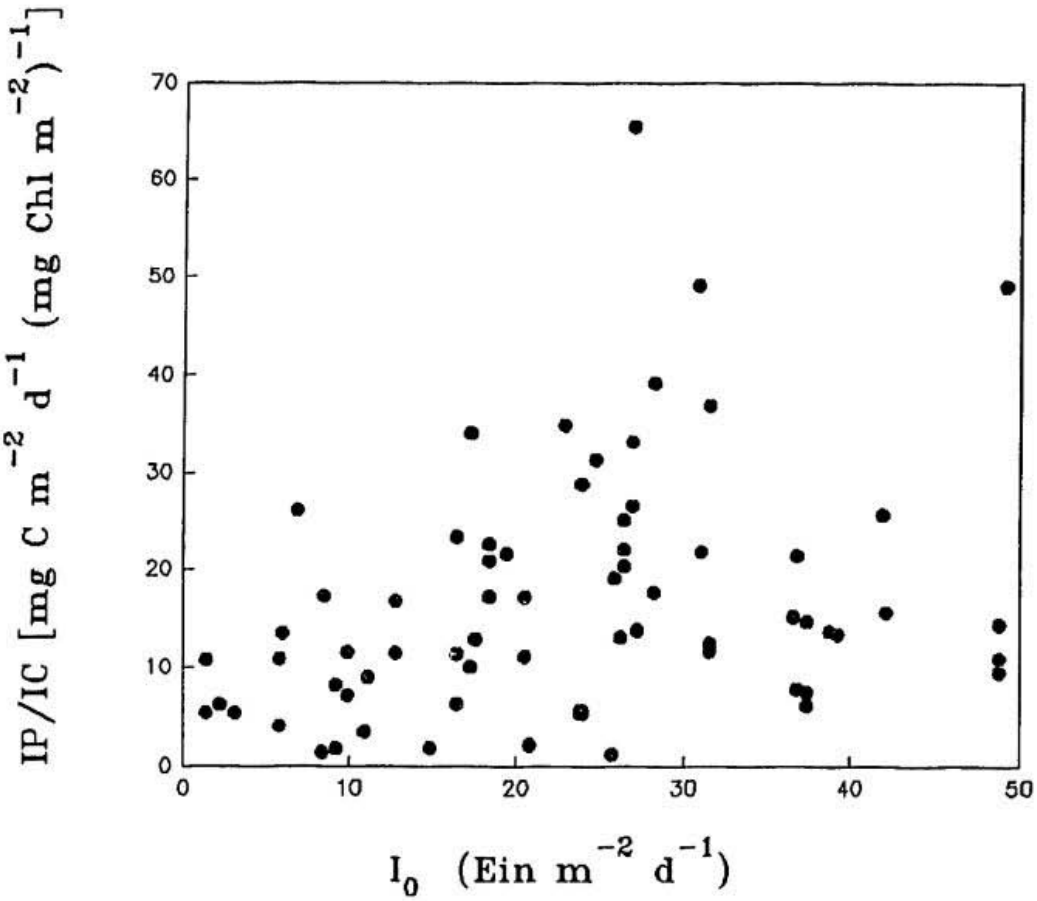

Figure 4. Biomass-specific production (IP/IC) versus total incident radiation (I_o) (n = 70, r^2 = 0.08).

The mean value of ψ averaged over all stations on the Grand Banks was 1.032 mg C (mg Chl*a*)$^{-1}$ m^2 Ein^{-1} (Prasad *et al.*, 1992). Therefore IP/IC cannot be predicted from incident radiation with either precision (because of low r^2) or accuracy (because of

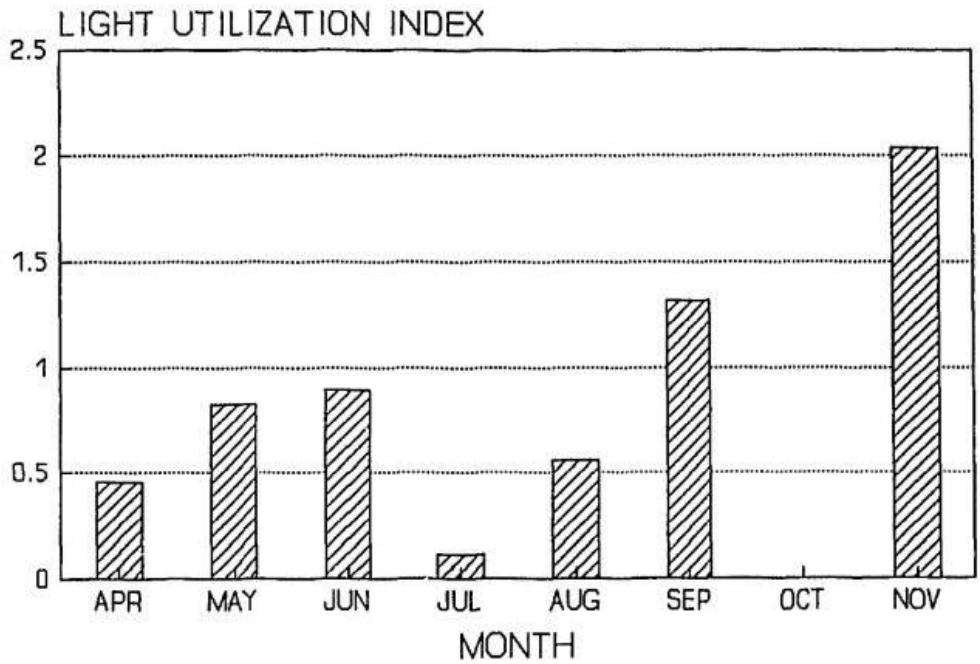

Figure 5. Temporal variation in the water column light utilization index ψ (mg C (mg Chl*a*)$^{-1}$ m^2 Ein^{-1}) on the Grand Banks.

dependence on date). Figure 5 shows how ψ varied according to month.

The relative constancy of ψ depends on the spectral quality of radiant energy available at different levels within the euphotic zone, the duration of the light period, the vertical distribution of algal biomass and the physical conditions that govern the availability of nutrients to the phytoplankton (Morel, 1991). Further analysis is necessary before ψ can be considered a constant in estimating water column production

anywhere, and particularly over large spatial scales.

Results from various test hypotheses using integral production, chlorophyll, and light, and from studies on the seasonal variability in production variables, suggest that some empirical models provide a good fit to data. However, because of dependence on date these models are not necessarily reliable . Therefore it was necessary to develop a more physiologically-based model to predict IP from IC and PAR. Such a model should take into account differences in the photosynthetic efficiency of phytoplankton.

2.6 The production algorithm

Most models for predicting integral production use chlorophyll and light, which vary with depth in the water column. Photosynthetic efficiency depends on PAR, on the concentration of chlorophyll in the phytoplankton cells, and on the chlorophyll specific absorption coefficient. Therefore, knowledge of the chlorophyll specific absorption coefficient, chlorophyll concentration at depth z and PAR at depth z are required for calculating the light absorption by chlorophyll at depth z (V_z). Theoretically, the product of light absorbed over the euphotic depth and quantum yield of the water column, $<K>$, should predict integral production. However, calculation of $<K>$ requires knowledge of production at depth z, but this value also happens to be a variable to be predicted. The model therefore is based on the light absorbed by phytoplankton and a computed value of quantum yield to predict IP.

The variables amenable to satellite measurement are the chlorophyll within one

attenuation length, and thus IC or the mean euphotic chlorophyll <C>, which can be predicted from SDC with sufficient accuracy. Therefore, the semi-empirical model is based on IP, IC, PAR, and the chlorophyll specific light absorption. A computed value of quantum yield in the IP is used in the model to eliminate the use of production values at discrete depths, which are not available from satellite imagery. Therefore, the semi-empirical model utilizes a combination of derived as well as measured variables to predict IP from discrete chlorophyll and PAR.

The quantum yield for the water column, K, is defined as the ratio of carbon fixed to light absorbed per m^2 by phytoplankton

$$K = \Sigma P_z w_z / \Sigma V_z w_z \tag{2.11}$$

where V_z is the absorption of light by phytoplankton at depth z, w_z is the width interval at depth z, P_z is the production at depth z, and

$$V_z = K_c C_z I_z \tag{2.12}$$

where K_c is the chlorophyll specific diffuse attenuation coefficient (= 0.017 m^{-2} (mg chl*a*)$^{-1}$ for natural populations of phytoplankton, Kirk, 1983), C_Z is the chlorophyll concentration at depth z and I_z is the PAR at depth z as estimated by PAR' (Eq. 2.6).

The product of light absorption V_z and the quantum yield K_z at depth z should

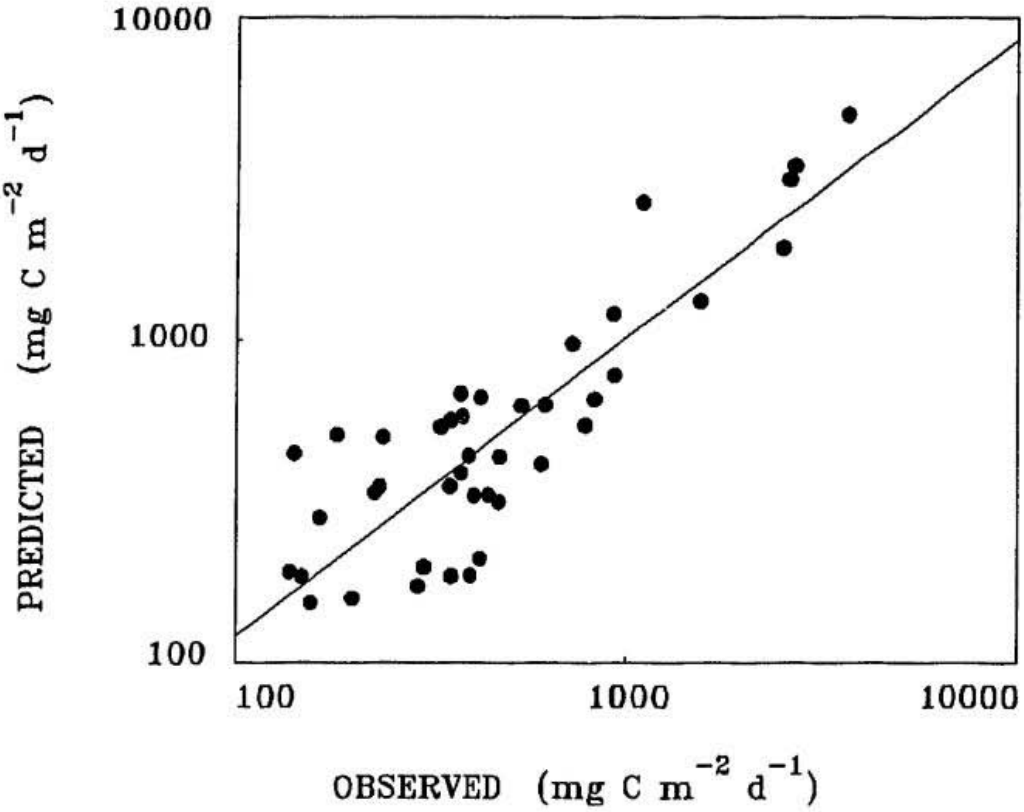

Figure 6. Fit between Log predicted versus Log observed production. Predicted values computed using the model.

account for the integral production down to the optical depth corresponding to the 1% light level. Physiologically these two variables are required for underwater photosynthesis, and from this

$$\Sigma IP_z = \Sigma K_z \; \Sigma V_z \qquad (2.13)$$

Similarly, accounting for K values over the optical depth corresponding to the 1% light level, we have

$$K_z = K/4.6 \qquad (2.14)$$

where 4.6 is the optical depth (m) corresponding to 1% of the subsurface light (Kirk,1983), and K is the quantum yield. Therefore this optical depth is a function of the light attenuation in the water column. Combining equations 2.11, 2.12, 2.13 and 2.14, the final model equation becomes

$$\Sigma\, IP_z = (K/4.6)\,(K_c\ \Sigma\, C_z\ \Sigma\, I_z) \qquad (2.15)$$

where it is assumed that the summation of discrete values of chlorophyll concentrations and light over the water column is equal to the sum of chlorophyll and light considered as if they were continuous variables.

The estimated production using the model was plotted against observed production to show the goodness of fit (Figure 6); the intention here has been to corroborate the model rather than to develop a regression model where IP is the predicted integral production. The quantum requirement for photosynthetic oxygen evolution is 10 ± 1 Einsteins absorbed per mol of oxygen evolved (Ley and Mauzerall, 1982, Dubinsky *et al.*, 1986). A practical upper limit, which is closer to 0.1 mol C Ein^{-1} (1200 mg C Ein^{-1})

(Kiefer and Mitchell, 1983; Kirk, 1983; Smith *et al.*, 1989), was used in the model. The fit is quite good ($r^2 = 0.80$, $n = 67$, $p < 0.0001$). The data are given in Appendix Table D.

To summarize, shipboard data have provided ample evidence that the pigment within the first attenuation length (= CZCS pigment) can be converted to production data through a series of interrelated steps. The approach adopted here is semi-empirical, and partly accounts for variable light absorption due to phytoplankton species and varying physiology. However, parameters like the quantum yield for photosynthesis (assumed as a constant in the algorithm) need further study and evaluation, especially with respect to temporal variability and its role in production estimates. This subject is dealt with more fully in Chapter 5.

With the refinement of pigment retrieval algorithms for satellite data, it has been possible to retrieve overall accurate pigment estimates ($\pm$ 0.3 $\log_{10}$ units). Pigment retrieval from the satellite still remains important and is the first step before accurate estimates of production are possible. Chapter 3 deals with retrieval of pigment information for the Grand Banks from the CZCS satellite.

CHAPTER 3. THE ANNUAL PICTURE FROM SHIP AND SATELLITE DATA

3.1 The Coastal Zone Color Scanner

The technical objective of the Coastal Zone Color Scanner (CZCS) was to determine if remote sensing of ocean color could be used to identify and quantify suspended or dissolved material in the water. If information concerning chlorophyll and sediment concentration could be derived from ocean color measurements, it could then help in the design and development of an operational satellite for use in future ocean exploration.

The CZCS provided estimates of near-surface concentrations of phytoplankton pigments and total seston by measuring the spectral radiance backscattered out of the ocean. This radiance is considerably less than the total signal, and therefore the CZCS sensor was designed with a very high radiometric sensitivity. This means that the CZCS sensor can detect, with high resolution, low radiances that are encountered in the sea. However, 70 to 80% of the signal sensed by the CZCS in band 1 (443 nm) originates in the atmosphere. The atmospheric effects are about 50% in band 3 (550 nm).

Estimating these atmospheric effects and removing them from the total signal seen

by the sensor has received considerable attention. Principal effects are from Rayleigh scattering (scattering from the air molecules) and aerosol scattering (scattering from particles suspended in the air). Aerosol scattering can vary greatly on small temporal and spatial scales, making its estimation more tedious than that for Rayleigh scattering. This is due to the fact that the scattering function is dependent on the aerosol size distribution (Quenzel, 1983).

Once atmospheric effects have been removed, the water-leaving radiance can be converted to give near-surface pigment concentration. The CZCS can detect chlorophyll to about one optical depth, approximately down to the 37% light level depth, which has been found to vary from 10-15 m on the Grand Banks. From October of 1978 until 1986, the CZCS allowed synoptic year-round estimates of near-surface chlorophyll concentrations (Hovis *et al.*, 1980) with reasonable accuracy (Gordon *et al.*, 1980; Gordon *et al.*, 1983a; Barale *et al.*, 1986). This accuracy is about $\pm$ 30% of the retrieved pigment.

CZCS data have added greatly to the information available on spatial and temporal patterns in the distribution of phytoplankton (Smith and Baker, 1982; Gordon *et al.*, 1983a). As a result of extensive ocean color measurement it has been possible to develop algorithms for derived products from the CZCS. Atmospheric, radiometric and geometric corrections are included in the processing algorithm. The final processing goal has been to take the observed radiance, determine the radiance that would be seen directly above the ocean surface, and then derive, from that radiance, the pigment

content of the water below the ocean surface.

3.2 CZCS design

The CZCS on the Nimbus-7 satellite system was a high-gain multispectral scanner designed to image the ocean in six co-registered spectral bands centered at 443, 520, 550, 670, 700 and 11,500 nm. The first four bands had a spectral width of 20 nm, while the fifth and sixth, respectively, had spectral widths of 100 and 2000 nm. The ground resolution was 825 metres for all bands. Scanning was accomplished through the use of a rotating mirror. The CZCS was operational during the period 1978-1986. The data from the thermal channel (11,500 nm), although available, were not utilized by investigators. This was due to the fact that the NOAA-AVHRR thermal data were more sensitive than the thermal channel in CZCS for mapping SST (Gordon and Morel, 1983). Therefore, due to progressive loss in the sensitivity of the thermal channel, the CZCS was less reliable than the NOAA-AVHRR for this information.

In spite of intermittent data acquisition, the CZCS data can be used to validate methods to be applied in future, in particular for deriving primary production and its associated carbon flux at a global scale (Platt and Sathyendranath, 1988).

The phytoplankton pigment algorithm currently used relates the pigment concentration to the three ratios of upwelling radiance just beneath the sea surface which can be formed from the wavelengths 443, 520, and 550 nm. The pigment algorithm developed by Gordon and Clark (1980) explains from 94 to 98% of the variance in

$\log_{10}C$ over three orders of magnitude in pigment concentration.

3.3 CZCS Image analysis

3.3.1 *Data for the Grand Banks*

CZCS satellite data obtained from NASA's Goddard Space Center, Greenbelt, Maryland, were processed using the image analysis system at the Bedford Institute of Oceanography (BIO), Dartmouth, Nova Scotia. MIAMI, an image processing software developed by University of Miami (Rosenstiel School of Marine and Atmospheric Science) (Feldman *et al.*, 1989), was used for CZCS image processing. Initial video display allowed elimination of 39 images with more than 50% cloud cover. For the 1980-81 period, six good images were chosen. The NASA scene number and the processed tape identification filename for the CZCS images are listed in Table 2. Air temperatures and wind speeds on the day of the satellite pass were not recorded. Out of the six images analysed, four images are presented in the thesis. The four images were selected because they represent the phytoplankton distribution before, during, and after the spring bloom on the Grand Banks.

Visible radiances from the CZCS were processed with an algorithm based on Gordon *et al.*, (1983a) to remove effects of Rayleigh and aerosol scattering and to compute pigment concentrations from corrected blue (443 nm) to green (550 nm) radiance ratios. The initial processing utilizes atmospheric correction algorithms for

Table 2. NASA scene numbers and file identification information for processed CZCS

images. The file backup is archived and available on 9-track computer tape at the Ocean Sciences Centre (NICOS).

NASA Scene No.	Date	Processed File ID
80051145328.N17;1	20.02.80	[MIAMI.RMG]C80051145328.RMG;1
80106145100.N17;1	16.04.80	[MIAMI.RMG]C80106145100.RMG;1
80123145808.N17;1	03.05.80	[MIAMI.RMG]C80123145808.RMG;1
80249143554.N17;1	05.09.80	[MIAMI.RMG]C80249143554.RMG;1
80261145144.N17;1	17.09.80	[MIAMI.RMG]C80261145144.RMG;1
81183143208.N17;1	02.07.81	[MIAMI.RMG]C81183143208.RMG;1

application to the raw satellite data.

Epsilon (ratio of aerosol radiance at 440, 520, and 550 nm to the aerosol radiance at 670 nm wavelength) values were calculated for each of the selected images. For example the epsilon at 443 nm could be calculated as:

$$\text{epsilon } (443,670) = (670/443)^{-\nu} \tag{3.1}$$

where ν is the Angström coefficient (Robinson, 1985).

CZCS pigment algorithms are appropriate for estimating phytoplankton pigment concentration only in Case 1 waters (Morel and Prieur, 1977), where phytoplankton cells and associated products are the only important determinants of optical properties (Gordon

and Morel, 1983). This is the case on the Grand Banks.

3.3.2 *Algorithm overview*

A series of interrelated steps are performed during CZCS data processing to obtain chlorophyll (chl), diffuse attenuation length (K490), normalized water leaving radiance (440, 520, 550), and aerosol radiance (670). These wavelengths correspond to the channels on the CZCS sensor. Basically these steps follow the algorithm presented by Gordon and Morel (1983), and use a linear decomposition of the total radiance sensed at the satellite

$$L_T = L_R + L_A + tL_W \tag{3.2}$$

where L_T is the total radiance, L_R is the Rayleigh scattering path radiance, L_A is the aerosol path radiance, L_W is the water-leaving radiance, and t is the diffuse transmittance of the atmosphere.

3.3.3 *Rayleigh Model*

The effect of Rayleigh scattering is determined by analytic modeling to give the L_R term in equation 3.2. Two Rayleigh models are available: a single scattering model (Gordon *et al.*, 1983a) that is valid for calculations within 55 degrees of the solar equator, and a multiple-scattering polarization model (Gordon and Castano, 1987), that

extends quantitative calculations out to 65 degrees of the solar equator and qualitative calculations to within 75-80 degrees. Calculations nominally are based on the multiple-scattering algorithm.

3.3.4 *Aerosol correction*

Aerosol correction involves the calculation of the L_A term in equation 3.2. L_A can be estimated for the 670 nm channel by assuming that there is essentially no water-leaving radiance at this wavelength (i.e., $L_W(670) = 0$). $L_A(670)$ is then calculated as the difference between L_T and L_R calculated from the Rayleigh model

$$L_A(670) = L_T(670) - L_R(670). \tag{3.3}$$

The L_A at the other wavelengths (440 nm, 520 nm, 550 nm) is then related to L_A670 by a set of epsilon coefficients. The atmospheric correction assumes that one aerosol type (set of epsilons) is sufficient to characterize the aerosols (aerosol size distribution) across a specific two-minute CZCS scene.

3.4 Ship-to-Satellite comparison

A ship-to-satellite calibration was necessary on the Grand Banks because existing CZCS pigment retrieval algorithms were based on mid-latitude and low-latitude calibration data. The pigment algorithm used in CZCS data processing is based on the

results of Clark (1981). The NASA CZCS pigment algorithm applied universally to produce pigment images is

$$chl = 1.13\ (L_{ss},443/L_{ss},550)^{-1.71} \qquad (3.4)$$

where L_{ss} is the subsurface radiance. In practice, it has been found that equation 3.4 is good only when chl < 1.5 mg m^{-3}. Therefore when the chl concentration exceeds 1.5 mg m^{-3}, the CZCS processing algorithm switches to

$$chl = 3.326\ (L_{ss},520/L_{ss},550)^{-2.439} \qquad (3.5)$$

The reason behind this algorithm switching is that at higher chl absorption values the L_{ss} at 443 nm becomes so small that the ratio algorithm (equation 3.4) no longer works efficiently.

The CZCS senses the chlorophyll concentration down to one optical depth, which may vary from 10 to 15m on the Grand Banks. As a calibration, ship observations of chlorophyll were correlated with CZCS-derived pigment concentrations along a transect at 47°N (Figure 7). Ship data were available for calibration only for February, May, and September, 1980. Pixel level pigment information were obtained by "clicking" the mouse on the satellite image corresponding to the ship's position (latitude and longitude).

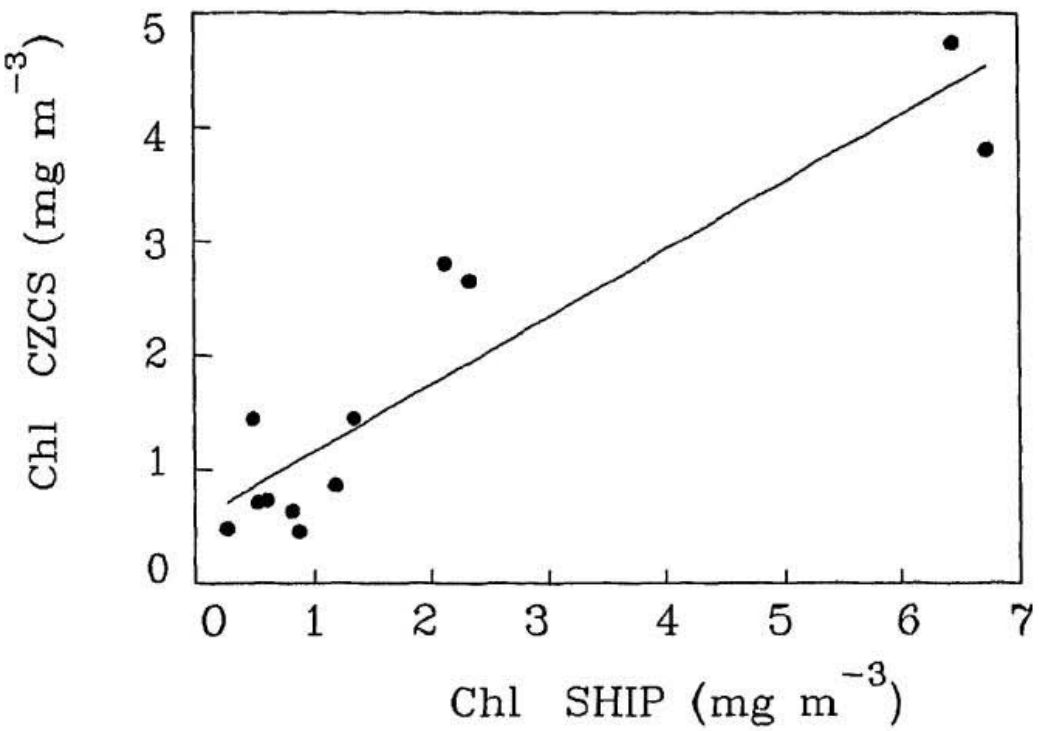

Figure 7. Ship-to-Satellite comparison of pigment concentrations on the Grand Banks. Ship data are from a transect at 47°N; see Fig. 1.

The calibration regression equation derived was

$$Chl_{CZCS} = 0.5651 + 0.5896 \times Chl_{SHIP} \quad (3.6)$$

with an $r^2 = 0.85$, $n=12$, $p < 0.0001$. The data appear in Table 3.

Table 3. CZCS and ship pigment data used for calibration. Positions given are for the individual satellite pixel clicked on the mapped ship position.

CZCS Image No.	Date	Lat.°N	Long.°W	chl_{CZCS} (mg m^{-3})	chl_{SHIP} (mg m^{-3})
80051145328.N17	20 FEB 1980	47.095	52.756	0.45	0.87
		47.075	52.550	0.85	1.17
		47.095	52.215	3.80	6.73
		47.045	51.802	0.70	0.50
		47.095	51.466	0.63	0.81
80123145808.N17	03 MAY 1980	47.040	51.370	1.44	1.33
		47.097	50.512	2.80	2.13
		47.097	49.720	4.74	6.45
		47.090	56.000	0.72	0.59
		47.055	51.879	2.65	2.33
		47.025	50.847	1.44	0.46
80249143554.N17	05 SEP 1980	47.025	55.980	0.47	0.24

3.5 CZCS images of the Grand Banks

The color plates in this section show the evolution of the spring bloom on the Grand Banks in 1980. Ship-board observations were obtained from the Hibernia EIS survey performed on the Grand Banks during the period 1980-81.

In winter (February), before the spring bloom begins, overall pigment concentrations are low (Figure 8). There were, however, patches of elevated pigment

concentration off the Avalon Channel and particularly in Bonavista and Trinity Bays. Offshore on the Grand Banks, high nutrients and low stability in the water column during this time of the year may account for the low pigment concentrations observed. These bays both support winter fisheries, and the elevated concentration of pigments may be indicative of the phytoplankton production which sustains the zooplankton there. In April, just prior to the bloom, the image is interesting in that early indications of the coming bloom appear inshore in Trinity and Conception Bays (Figure 9). A plume of phytoplankton moves north and eastward from the mouth of Conception Bay; the same pattern was observed in shipboard observations made during the COPE (Cold Ocean Productivity Experiment) investigation of 1986-90 (Pomeroy *et al.*, 199!). Overall nutrient concentrations were high during this time, although reduced nitrate concentrations and phytoplankton standing crop were observed in the surface layer. The image reveals upwelling events along the Avalon Channel. This upwelling is locally well-documented, and can be attributed to alongshore wind stress from the south (Schneider and Methven, 1988).

Three weeks later, in early May, the spring bloom of 1980 was at its peak (Figure 10). The images show that development of the bloom on the Grand Banks took place almost within a fortnight. This rapid evolution can also be seen in a plot of April *vs* May CZCS pigment concentrations along a transect at 47°N as a function of distance from shore (Figure 11). The extent of the growth of phytoplankton from inshore to offshore is clearly seen.

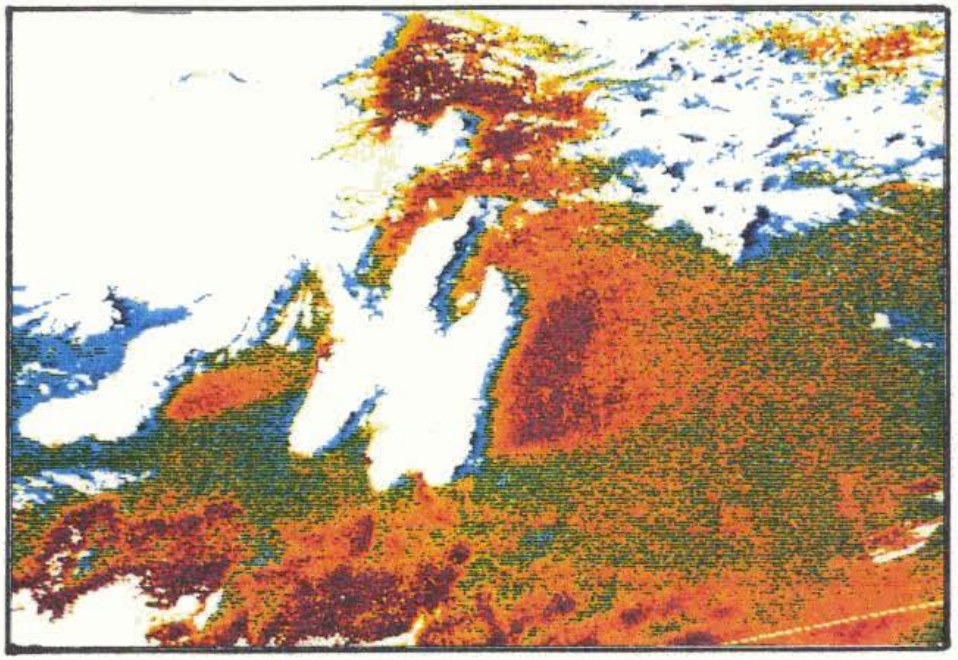

Figure 8. Nimbus-7 CZCS image of the Grand Banks region, 20 February 1980.

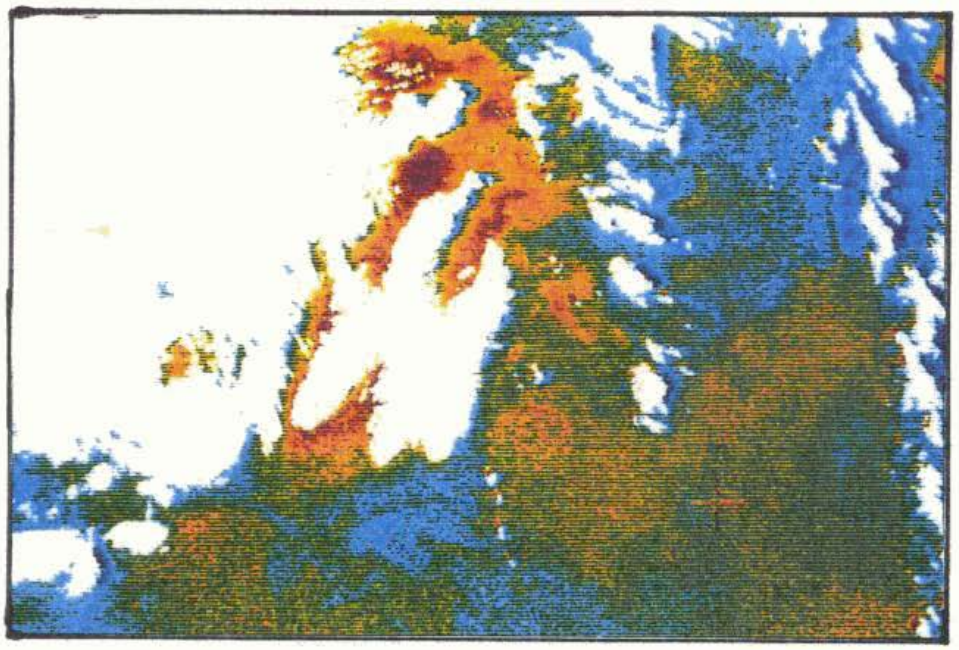

Figure 9. Nimbus-7 CZCS image of the Grand Banks region, 16 April 1980.

Figure 10. Nimbus-7 CZCS image of the Grand Banks region, 3 May 1980.

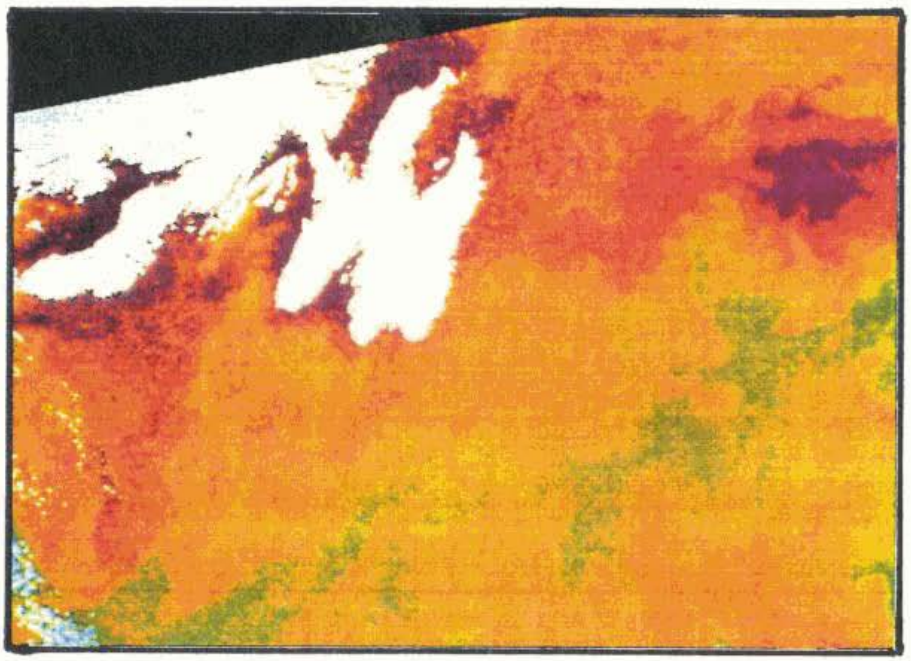

Figure 14. Nimbus-7 CZCS image of the Grand Banks region, 17 Sept 1980.

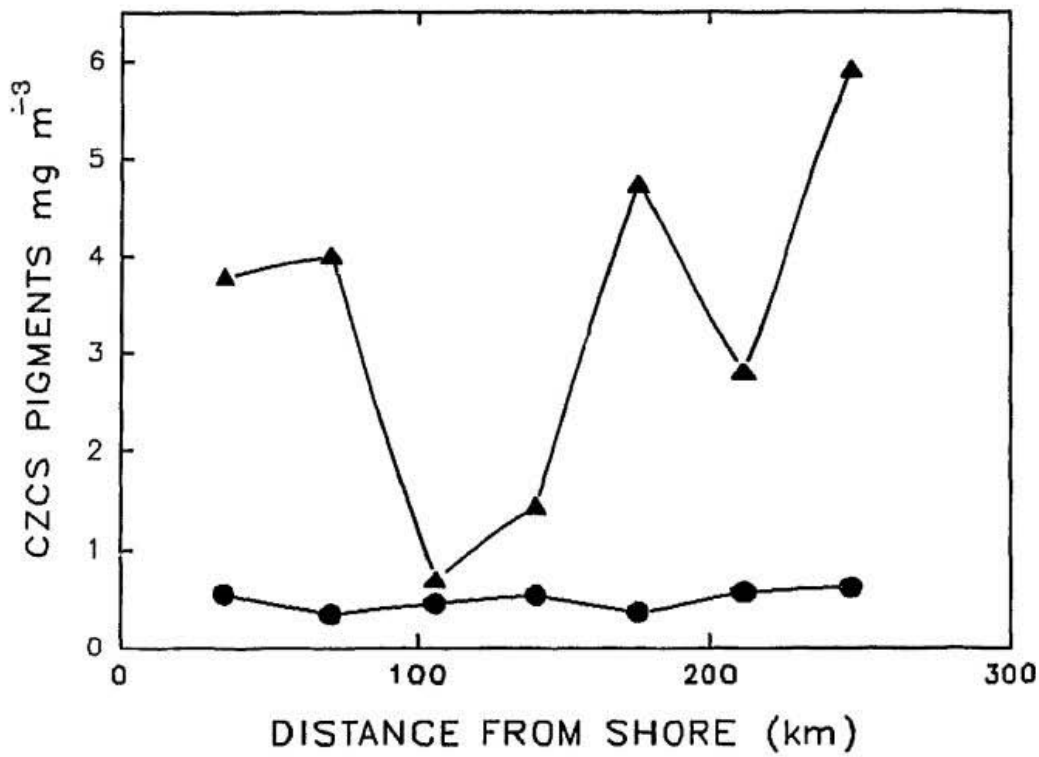

Figure 11. Pigment concentration for April (●) and May (▲) along a Grand Banks transect at 47°N. Measured from Nimbus-7 Coastal Zone Color Scanner sensor.

The rapidity and extent of phytoplankton growth from inshore to offshore regions is also reflected in a plot of the concentration of nitrate in the upper 50m of the water column. These data were measured on shipboard. Nutrient depletion in May relative to February along the same transect as the CZCS plots is evident in Figure 12.

Water column stability is a measure of the surface to 50m gradient in sigma-*t* (Chapter 4, equation 4.1). Water column stability varies considerably over the season on

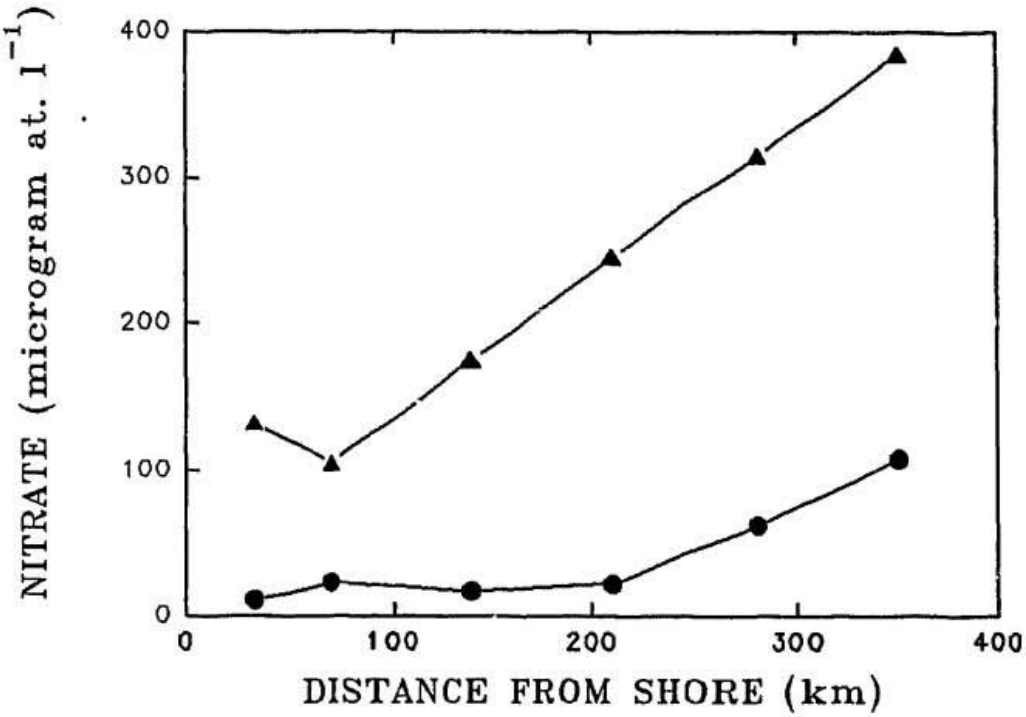

Figure 12. Nitrate concentrations of February (▲) and May (●) along a Grand Banks transect at 47°N. Survey data measured on shipboard.

the Grand Banks (Figure 13). Analyses show that water column stability is highly correlated to sea surface temperature on the Grand Banks (Chapter 4, equation 4.2), and thus stability continues to increase from spring into fall.

Once water column stability is established and nitrate depleted, the composition of the phytoplankton changes. Instead of the diatoms which dominated during the spring bloom, motile forms take over (Hollibaugh and Booth, 1981). Dinoflagellates and other

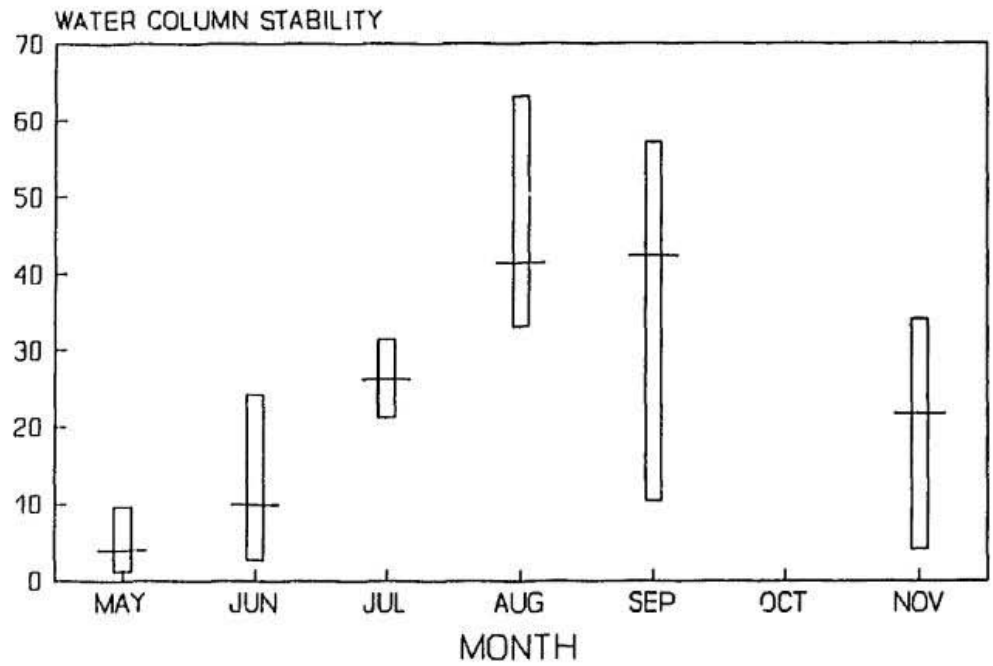

Figure 13. Temporal variability in water column stability (m^{-1}) on the Grand Banks. The horizontal line indicates the mean value for the month; the vertical bars show the range of values.

forms with low sinking rates make efficient use of nitrogen regenerated as ammonia in the stable surface layer. This regenerated nitrogen sustains phytoplankton growth until autumn storms increase the mixing of nitrate upward into the euphotic zone. At this point, another bloom may occur. The satellite image for September shows a large bloom centered at about 47° N 50° W (Figure 14). The shipboard data indicate that this is not a diatom bloom, but was practically a pure culture of the dinoflagellate *Gymnodinium sp.*

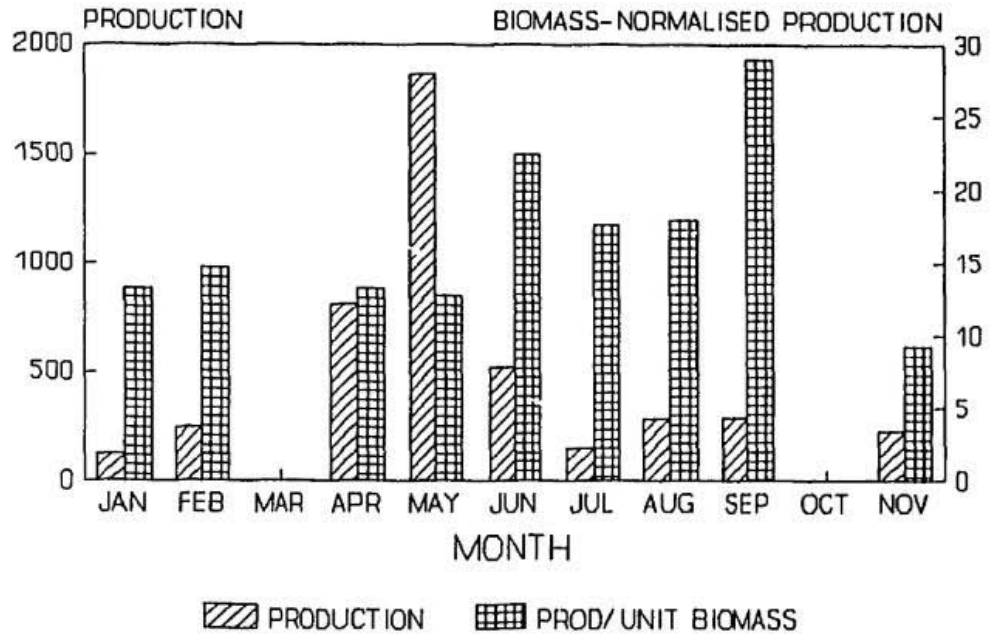

Figure 15. Comparison between production (mg C m^{-2} d^{-1}) and biomass-normalized production (mg C (mg Chl)$^{-1}$ d^{-1}) over the season on the Grand Banks.

Even though the standing crop of phytoplankton and integrated production peaked during May, biomass-normalized production peaked at even higher values in August and September (Figure 15). The data indicate that the dominant species in late summer or early fall are probably dinoflagellates, and the suggestion of Figure 15 is that these presumed dinoflagellates may be more efficient carbon fixers than are the spring bloom diatoms.

One of the key factors to be considered during phytoplankton seasonal succession is cell size, which presumably decreases through succession. Such changes in cell size may be functionally important since a larger surface-to-volume ratio may favor higher nutrient uptake rates, change sinking rates, and affect susceptibility to consumers. Diatoms range from 5 to 200 μm in size. However, larger cells are less common in late succession. Nanoplankton (2 - 20 μm) carry out most phytoplankton production (Malone *et al.*, 1979), and become more prominent late in succession. Therefore, when nutrients are renewed (early succession), the nanoplankton account for 5 - 20% of the chlorophyll, and under stratified summer conditions in the water column (late succession), 50 - 99% of the chlorophyll is due to nanoplankton (Hallagraeff, 1981).

The CZCS K490 algorithm has been demonstrated to be robust based on an analysis of *in situ* optical profiles from widely distri ıted stations in the North Pacific, the North Atlantic and the Greenland Sea (Mueller and Lange, 1989). It was encouraging to find that the diffuse light attenuation coefficient at 490nm (K490) on the Grand Banks is highly correlated with the satellite detectable chlorophyll (r^2=0.91, n=63, $p < 0.0001$, Figure 16). This finding further supports the general conclusion that K490 data could be used for characterizing water quality. The data on which the regression is based appear in Appendix Table E.

Patterns in near-surface pigment concentration are associated with the evolution of the spring bloom. First indications of the bloom were inshore, and the bloom developed very rapidly all over the Grand Bank at the onset of stratification in May.

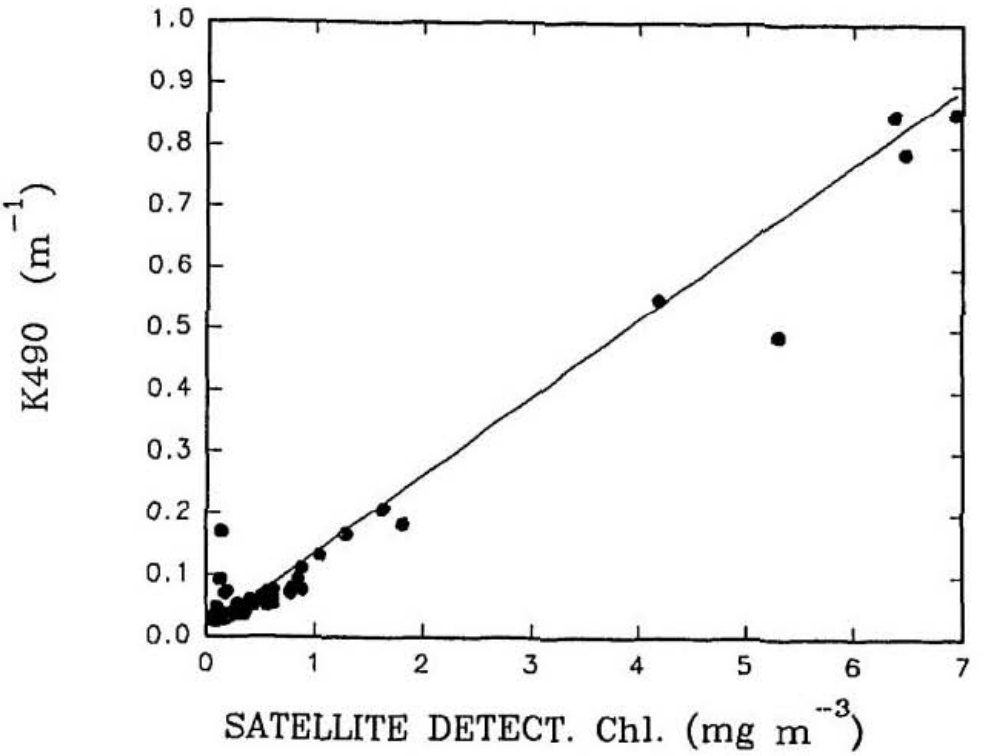

Figure 16. Diffuse attenuation coefficient at 490 nm (K490) versus satellite detectable chlorophyll (SDC) on the Grand Banks.

Satellite and nutrient data suggest that the bloom was ultimately stronger offshore. Diatoms comprised the dominant species, but were replaced by other species later in the season; dinoflagellates dominated an early fall bloom. As the season progressed, water column stratification and stability (associated with surface temperature) increased, and there was a fairly abrupt increase in the production-to-biomass ratio, perhaps attributable to a change in phytoplankton species composition.

CHAPTER 4. A SEMI-EMPIRICAL MODEL BASED ON SECONDARY VARIABLES

4.1 Introduction

Early primary production models developed for satellite data relied on knowledge of pigment concentration, light absorption and incident light in the water column. All three of these variables are closely related, and focus on the light harvesting capacity of phytoplankton. Seasonal variability in these variables has resulted in considerable scatter in predictions of annual primary production.

Most empirical approaches for predicting primary production depend on a constant relationship between chlorophyll and primary production. However, this relation can vary (Harrison and Platt, 1986) as a function of factors such as light level, nutrients, and mixing stress. Therefore, secondary variables have been investigated for their possible utility. Algorithms which include sea surface temperature along with chlorophyll, for example, account for the variability in predicted values of production (Balch *et al.*, 1989c). However, Campbell and O'Reilly (1988) found that, although SST and PAR were correlated to productivity on a temporal scale, their data within cruises were uncorrelated. Therefore, they were unable to use the relationship between SST and productivity.

4.2 Importance of secondary variables

Improving the predictive capability of semi-analytical algorithms for remote sensing of primary production will depend on the accuracy of variables such as quantum yield and chlorophyll-specific light absorption (Balch *et al.*, 1989b). These parameters vary as a function of species, depth, and light history, and they contribute to a large, unexplained variance in semi-analytical models. Local algorithms which include temperature perform well and can account for considerable variance in primary production. Therefore the virtue of semi-analytical models is not their accuracy as much as their applicability to any water mass.

The challenge, however, lies in utilizing parameters besides pigment concentration that can be derived *via* satellite and that provide new information about primary production. Therefore the use of variables besides pigment concentration to improve primary productivity prediction constitutes a new challenge worth investigating on the Grand Banks.

Three secondary variables from the Grand Banks shipboard data (water column stability, sea-surface temperature, and the remote sensing optical depth) were used for predicting integral production. Relationships among these variables were investigated for the purpose of predicting the integral chlorophyll in the water column. Some of the important questions addressed in this Chapter are:

1) How is sea-surface temperature related to water column stability on the Grand Banks?

2) How are water column stability and remote sensing optical depth related to integral

chlorophyll in the water column?

3) Can estimated integral chlorophyll be used to predict production on the Grand Banks?

4.3 Computation of secondary variables

Vertical stability of the water column (VS) was computed from the relation

$$VS = (\Delta \sigma_t / \Delta z) \times 10^3 \qquad (4.1)$$

where ($\Delta \sigma_t / \Delta z$) is the surface to 50m gradient in sigma-*t* (Anderson and Gardner, 1986). Values of thermosteric anomaly, the anomaly of specific volume with the secondary pressure effects neglected, were extrapolated from vertical section plots. A conversion was used for equating thermosteric anomaly to sigma-*t*. A contour interval of thermosteric anomaly of 20 cl/ton is equivalent to a contour interval of 0.21 sigma-*t* units.

The diffuse light attenuation coefficient at 490nm wavelength (K490) was calculated using a statistical relationship presented by Morel (1988) (Chapter 2; equation 2.7).

GLM procedure (SAS 1985) was used to fit linear regression models. Residuals from the models were examined for patterns by the method of Draper and Smith (1981).

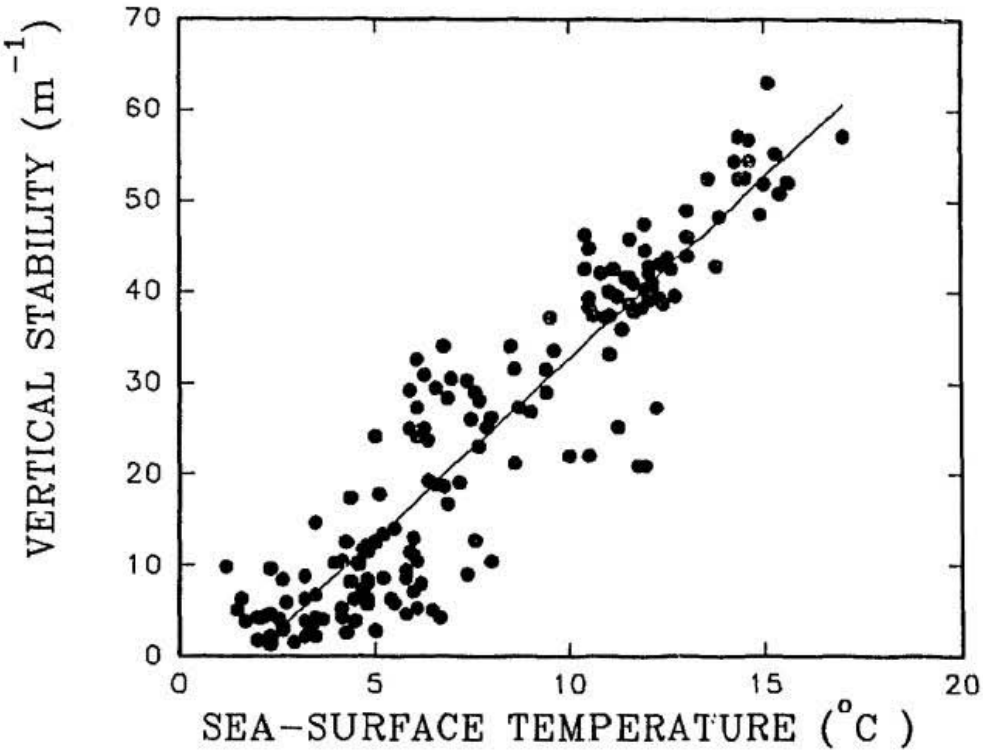

Figure 17. Sea surface temperature versus water column stability on the Grand Banks.

4.4 Vertical stability and integral chlorophyll

Water column stability (VS) in the Grand Banks data was a linear function of sea surface temperature (SST) (Figure 17). The level of explained variance was high and significant ($r^2 = 0.86$, $n = 173$, $p < 0.0001$), and the regression equation was

$$VS = -7.45 + 4.002\ SST \qquad (4.2)$$

The data appear in Appendix Table F.

SST, VS and 1/K490 were normalized *via* logarithmic transformation to achieve a normal distribution of data (Sokal and Rohlf, 1981), and then used to predict integral chlorophyll (IC) with an empirical linear regression equation. When SST was included in the equation, the model could explain about 96% of the variance in IC. The data were also analysed using only VS and 1/K490 as independent variables in a multiple regression to estimate IC. About 96% of the variance in IC could be explained by VS and 1/K490 ($r^2 = 0.96$, $n = 50$, $p < 0.0001$). The regression model obtained using both variables was

$$\log_e(IC) = 8.154 - 0.089 \log_e(VS) - 1.78 \log_e(1/K490) \qquad (4.3)$$

Equation 4.3 was checked for part-whole correlation effects due to the fact that K490 was estimated using mean euphotic chlorophyll (eq. 2.7). The correlation between $\log_e(IC)$ and $\log_e(1/K490)$, depends on the degree of correlation between $\log_e(VS)$ and $\log_e(1/K490)$ and was predicted as described by Sokal and Rohlf (1981). The part-whole correlation was 0.78, indicating that the explained variance in equation 4.3 was still quite high and could be used to estimate integral chlorophyll after eliminating the part-whole effects.

Remotely-sensed data to derive integral chlorophyll (IC') had to be simulated by using shipboard measured values of VS and 1/K490 in equation 4.3. SST can be sensed

from NOAA-AVHRR and K490 from Nimbus-7 CZCS satellite sensors.

Water column stability, which is a function of SST, can be predicted with sufficient accuracy from equation 4.2. This is because of the high r^2 obtained in equation 4.2 from the Grand Banks data. VS is the preferred variable as it partly eliminates the seasonal variations of SST.

The simulated integral chlorophyll (IC') values from equation 4.3 were used in a model to estimate integral production (IP'). The values of IP' were then compared to ship-measured values of primary production on the Grand Banks.

4.5 Test of the Model

The model utilizes remotely sensed pigment concentration (IC') to infer the potential carbon fixed by phytoplankton. A simple solution (Smith *et al.*, 1982) consists of assuming a constant proportionality between carbon fixation per unit of chl*a* present within the euphotic zone and the PAR at the sea surface. This leads to an estimation of the photosynthetically stored energy (PSR) within the euphotic zone (Morel, 1978; Platt, 1986)

$$PSR = PAR\ IC'\ \psi^{*} \qquad (4.4)$$

where PAR (Ein m^{-2} d^{-1}) is the photosynthetically available radiation, IC'(mg (chl*a*) m^{-2}) is the estimated integral chlorophyll, and ψ^{*} (m^2 (mg chl)$^{-1}$) is the cross-section for

photosynthesis. A mean value of ψ^* (= 0.05 m^2 (mg chl)$^{-1}$) was used in the model. This mean value corresponds to the value proposed by Morel and Berthon (1989) from field experiments for trophic category "e" based on pigment concentration.

Morel and Berthon (1989) analysed about 4000 vertical profiles of pigment (chl*a* + phaeo*a*) and defined trophic categories for most waters, including the Antarctic, based on pigment concentration within the surface layer and total pigment in the euphotic layer. Therefore, their relationships were based on a wide variety of water types including the tropical, temperate, and Antarctic waters. Hence their relationships based on trophic categories should be very robust. Values of surface layer and total pigment concentration in the Grand Banks region agree well with Morel and Berthon (1989) trophic category "e". Thus a mean value of 0.70 for ρ, the ratio of chl*a* to (chl*a* + phaeo*a*), is used here. ρ accounts for the active chlorophyll pigments in IC', a fraction that is normally less than the total chlorophyllous pigments encountered in coastal waters.

To derive an equation to predict integral production from equation 4.4, which estimates the photosynthetically stored radiant energy in the water column, the quantum yield for photosynthesis has to be included. In bio-optical models, the apparent maximum quantum yield is treated as a constant, commonly accepted to approximate 0.1 mol C Ein^{-1} if an O_2:CO_2 ratio of unity is assumed.

Morel and Berthon (1989) use a factor (1/39) which corresponds to the fixation of 1mg of carbon for a storage of 39J of PAR. However, a value of 1200 mg C Ein^{-1} (= 0.1 mol C Ein^{-1}) has been used for quantum yield, ϕ, assuming the ratio O_2:CO_2 is

unity. This value comes from an earlier analysis of data on the Grand Banks (Chapter 2; Prasad *et al.*, 1992). Therefore, equation 4.4 can be rewritten as

$$IP' = \phi \, PAR \, \rho \, IC' \, \psi^{*} \qquad (4.5)$$

where IP' (mg C m^{-2} d^{-1}) is the predicted integral production. Simulated IC' values from equation 4.3 were used in equation 4.5 along with a constant value of quantum yield for carbon fixation to predict primary production. Figure 18 shows the plot of observed *vs* predicted production. The predicted values come from equation 4.5 and the observed values were from direct measurements made on board the research vessel. The goodness of fit was satisfactory ($r^2 = 0.83$, $n = 66$, $p < 0.0001$).

4.6 Applicability of the model

The utility of SST and pigment maps for estimating production over the Grand Banks shows promise. Now that the use of satellites to measure SST is an established operational practice, it is worthwhile considering these data in extracting information on the vertical distribution of stability and pigment concentration in conjunction with satellite- derived pigment maps.

Estimation of IC' is critical in the model proposed. There may be a need to quantify the impact of non-uniformity in the vertical biomass on production in oligotrophic waters. In the Grand Banks data set, IC has been determined from discrete

a great extent. Finally, the trophic categories defined by Morel and Berthon (1989), from pigment concentration were highly useful, as their values permit the use of appropriate values for ψ^* and ρ in the model.

The results also show that VS is a function of SST. The importance of VS and 1/K490 in estimating integral chlorophyll is well demonstrated. Temporal variations in 1/K490 coincide with changes in IC, that is optical depth decreased with increase in chlorophyll concentration as the spring bloom developed from January into May (Figure 19). K490 mean and standard deviation values from CZCS data have helped in defining the optical properties of water masses. This is key to revealing the biological structure of the water column, especially in Case 1 (Chapter 3, section 3.3.1) waters where phytoplankton cells and associated products are the only important determinants of optical properties.

A good estimate of IC' allows prediction of production with greater precision than has been possible with other semi-empirical models. Simultaneous assimilation of SST and 1/K490 into one model for predicting log (IC) (equation 4.3) demonstrates the usefulness and need for a thermal channel in future ocean color sensors. Thermal data can be considered a key to both the physical and biological structure of the water column.

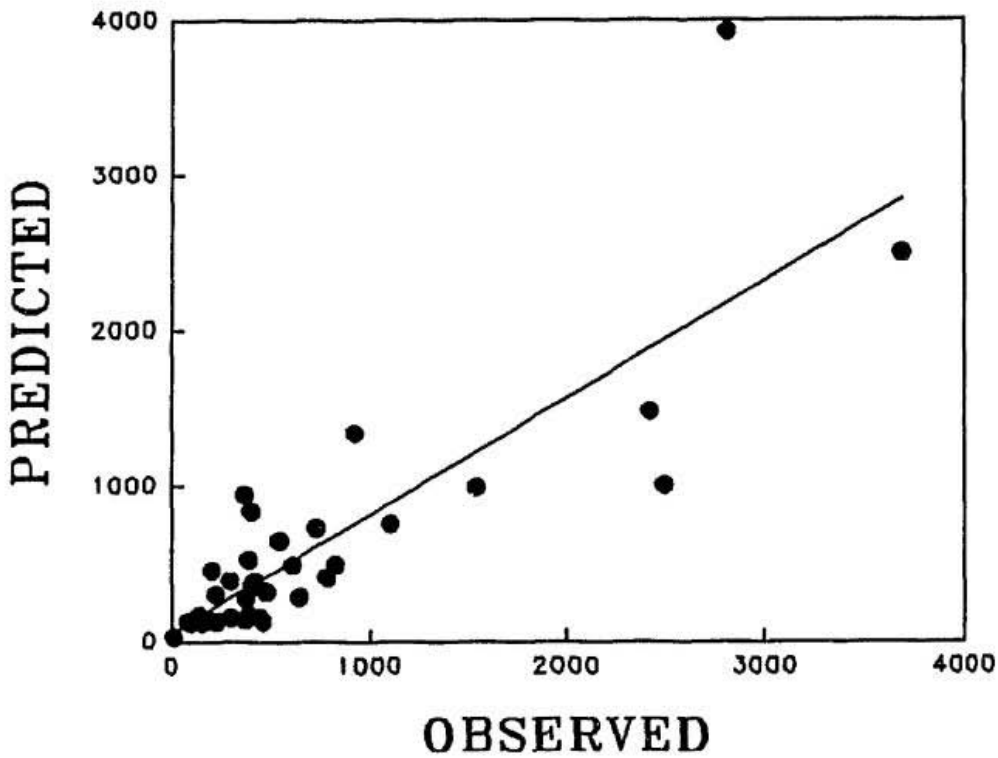

Figure 18. Observed versus predicted values of production (mg C m^{-3} d^{-1}) on the Grand Banks. Predicted values are from equation 4.5. Line is least-square linear fit.

depths. Vertical profiles of chlorophyll concentration (mg m^{-2}) show subsurface peaks in the upper portion of the water column in some stations during May (peak spring bloom). Sampling at fixed depths makes recording of narrow chlorophyll maxima difficult. Continuous sampling by chlorophyll fluorescence could certainly detect these peaks. Parameterization of the actual profiles based on the mean pigment concentration within the euphotic layer (see Morel and Berthon, 1989) could resolve this problem to

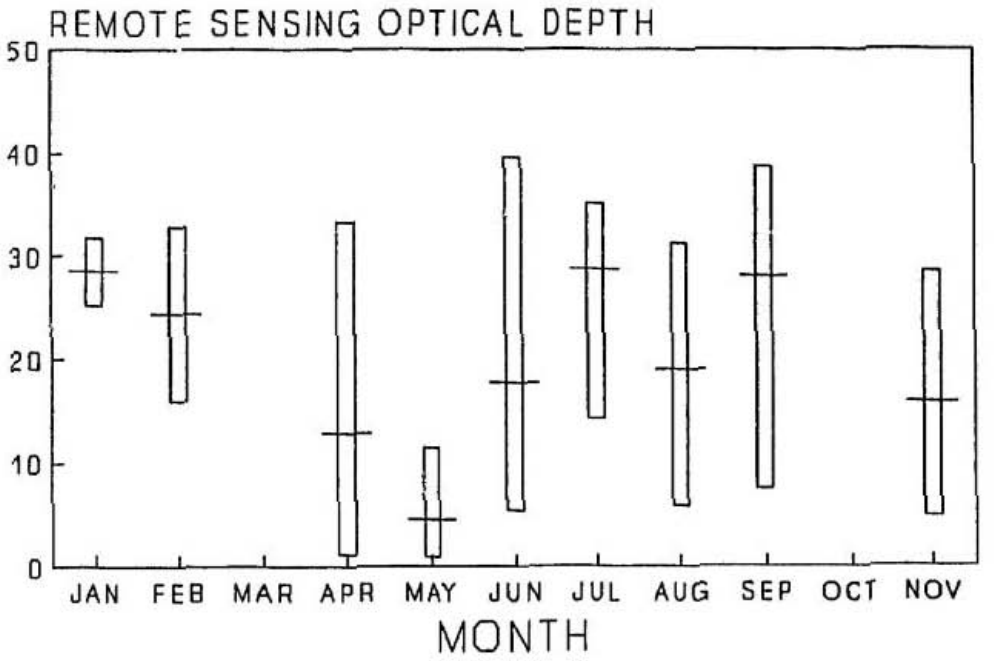

Figure 19. Temporal variation in remote sensing optical depth (1/K490) (m) by month. Horizontal lines indicate the mean value for the month and bars show the range.

4.7 Summary

The Grand Banks are subject to marked seasonal events, one of the most dramatic being the spring bloom of phytoplankton (Chapter 3; Prasad and Haedrich, 1992), and these must be taken into account in remote-sensing models. Variance in models of relationships between environmental parameters and primary production can be reduced

through the use of estimates which themselves vary with the season, and by parameterizing certain physiological properties of the phytoplankton.

The maximum quantum yield is a very important parameter. Any factors that reduce quantum yield will reduce the production estimates of bio-optical models, a situation which can result in poor agreement of calculated with measured values (Smith *et al.*, 1989). On the Grand Banks, seasonal changes in light absorption and in the efficiency of light utilization by phytoplankton affect quantum yield significantly (Prasad and Hollibaugh, 1992). The possibility of using variables other than pigment concentration derived from satellites holds promise.

This area of research needs more focus as accuracy in bio-optical algorithms is a current limitation. The loss in accuracy can be attributed mainly to the lack of knowledge about the photoadaptive parameters in the spatial and temporal scale. Chapter 5 deals with seasonal variability in two important phytoplankton photoadaptive parameters, the quantum yield for photosynthesis and the chlorophyll-specific light absorption.

CHAPTER 5. PHYSIOLOGICAL FACTORS OF IMPORTANCE IN PRODUCTION ALGORITHMS

5.1 Quantum yield for photosynthesis

Satellite-based estimates of ocean productivity are limited by the inherent inability of passive remote sensors to resolve variation in vertical scale (Campbell and O'Reilly 1988). Therefore, knowledge of integrated pigment concentration and its vertical distribution is required for light production models (Platt and Sathyendranath, 1988). However, temporal and spatial requirements for monitoring marine photosynthesis can be met only by satellites, and thus there is a need to parameterize adequately various physiological processes which control the light-harvesting and photosynthetic capabilities of algae. Although it has been possible to parameterize the physical factors accurately, the physiological factors remain elusive (Morel, 1991). However, there is an internal association between the bulk properties measured on shipboard (integrated production of the euphotic column) and the *in vitro* physiological properties of the phytoplankton.

Due to spatial and temporal variations in the photochemical properties of phytoplankton, photosynthesis in the sea is difficult to describe with one formulation. However, with the advent of satellite remote sensing and the availability of enormous

quantities of data on pigment distributions in the ocean, a substantial effort has been made to develop a simple, general algorithm to relate pigment concentration to primary productivity (Eppley *et al.*, 1985; Perry, 1986; Platt, 1986; Balch *et al.*, 1989c; Prasad *et al.*, 1992).

Even though a single, biomass-specific photosynthesis (P_B) *vs* irradiance (I) curve, specified by parameters with biophysical meaning, is able to describe photosynthesis of a marine diatom over a very broad range of conditions, it cannot be concluded that certain properties of the photochemical mechanisms of the diatoms, such as chlorophyll-specific absorption coefficient, chlorophyll-specific cross-section and maximum quantum yield, are invariant. Because the maximum rate of photosynthesis (assuming there is no photoinhibition), P_S^B, the photosynthetic efficiency, α, and the light saturation parameter, I_K, are known to vary with growth conditions (Harrison and Platt, 1980; Osborne and Geider, 1986), the photochemical parameters will also vary.

The optical properties of the euphotic layer and the availability of PAR at depth are mechanistically linked to phytoplankton production (Smith *et al.*, 1989). The estimation of plant biomass from the optical properties of seawater has been relatively successful using simple regression methodology and/or semi-empirical models (Brown *et al.*, 1985). However, this approach of relating biomass to production suffers from a large variance in the assumed covariability between incident PAR and the quantum yield of photosynthesis (Eppley *et al.*, 1985). Thus the variance observed is due to the fact that phytoplankton biomass and production rates can be differentially regulated by the

availability of nutrients and radiant energy in the upper ocean, and these are in turn determined by the physical, biological, and optical properties of the water column. The variance in the modelling of relationships between key environmental parameters and primary production can be reduced through the use of seasonally variable estimates of quantum yield of photosynthesis and the specific absorption coefficients of phytoplankton.

Sosik and Mitchell (1991) suggested that, for the absorption of light in the blue region of the electromagnetic spectrum, the observed variability was equally partitioned between package effects (non-uniform distribution of pigment within cells) and pigment composition. Although the absorption properties of phytoplankton generally vary by less than threefold (Morel *et al.*, 1987; Sathyendranath *et al.*, 1987; Campbell and O'Reilly, 1988), the quantum yield of photosynthesis can vary up to 10-fold (Kishino *et al.*, 1985; Campbell and O'Reilly, 1988).

Berthon and Morel (1992) have demonstrated the importance of the maximum quantum yield and chlorophyll specific absorption by phytoplankton in production models, and of using constant values as the principle causes for deviation between measured production values and those predicted from remote sensing data.

Therefore, it has been necessary to examine the seasonal variability of quantum yield, ϕ_C, and the absorption coefficient of phytoplankton, $a_{ph} \cdot Chl^{-1}$, on the Grand Banks and present estimates of their monthly means for use in primary production models. An attempt has been made to identify possible factors responsible for the seasonal variance in $a_{ph} \cdot Chl^{-1}$ and ϕ_C and to determine the relationship between surface incident PAR (I_o)

and normalized quantum yield.

5.2 Theory and calculation of quantum yield

The theoretical limit for maximum quantum yield of photosynthesis (ϕ_{max}) is 0.125 mol C Ein^{-1} (i.e. 8 quanta per molecule of CO_2 reduced), assuming a photosynthetic quotient of unity. In bio-optical models, the apparent ϕ_{max} is treated as a constant that is commonly accepted to approximate 0.1 mol O_2 Ein^{-1} or 0.1 mol C Ein^{-1} if a temperature-independent O_2:CO_2 ratio of unity is assumed (Tanada, 1951). This approximation of 0.1 mol C Ein^{-1} is due to the fact that the quantum yield for growing natural assemblages of phytoplankton cells can never exceed this value, even under ideal growth conditions (Kirk, 1983). This assumption holds when the ^{14}C primary production method is used to measure gross photosynthesis. A photosynthetic quotient >1.0 may result from alternation in photosynthate pathways, nutrient depletion, or light stress, and all can act to lower maximum quantum yield twofold to threefold (Peterson *et al.*, 1988). Kiefer and Mitchell (1983) showed that nutrient uptake rates could adequately describe the irradiance dependence of maximum quantum yield and provide an adequate estimate of light-limited growth for a marine diatom.

The quantum yield is controlled by several factors in the aquatic environment. The principle factors are the light harvesting capacity of phytoplankton at reduced subsurface irradiances and the high carbon fixation capacity of phytoplankton per unit chlorophyll at moderate irradiance. Quantum yield can also be affected by increases in

irradiance which can lead to photoinhibition. If nutrients are not limiting, the quantum yield value close to the euphotic depth may reach the maximum quantum yield (i.e., $\phi_{C(z)} \simeq \phi_{max}$). However, the $\phi_{C(z)}$ value will attain ϕ_{max} at a depth closer to the surface under conditions of light saturation (Campbell and O'Reilly 1988). The mean values for water column quantum yield and the phytoplankton absorption coefficient $a_{ph}\cdot Chl^{-1}$, along with integral chlorophyll (IC) and the PAR at the surface (I_o), should predict the integral production (IP) as follows:

$$IP = (\bar{\phi}_C \, a_{ph}\cdot Chl^{-1}/4.6) \, IC \, I_o. \tag{5.1}$$

Rearranging equation 5.1 (as in Campbell and O'Reilly, 1988), limits the right-hand side of the equation to measured variables. Campbell and O'Reilly (1988) use the notation k_c, the chlorophyll-specific diffuse attenuation coefficient for PAR, instead of my notation, $a_{ph}\cdot Chl^{-1}$, the chlorophyll specific absorption coefficient. In this case, $a_{ph}\cdot Chl^{-1}$ is a more appropriate notation than k_c, because scattered light is not used for photochemistry (Prasad and Hollibaugh, 1992). It follows that

$$a_{ph}\cdot Chl^{-1}(z) \, \phi(z) = P_z / C_z \, I_z \tag{5.2}$$

where P_z is production at depth z, C_z is the chlorophyll concentration at depth z and I_z is the PAR at depth z. The ratio on the right is known as the photosynthetic yield

(Morel, 1978). Normalized by the theoretical maximum, i.e. ϕ_{max} = 1,200 mg C Ein^{-1}, equation 5.2 becomes

$$a_{ph} \cdot Chl^{-1}(z)\ \phi_{C(z)}/\phi_{max} = P_z / 1200\ C_z\ I_z \qquad (5.3)$$

Equation 5.3 was used to estimate the normalized photosynthetic yield (Campbell and O'Reilly, 1988) at the surface, 5 m, 10 m, 20 m, 30 m, and the 1% light level depths at every station for all Grand Bank cruises (see section 2.4 on sampling). Instead of assuming $\phi_C = \phi_{max}$ at the three lowest sampling depths (20 m, 30 m, and 1% light level depth) for computing $a_{ph} \cdot Chl^{-1}$, this value was computed with respect to depth using the quantum yield value (= 0.06 mol C Ein^{-1}) suggested by Bannister (1974).

5.3 Spatial variability of quantum yield

Normalized quantum yield varied considerably in the water column. A depth-wise frequency distribution of quantum yield revealed a marked variability of $a_{ph} \cdot Chl^{-1}\ \phi_C/\phi_{max}$ and $a_{ph} \cdot Chl^{-1}$ on the Grand Banks. Histograms of $a_{ph} \cdot Chl^{-1}\ \phi_C/\phi_{max}$ for each sampling depth are presented in Figure 20 a-f. Figure 20 a to d show that most normalized quantum yield values are $\leq$ 0.001. There is a shift in the distribution of $a_{ph} \cdot Chl^{-1}\ \phi_C/\phi_{max}$ toward lower values in the upper 20 m which suggests the occurrence of frequent light saturation. There is a gradual shift in the quantum yield values to the 0.01 to 0.1 range from 20m to the 1% light level depth. This could indicate that the radiation utilization

efficiency of the phytoplankton is higher at depth than in the surface layers leading to higher quantum yield values.

The chlorophyll specific absorption coefficient (a_{ph}·Chl^{-1}) also varied with depth. Values of a_{ph}·Chl^{-1} showed a twofold to threefold increase at the base of the euphotic zone. The mean value from the Grand Banks was 0.015 m^2 (mg Chl a)$^{-1}$, consistent with reported values for a_{ph}·Chl^{-1} of 0.007 to 0.027 m^2 (mg Chl a)$^{-1}$ (Campbell and O'Reilly 1988). The analysis was repeated for data from different months and for different sampling depths. Results appear in Table 4 a-g.

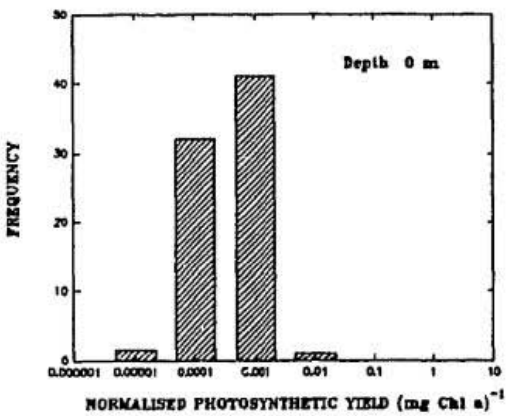

Figure 20 a. Histogram of normalized photosynthetic yield at 0 m depth.

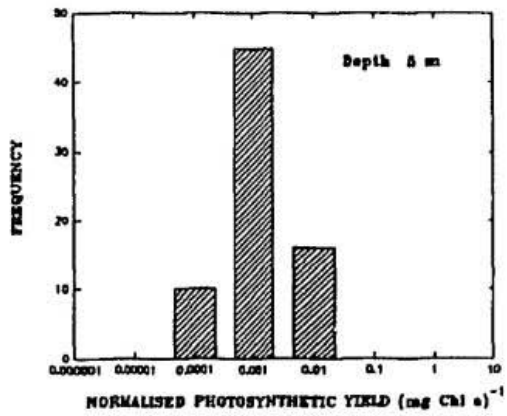

Figure 20 b. Histogram of normalized photosynthetic yield at 5 m depth.

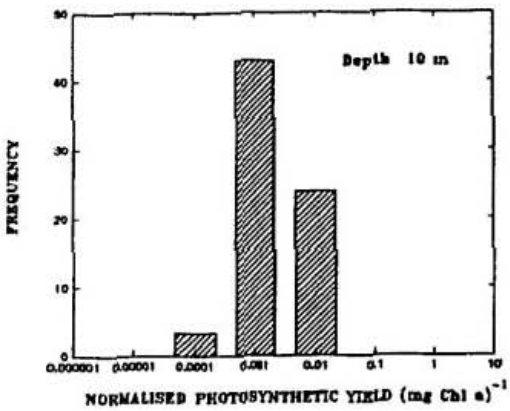

Figure 22 c. Histogram of normalised photosynthetic yield at 10 m depth.

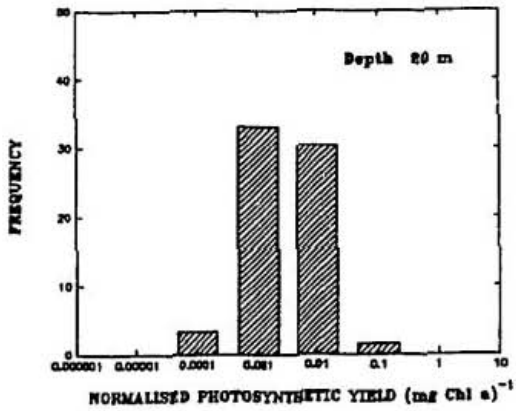

Figure 20 d. Histogram of normalized photosynthetic yield at 20 m depth.

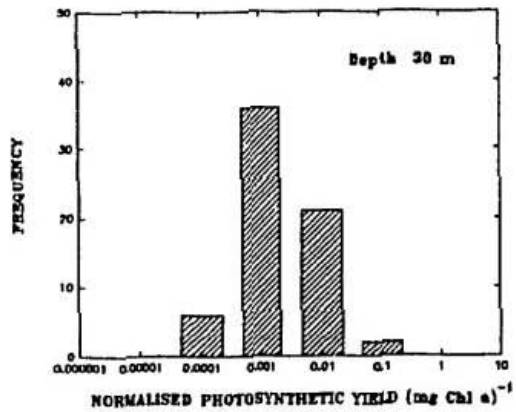

Figure 20 e. Histogram of normalized photosynthetic yield at 30 m depth.

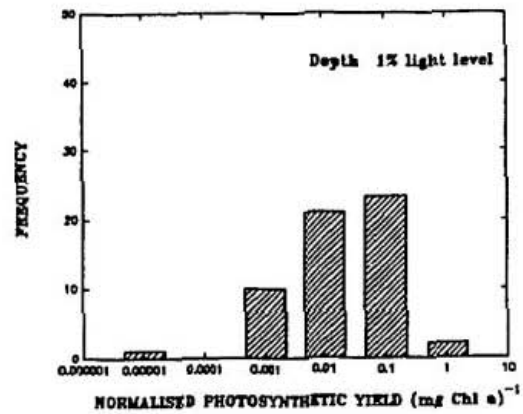

Figure 20 f. Histogram of normalized photosynthetic yield at the 1% light level depth.

Table 4a. Summarized shipboard data from the Grand Banks Hibernia EIS Survey for a_{ph} Chl^{-1} ϕ_C/ϕ_{max}, ϕ_C/ϕ_{max}, and a_{ph} Chl^{-1}. *R.V. Meta* cruise 80M03, April 1980. Number of stations = 49.

DEPTH	a_{ph} Chl^{-1} ϕ_C/ϕ_{max}		ϕ_C/ϕ_{max}		a_{ph} Chl^{-1}
meters	Std. Dev.	Mean	Std. Dev.	Mean	Mean
0	0.002	0.00008	0.012	0.005	0.0002
5	0.0007	0.0004	0.046	0.026	0.0009
10	0.001	0.0006	0.077	0.038	0.001
20	0.004	0.004	0.265	0.268	0.005
30	0.003	0.003	0.219	0.199	0.004
1% PAR	0.032	0.047	1.93	2.81	0.041
Average	0.004	0.014	0.255	0.879	0.009

Table 4b. Summarized shipboard data from the Grand Banks Hibernia EIS Survey for a_{ph} Chl^{-1} ϕ_C/ϕ_{max}, ϕ_C/ϕ_{max}, and a_{ph} Chl^{-1}. *R.V. Meta* cruise 80M05, May 1980. Number of stations = 76.

DEPTH	a_{ph} Chl^{-1} ϕ_C/ϕ_{max}		ϕ_C/ϕ_{max}		a_{ph} Chl^{-1}
meters	Std. Dev.	Mean	Std. Dev.	Mean	Mean
0	0.001	0.001	0.065	0.081	0.001
5	0.002	0.002	0.161	0.143	0.003
10	0.004	0.003	0.283	0.225	0.006
20	0.008	0.006	0.470	0.388	0.010
30	0.014	0.019	0.873	1.170	0.018
1% PAR	0.029	0.035	0.172	0.211	0.036
Average	0.052	0.16	0.305	0.994	0.012

Table 4c. Summarized shipboard data from the Grand Banks Hibernia EIS Survey for a_{ph} Chl^{-1} ϕ_C/ϕ_{max}, ϕ_C/ϕ_{max}, and a_{ph} Chl^{-1}. *R.V. Meta* cruise 80M07, June 1980. Number of stations = 76.

DEPTH	a_{ph} Chl^{-1} ϕ_C/ϕ_{max}		ϕ_C/ϕ_{max}		a_{ph} Chl^{-1}
meters	Std. Dev.	Mean	Std. Dev.	Mean	Mean
0	0.001	0.001	0.109	0.095	0.002
5	0.002	0.003	0.152	0.177	0.003
10	0.007	0.013	0.439	0.807	0.009
20	0.003	0.002	0.232	0.169	0.004
30	0.004	0.006	0.257	0.38	0.005
1% PAR	0.070	0.065	4.125	3.82	0.087
Average	0.013	0.033	0.803	1.99	0.018

Table 4d. Summarized shipboard data from the Grand Banks Hibernia EIS Survey for a_{ph} Chl^{-1} ϕ_C/ϕ_{max}, ϕ_C/ϕ_{max}, and a_{ph} Chl^{-1}. *R.V. Meta* cruise 80M07, July 1980. Number of stations = 26.

DEPTH	a_{ph} Chl^{-1} ϕ_C/ϕ_{max}		ϕ_C/ϕ_{max}		a_{ph} Chl^{-1}
meters	Std. Dev.	Mean	Std. Dev.	Mean	Mean
0	0.001	0.0006	0.060	0.037	0.001
5	0.0002	0.001	0.167	0.078	0.003
10	0.006	0.002	0.390	0.133	0.008
20	0.004	0.003	0.270	0.214	0.005
30	0.028	0.035	1.668	2.064	0.035
1% PAR	0.029	0.031	1.750	1.880	0.037
Average	0.011	0.020	0.667	1.207	0.015

Table 4e. Summarized shipboard data from the Grand Banks Hibernia EIS Survey for a_{ph} Chl^{-1} ϕ_C/ϕ_{max}, ϕ_C/ϕ_{max}, and a_{ph} Chl^{-1}. *R.V. Meta* cruise 80M11, August 1980. Number of stations = 20.

DEPTH	a_{ph} Chl^{-1} ϕ_C/ϕ_{max}		ϕ_C/ϕ_{max}		a_{ph} Chl^{-1}
meters	Std. Dev.	Mean	Std. Dev.	Mean	Mean
0	0.002	0.001	0.170	0.064	0.003
5	0.009	0.003	0.534	0.222	0.011
10	0.007	0.004	0.415	0.283	0.008
20	0.005	0.001	0.339	0.091	0.007
30	0.003	0.002	0.179	0.117	0.003
1% PAR	0.010	0.003	0.627	0.231	0.013
Average	0.005	0.003	0.345	0.216	0.008

Table 4f. Summarized shipboard data from the Grand Banks Hibernia EIS Survey for a_{ph} Chl^{-1} ϕ_C/ϕ_{max}, ϕ_C/ϕ_{max}, and a_{ph} Chl^{-1}. *R.V. Meta* cruise 80M13, September 1980. Number of stations = 81.

DEPTH	a_{ph} Chl^{-1} ϕ_C/ϕ_{max}		ϕ_C/ϕ_{max}		a_{ph} Chl^{-1}
meters	Std. Dev.	Mean	Std. Dev.	Mean	Mean
0	0.002	0.001	0.143	0.078	0.003
5	0.006	0.005	0.366	0.305	0.007
10	0.005	0.004	0.314	0.245	0.006
20	0.007	0.004	0.448	0.239	0.009
30	0.005	0.006	0.311	0.359	0.006
1% PAR	0.037	0.057	2.204	3.391	0.046
Average	0.010	0.025	0.622	0.150	0.0014

Table 4g. Summarized shipboard data from the Grand Banks Hibernia EIS Survey for a_{ph} Chl^{-1} ϕ_C/ϕ_{max}, ϕ_C/ϕ_{max}, and a_{ph} Chl^{-1}. *R.V. Meta* cruise 80M14, November 1980. Number of stations = 77.

DEPTH	a_{ph} Chl^{-1} ϕ_C/ϕ_{max}		ϕ_C/ϕ_{max}		a_{ph} Chl^{-1}
meters	Std. Dev.	Mean	Std. Dev.	Mean	Mean
0	0.0004	0.0004	0.029	0.023	0.006
5	0.008	0.014	0.509	0.828	0.010
10	0.008	0.010	0.498	0.615	0.010
20	0.011	0.016	0.658	0.943	0.013
30	0.004	0.004	0.237	0.281	0.005
1% PAR	0.038	0.209	0.576	1.233	0.122
Average	0.020	0.087	1.222	0.512	0.028

The concentration of photosynthetic pigments in the marine environment is dependent on the species composition and photoadaptive state of the phytoplankton. Tables 4 a to g give the depthwise values for normalized quantum yield and the chlorophyll specific absorption coefficients on the Grand Banks along with their mean and standard deviation values. It can be seen from the Tables that $a_{ph}\cdot Chl^{-1}$ which is normally treated as a constant in production models, is highly variable. The low mean values of $a_{ph}\cdot Chl^{-1}$ were seen in April and August. Highest value of $a_{ph}\cdot Chl^{-1}$ occurred during November. The values of $a_{ph}\cdot Chl^{-1}$ progressively increase from April up to June. This increase reflects the rapid evolution of the spring bloom. After June the mean value of $a_{ph}\cdot Chl^{-1}$ starts to decrease. The variations in $a_{ph}\cdot Chl^{-1}$ depend on the phytoplankton

species composition and size.

The larger net plankton on the Grand Banks had lower $a_{ph} \cdot Chl^{-1}$ (= 0.009 m^2 (mg Chl *a*)$^{-1}$ (Table 4a), than the nanoplankton which usually dominate during the postbloom season (June-July) *via* species succession. This value is comparable to the $a_{ph} \cdot Chl^{-1}$ estimates obtained from the North Atlantic for net plankton. The $a_{ph} \cdot Chl^{-1}$ increased during the postbloom season to 0.018 m^2 (mg Chl *a*)$^{-1}$ (Table 4c), an observation consistent with "packaging" effects (Kirk, 1983; Morel *et al.*, 1987), where the distribution of pigment within cells are not homogeneous and can influence the overall radiation absorption and utilization characteristics of phytoplankton.

Highest mean value of ϕ_C/ϕ_{max} occurred during May, corresponding to the peak of the phytoplankton spring bloom, and the lowest mean value occurred during September. This variation in ϕ_C/ϕ_{max} clearly reflects the light harvesting capacity of the phytoplankton. The PAR levels during May are about three times higher than the PAR levels during September. It is interesting to note that values of ϕ_C/ϕ_{max} are variable both as a function of depth and of month. Therefore, treating the maximum quantum yield as a constant in production models may result in either underestimation or overestimation of the predicted values. Certainly, however, it is incorrect to treat ϕ_{max} as a constant in remote sensing algorithms.

Figure 21 shows the dominance of the 10-20 μm size phytoplankton contributing to the phytoplankton carbon (μg l^{-1}) during peak spring bloom on the Grand Banks. The dominance of net plankton in the spring may account for the lower $a_{ph} \cdot Chl^{-1}$ distribution

at that time of the year, an observation consistent with Malone *et al.*, (1983) for the New York Bight area in the Northwest Atlantic. Mean values of ϕ_C showed a twofold to sixfold seasonal variation from spring through winter.

The variability in $a_{ph}\cdot Chl^{-1}$ can also be attributed to changes in the abundance of accessory pigments relative to chl *a* (Sathyendranath *et al.*, 1987; Berner *et al.*, 1989). However, Ridout and Morris (1988) have shown that the relative proportions of total chloropigment to total carotenoid remained almost constant throughout the period of the bloom. I do not have the carotenoid:chlorophyll ratios for my study period to support any views concerning the influence of the accessory pigments in $a_{ph}\cdot Chl^{-1}$ variability.

5.4 Estimation of mean quantum yield

Estimation of the mean quantum yield for the water column requires knowledge of the mean water column phytoplankton absorption coefficient $a_{ph}\cdot Chl^{-1}$ and the water column light utilization index ψ (Campbell and O'Reilly 1988). Values of ψ computed during an earlier analysis on the Grand Bank (Chapter 2; Prasad *et al.*, 1992) were used in the present analysis. $\bar{\phi}_C$ was computed as

$$\bar{\phi}_C = (4.6\ \psi)/a_{ph}\cdot Chl^{-1} \qquad (5.4)$$

If mean values of ψ (= 1.037 mg C (mg Chl*a*)$^{-1}$ m^2 Ein^{-1}) and $a_{ph}\cdot Chl^{-1}$ (= 0.015 m^2 (mg Chl *a*)$^{-1}$) for the Grand Banks are used in equation 5.4, ϕ_C is computed to be 318.0

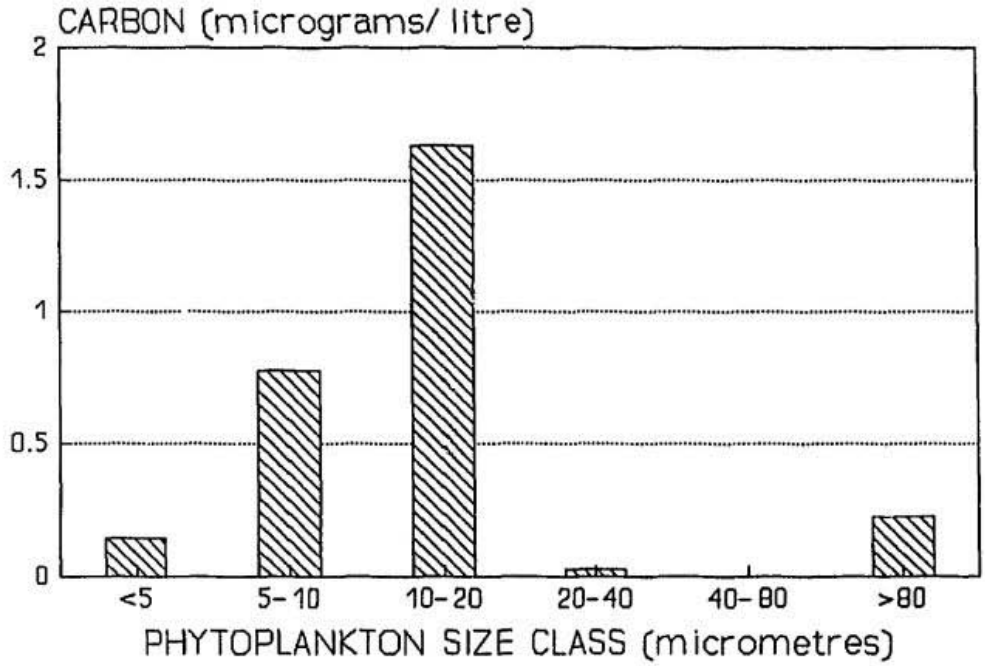

Figure 21. Phytoplankton during peak spring bloom (May) indicating the dominance of 10-20 μm size class.

mg C Ein^{-1} or $0.26\phi_{max}$, somewhat higher than the factor of 0.1 suggested by Platt (1986).

Platt (1986), in his analysis to estimate the magnitude of ψ, assumes a quantum yield value of 0.1 mol C Ein^{-1} and a efficiency factor of 10^{-2} mol C Ein-1. According to his calculations the thermodynamic efficiency factor should be about 0.1. Further, his results suggest that this factor is consistent enough for use as a constant in production

models. The value of ϕ_C from the Grand Bank (areal extent 28,000 km^2) was, however, even lower than estimates derived from the Atlantic continental shelf (= $0.4\phi_{max}$: Campbell and O'Reilly, 1988) obtained from shipboard data collected over a large areal extent (250,000 km^2) and under more variable oceanographic conditions. Areal extent of the study area may be an factor in the variability and magnitude of ψ. This could be due to the fact that radiation utilization efficiencies and the specific absorption coefficients of the phytoplankton depend on the species composition of the study area.

5.5 PAR and normalized quantum yield

Cruise means of ϕ_C/ϕ_{max} were regressed against log transformed I_o values (incident radiation) and found to be moderately correlated ($r^2 = 0.70$, $n = 51$, $p < 0.0001$). The regression equation obtained was

$$\bar{\phi}_C/\bar{\phi}_{max} = 0.71 - 0.17 \log_e (I_o). \qquad (5.5)$$

The data on which this relationship is based appear in Appendix Table G.

Figure 22 and equation 5.5 suggest that it may be possible to predict $\bar{\phi}_C$ on the Grand Banks from incident light.

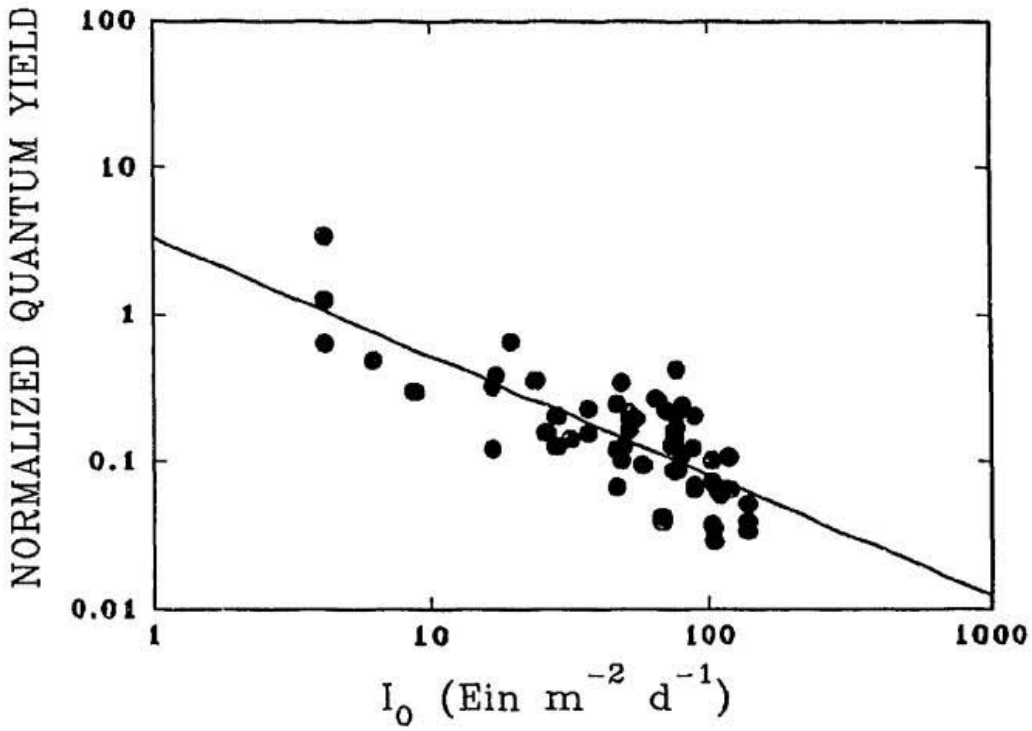

Figure 22. Normalized quantum yield versus incident radiation.

5.6 Conclusion

Seasonal changes in the efficiency of light utilization by phytoplankton, and variations in light absorption coefficients (Figure 23), can significantly effect quantum yield values (Figure 24). The light absorption rates of phytoplankton appear to control photosynthetic efficiency, particularly in the lower half of the euphotic zone. For estimating primary production, the maximum quantum yield, ϕ_{max}, is a very important

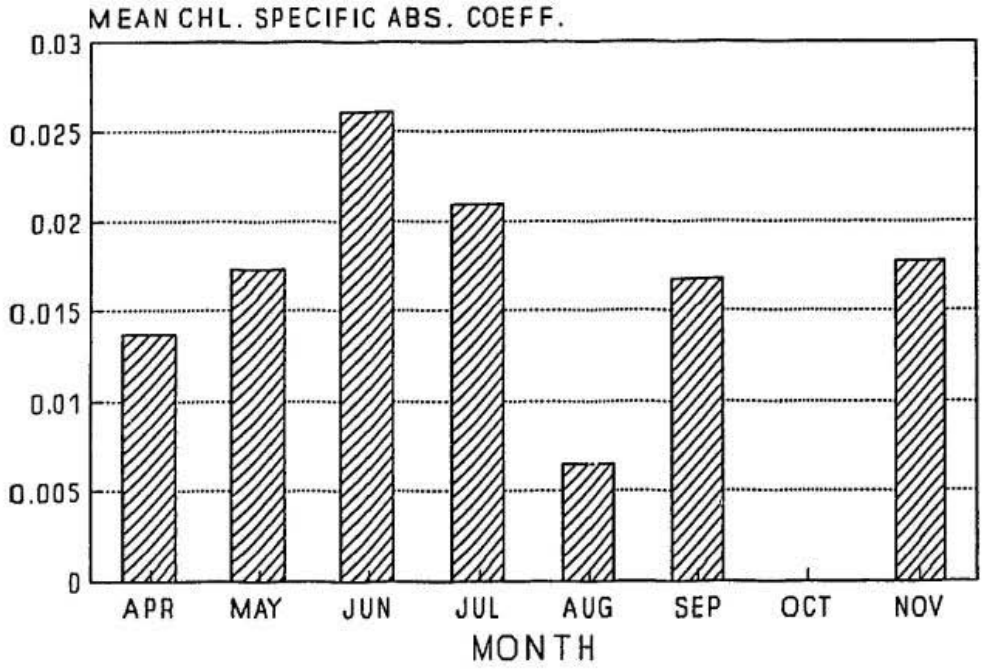

Figure 23. Temporal variations in chlorophyll specific absorption coefficient on the Grand Banks.

parameter in photosynthetic-irradiance (P-I) models. Therefore, factors that reduce ϕ_{max} will reduce the productivity estimates of the bio-optical models, a situation which could result in poorer agreement with the ^{14}C values (Smith *et al.*, 1989).

Recent work in the Antarctic Ocean (Mitchell and Holm-Hansen, 1991) suggests that predictions using current remote sensing algorithms for pigment estimation may lead to significant errors due to variability of a_{ph}·Chl^{-1} and relative abundance of

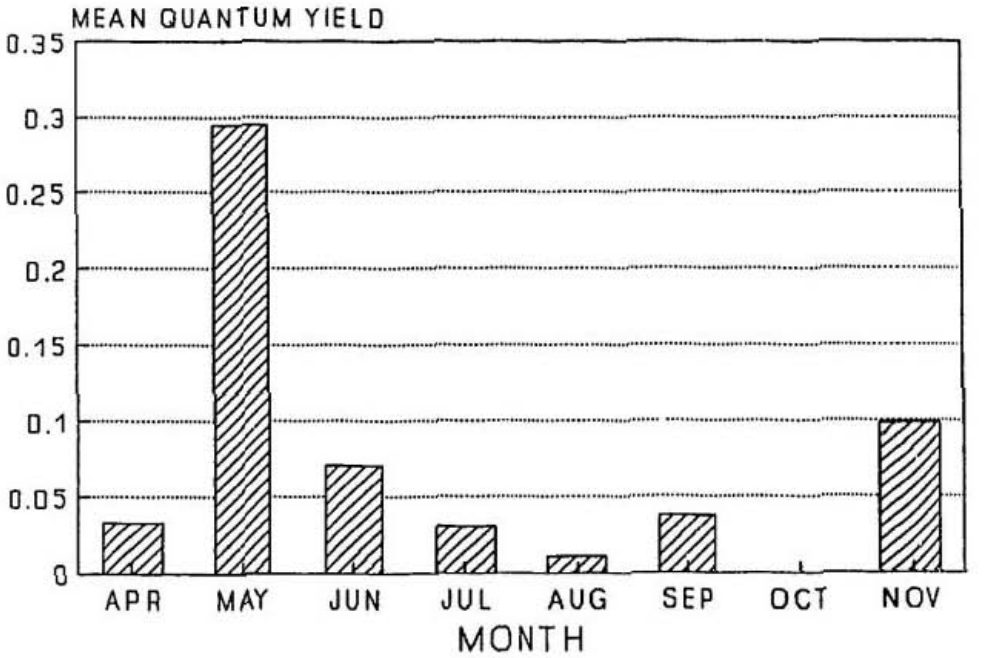

Figure 24. Temporal variations in mean normalized quantum yield by month on the Grand Banks. The value for May corresponds to the peak spring bloom.

phytoplankton and other absorbing material in the water column. The values presented here will allow fine tuning of satellite remote sensing algorithms by incorporating monthly effects of $\bar{\phi}_C$ and $a_{ph} \cdot Chl^{-1}$ on the Grand Banks. Equation 5.5 allows a reasonable prediction capability for $\bar{\phi}_C$ using incident radiation values.

CHAPTER 6. CALCULATING PRIMARY PRODUCTION ON THE GRAND BANKS

6.1 Introduction

The steps involved in converting ocean color data to estimates of integral production have been difficult to perform due to several factors. These include the satellite being able to sense pigment only in the top attenuation length (to approximately the 37% light level depth), variation in the ratio of phaeopigments to chlorophyll *a*, variation in the phytoplankton species composition and variation in phytoplankton physiology.

The error in deriving information from deeper than one attenuation length is further increased by subsurface chlorophyll maxima, and requires production models to take their effects into account. One solution is to assume a uniform chlorophyll profile (Platt, 1986). However, error analyses indicate that the maximum error incurred by this assumption can be as high as 90% or less of the estimate of integral biomass (Sathyendranath and Platt, 1989).

Other methods for estimating integral chlorophyll from surface pigments have involved integrating pigments over each optical depth and plotting this *vs* optical depth

(Balch *et al.*, 1989b), and normalizing the depth profiles of chlorophyll to the depth-dependent variance in pigment concentration (Morel and Berthon, 1989). Morel and Berthon (1989) have shown that the simulated, satellite-derived, pigment concentration (analogous to satellite detectable chlorophyll in Prasad *et al.*, 1992) is well-correlated to actual integral pigment concentration. The term "simulated" is used by Morel and Berthon because they used shipboard pigment data to compute the pigment concentration which would have been detected by the satellite sensor. Their studies, involving correlations between simulated, satellite-derived, pigment and integral pigment at 3500 stations in the west African upwelling region, the Mediterranean, Sargasso Sea, and the Antarctic, resulted in a correlation coefficient (r^2) of 0.872 for low latitudes, 0.869 for moderate latitudes, and 0.930 for high latitudes. Their analyses included data from a wide variety of water types, making their results quite robust. They suggest that, although surface pigments may not always be correlated with integral pigment, the average relationship is well-defined and highly significant. Maximum relative error of the Morel and Berthon (1989) relationship was $\pm$ 30% (Balch *et al.*, 1992). Campbell and O'Reilly (1988) reported that satellite chlorophyll was highly correlated with the mean euphotic chlorophyll. Their relationship had an r^2 of 0.93.

The sources of error may be variable over time and space and therefore pose challenge before any calculations of productivity can be attempted. However, Balch *et al.* (1989b, 1992) and Morel and Berthon (1989) indicate that oligotrophic regions present the biggest challenge in calculating integral pigment concentration using satellite

data. Fortunately, the Grand Banks is one of the more eutrophic of the ocean regions.

My estimate of primary production on the Grand Banks has involved investigation into the relationships between phytoplankton and other environmental variables through a series of interrelated steps. Chapter 1 reveals the need for oceanographic remote sensing in general, and especially on the Grand Banks where ship surveys are never synoptic for estimating primary production. Chapter 2 presents a semi-empirical model for estimating primary production, and suggests the need for evaluation of parameters such as quantum yield of photosynthesis. Chapter 3 provides an annual picture of the spring phytoplankton bloom on the Banks using satellite and ship data. A ship-to-satellite calibration is presented for this cold mid-latitude region for estimating satellite chlorophyll. Chapter 4 demonstrates the use of variables other than satellite chlorophyll (sea-surface temperature, water column stability and remote sensing optical depth) in estimating integral chlorophyll and, thence, primary production. The need for the use of a thermal channel alongside visible channels for simultaneous mapping of ocean color and temperature is demonstrated. Chapter 5 suggests that quantum yield varies both spatially (vertically) and temporally. Assuming quantum yield as a constant could lead to twofold to threefold overestimation of production.

Finally, the present Chapter summarizes the results in the first five Chapters and utilizes the algorithm to estimate mean monthly values of integrated chlorophyll and primary production on the Grand Banks. Such estimates can provide baseline information for programs such as JGOFS whose focus is on the understanding of carbon

cycling in world oceans.

6.2 Computation of production for the Grand Banks

Computation of production on the Grand Banks involves the use of local input variables. These are satellite-detectable chlorophyll, surface pigment within the euphotic zone, PAR (photosynthetically available radiation), and ψ^* (chlorophyll specific cross-section for photosynthesis). Computed quantum yield estimates for phytoplankton (Prasad and Hollibaugh, 1992) are also used in the model to reduce the variance in the predicted production values. Some of the methods used by Morel and Berthon (1989) were adapted for computing ψ^*.

Methods for calculating the satellite detectable chlorophyll, PAR, the water column light utilization index, and integrated pigment have been discussed in Chapter 2 (sections 2.4.1 to 2.4.6) and also in Prasad *et al.* (1992). Calculations of variables not listed in the above are given below.

6.2.1 *Estimating IC directly*

Morel and Berthon (1989) present empirical relationships to calculate IC (which they refer to as $<C_{TOT}>$) using surface chlorophyll (which they refer to as C_{SAT}). My calculated values of IC agree well with measured values when Morel and Berthon's (1989) equation for well-mixed waters is used. From the Grand Banks data, the empirical relationship was

$$\log_e IC = 3.822 + 0.8408 \log_e Chl_{CZCS} \quad (6.1)$$

where 88% of the variance is explained and n = 54. IC values calculated by this equation were used in the model for estimating primary production on the Grand Banks. If the satellite observations had not been available, I could have used the equation for IC calculated using secondary variables (Chapter 4, equation 4.3).

6.2.2 *Computation of chlorophyll specific cross section*

The chlorophyll specific cross section, ψ^*, is required to run the light-photosynthesis model (Morel and André, 1991). ψ^* has been considered a constant in production models by some investigators (Platt, 1986; Malone, 1987). The value of ψ^* is partly dependent on the trophic category, which is again a function of the chlorophyll concentration. The dependence of ψ^* holds good for chlorophyll values less than 1 mg m^{-3}. However, when waters become more productive (eutrophic), the value of ψ^* tends to decrease. The value of ψ^* is more dependent on the surface light field than it is on photosynthetic pigment levels. The value of ψ^* shows a relative increase in high latitudes which may be due to lower light levels. Higher values of ψ^* are characteristic of low light levels (<0.5 MJ m^{-2} d^{-1}). Thus low light levels and higher values of ψ^* contribute to low production. Values reported for ψ^* range from 0.055 to 0.080 m^2 (g chl)$^{-1}$ for 60°N (Morel, 1991).

The value of photosynthetically stored radiant energy (PSR) (Morel, 1978) over the euphotic depth is needed for the calculation of ψ^*. PSR is a function of photosynthetically available radiation at the surface, PAR', and the integrated pigment content IC, as follows

$$\psi^* = \overline{PSR}/\overline{PAR'}\ IC \tag{6.2}$$

where $\overline{PSR}$ and $\overline{PAR'}$ are in MJ m^{-2} d^{-1} and IC is in mg m^{-2}. The daily integrated quantities are denoted by the overbars (Morel, 1991).

Morel (1991) reported an equivalence between ψ (the light utilization index of Falkowski, 1981) and ψ^*, as follows

$$\psi = 6.174\ \psi^* \tag{6.3}$$

This relationship was based on values reported by Platt (1986). His values of ψ ranged from 0.31 to 0.66 gC (g chl)$^{-1}$ (Ein m^{-2})$^{-1}$. Platt (1986) suggested that ψ was a relatively constant parameter. Higher values, however, have been published (e.g. Yoder *et al.*, 1985; Campbell and O'Reilly, 1988; Prasad *et al.*, 1992). Computed values of ψ on the Grand Banks range from 0.432 to 3.708 m^2 (g chl)$^{-1}$, equivalent to a range in ψ^* of 0.07 to 0.6 m^2 (g chl)$^{-1}$.

Morel (1991) suggested that the stability of ψ^* in high latitudes depends on the

spectral quality of the light available at different levels in the euphotic zone and on the day length, among other environmental influences. Therefore, parameterization of ψ^* may be important in models that assimilate remotely-sensed pigment for calculating production values.

6.3 Pigment distribution and evolution in the upper layer

Pigment distribution in the upper layers of the Grand Banks is largely controlled by the evolution of the spring algal bloom. Ship and CZCS satellite data analysis suggests that the spring bloom during 1980-81 peaked during May (Chapter 3; Prasad and Haedrich, 1992). There was rapid phytoplankton growth within a fortnight beginning in April. CZCS imagery reveals that the growth of phytoplankton was from inshore to the offshore region, and this growth was reflected in the depletion of nitrate in the upper 50 m of the water column (Figure 12). Water column stability varied considerably over the season on the Grand Banks (Figure 13) and tend to control phytoplankton growth indirectly. Water column stability was associated with sea surface temperature, and there was a positive correlation between these two variables on the Grand Banks (Chapter 4, section 4.4). Therefore, once water column stability was established and nitrate depleted, the composition of the phytoplankton changed. Instead of the diatoms which dominated during the spring bloom, dinoflagellates and other forms with low sinking rates took over.

Spatially-averaged values of surface chlorophyll (mg m^{-3}) and pigment within the

euphotic zone (IC) for the North, Tail and entire Grand Banks appear in Table 5. The Northern part of the Bank is defined as the region above 46°N and the Tail of the Banks as the region below 44°N. This is an operational definition. It means that the shipboard production stations from transects at 46°N (7 stations × 8 cruises), 47°N (5 stations × 8 cruises) and 48.5°N (3 stations × 8 cruises) were used to determine the Northern production, and stations from the 44°N transect (6 stations × 8 cruises) were used to determine production on the Tail of the Banks (see Figure 1). Note that not all stations were re-visited on every cruise.

The Tail of the Grand Banks supports more algal biomass on an annual basis per unit area than the North. This is reflected in SDC and IC, and also in higher annual carbon fixation rates obtained from the Tail. Annual carbon fixation rates for the entire Grand Banks are 193.56 g C m^{-2} yr^{-1} (Table 5).

Table 5. Spatially averaged surface pigment concentration (SDC), pigment with the euphotic zone (IC), and annual carbon fixation rates IP, as computed from the model.

Zone	SDC (mg m^{-3})	IC (mg m^{-2})	IP (g C m^{-2} yr^{-1})
Northern Grand Banks	0.374	18.17	156.33
Tail of the Banks	0.439	19.95	181.80
Entire Grand Banks	0.418	19.27	193.56

Temporal evolution in the magnitude of IC for the Northern and Tail region of the Grand Banks is shown in Figure 25. A sixteenfold change in IC is encountered from spring to winter, a reflection of the fact that over 40 percent of the annual production of phytoplankton on the Grand Banks occurs during the spring bloom (Hollibaugh and Booth, 1981). It is interesting to observe that the Tail of the Grand Banks appears to support a higher mean annual biomass than the North. However, the area covered by the shipboard observations and used in the calculation in the Northern region is higher (1470 km^2) than that covered by the transects in the Tail region (570 km^2). This discrepancy may be due to the fact that annual estimates of primary production were extrapolated from monthly values by spatial averaging. Therefore, there is more production overall in the North even though the Tail of Banks is more productive per unit area. The monthly means suggest a difference in the vertical and temporal scales of IC. The mean value computed for IC amounts to about 19.27 mg m^{-2}, in relation to a mean SDC value of 0.418 mg m^{-3} for the entire Grand Banks.

The biota of the Grand Banks is heterogeneous seasonally and spatially. The northeastern and southern parts of the Bank are distinct from one another in groundfish species composition and in the nature of their food webs (Gomes, 1991; Gomes *et al.*, 1992). The annual regimes of primary production that drive these differences should be different as well, and calculations for the Northern part and Tail of the Grand Banks based on the model show that they are (Figure 26).

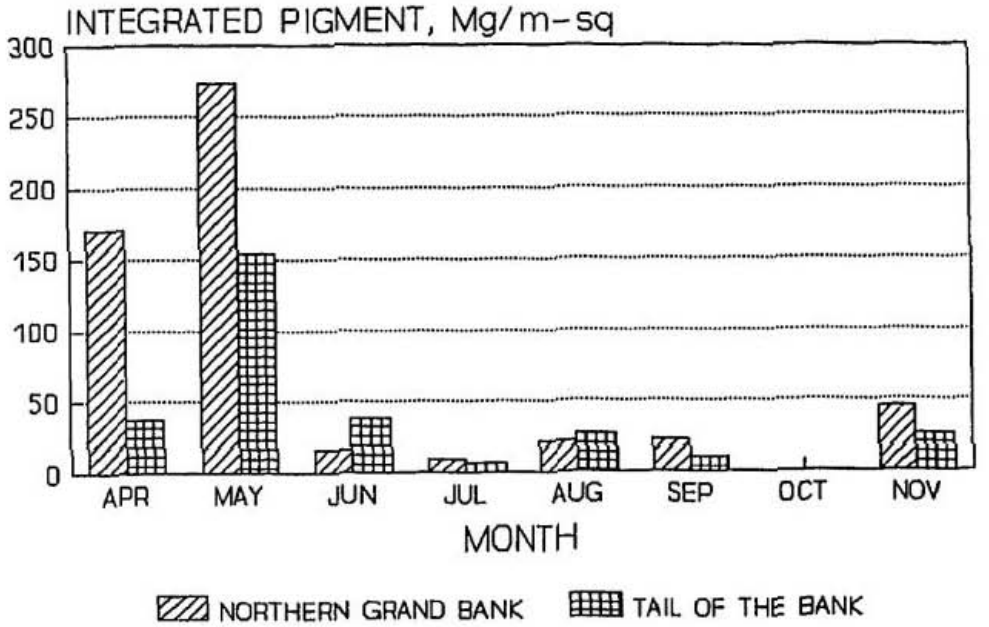

Figure 25. Temporal variations in Integral Chlorophyll (mg m^{-2}) on the Grand Banks. No observations were made in October.

6.4 Conclusions

The performance of semi-empirical algorithms should exceed that of simple empirical relations in predicting integral production. For a given location, the "P_m^b/K" model, that is one that predicts integral productivity from knowledge of maximum photosynthesis per unit chlorophyll in the top optical depth and divided by

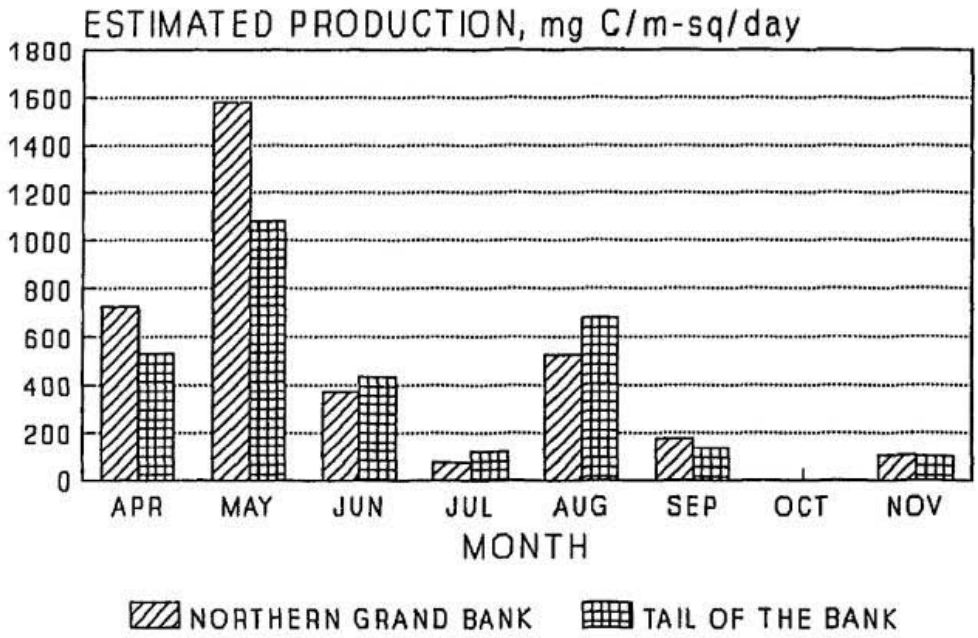

Figure 26. Calculated primary production on the northern and southern (= Tail of the Bank) Grand Banks, April to November 1980. Units are mg C m^{-2} day^{-1}.

the downward diffuse attenuation coefficient for wavelengths from 400 to 700 nm (Kd), seems to perform extremely well (see Platt and Sathyendranath, 1988). However, the P_m^b/K model has never been applied to large data sets. Recent evaluation of various production algorithms by Balch *et al.*(1992) indicates that algorithm complexity is not necessarily correlated to performance, and thus the development of the P_m^b/K model is

worth considering.

On the Grand Banks it has been encouraging to find a reasonable agreement between predicted and measured production rates. This success can be attributed to site-specific adjustments in the model parameters. Some of the site-specificity is due to changes in the phytoplankton species composition and photo-adaptation which result in variations in physiological responses in light absorption capability (Bricaud *et al.*, 1988), the maximum quantum yield for growth (Cleveland *et al.*, 1989; Prasad and Hollibaugh, 1992) and light and temperature dependence of growth.

One of the major challenges that still remains is the remote estimation of the photo-adaptive parameters from space for use as input in production models. Future research endeavours should focus on the relationship among temperature dependent photo-adaptive parameters from remotely sensed data. Satellite infrared data from the AVHRR sensor might allow derivation of P_m^b/K in surface waters based on the temperature dependent relationships of Eppley (1972).

Therefore, if the accuracy of remote sensing algorithms can be improved by incorporating pigment, temperature and light-dependent terms (Balch *et al.*, 1992), then primary production estimates from satellites will be invaluable for understanding the carbon cycling in the world ocean, a principle objective of the JGOFS program and the Biological Oceanographic community around the world.

My thesis has clearly demonstrated that despite the apparent difficulties that face remote sensing in mid-latitude, cloud-covered areas, it is possible to use satellite remote

sensing to develop workable production algorithms. This work represents a significant advance for oceanography in this area and has required calibration with synoptic shipboard data, the use of secondary variables, and the determination and parameterization of phytoplankton physiology.

The algorithms developed for the Grand Banks have been based on the CZCS data and are appropriate for use with data from other sensors. The results and algorithms presented in this thesis will provide invaluable baseline information for pigment retrieval and production estimation for the Grand Banks from the proposed ocean color sensor (SeaWiFS) on a regular synoptic basis. The algorithms can also be used with ocean color data collected by airborne surveys, a more practical means of remote sensing in areas such as the Grand Banks, where cloud cover is extensive. Data from airborne surveys can be used to fill in the gaps caused by the absence of satellite coverage.

CHAPTER 7. SUMMARY

7.1 Introduction

My purpose has been to investigate the potential and the availability of ocean color data for satellite remote sensing in the Grand Banks region, and, in particular, to develop approaches and algorithms useful for calculating primary production there. Ship-to-satellite calibrations are very rare for high latitude regions in general and there have been no previous attempts to derive these on the Grand Banks. Local calibration is important to set the framework for satellite pigment retrieval, and is the necessary first step before algorithms for primary production can be developed. Management of Newfoundland's ocean resources requires knowledge of the entire ecosystem, and therefore there is an especial need to investigate the use of ocean color remote sensing and to develop site-specific algorithms for estimating primary production on the Grand Banks.

7.2 Remote sensing as a tool

The importance of satellite remote sensing as a tool for measuring and quantifying

oceanographic processes is well recognized. Satellite sensors such as the Coastal Zone Color Scanner (CZCS) have provided oceanographers with maps of algal pigments at temporal and spatial scales not possible with traditional *in situ* oceanographic campaigns. Converting static measurements of algal biomass to rates of primary production has been the subject of much research since the early 50's. With the advent of satellite-derived estimates of algal pigment concentrations, the modelling of primary production over large scales has become quite feasible.

Algorithm development and evaluation has been an integral part of modelling primary production from the satellite-derived biomass estimates. However, due to the site-specificity induced by spatial and temporal variations in the photochemical properties of phytoplankton photosynthesis in the sea is considered too complicated to describe with one general formulation. This has necessitated the adaptation of general production models to the specific conditions found in different parts of the world ocean (Morel and André, 1991).

The ship-to-satellite calibration presented here will be highly useful for estimating chlorophyll from future satellites, such as the SeaWiFS, on the Grand Banks. Band 2 (443 nm), band 4 (510 nm), band 5 (555 nm), and band 6 (670 nm) of SeaWiFS, the proposed ocean color sensor, are compatible to the channels 1, 2, 3, and 4 of the CZCS. Therefore, in principle, the blue-to-green ratios obtained from the SeaWiFS sensor estimating pigment concentration should be similar to or better than CZCS pigment retrieval algorithms.

7.3 A primary production model for the Grand Banks

The Grand Banks of Newfoundland is a cold, mid-latitude region that is plagued by cloud and fog, and with large solar zenith angles which further complicate satellite data processing. Consequently, very little attention has been devoted to satellite remote sensing there. One aim of my investigations on the Grand Banks was to develop a semi-empirical model to predict production through a series of interrelated steps.

Relationships between satellite detectable chlorophyll, total chlorophyll, and mean euphotic zone chlorophyll were initially studied on the Grand Banks to predict integral production. Mean euphotic zone chlorophyll was a linear function of satellite detectable chlorophyll, with over 80% of the variance explained. Log integral chlorophyll, when regressed against log satellite detectable chlorophyll, showed an excellent linear fit with a correlation coefficient (r^2) of 0.88 (Figure 2; Equation 2.9).

The water column light utilization index, ψ, was found to vary seasonally over the Grand Banks (Figure 5). The indications are that ψ cannot be treated as a constant in estimating production from chlorophyll *a* in cold oceans as has been the practice. An analysis of covariance (Chapter 2, Table 1; Prasad *et al.*, 1992) indicated that empirical relationships based on integral chlorophyll may not give reliable predictions because the relation between IP and IC depends strongly on date and location. A semi-empirical model, which is in part physiologically based (Equations 2.11-2.15), utilizes integral chlorophyll, photosynthetically available radiation and light absorption by chlorophyll to predict integral production. Observed *vs* predicted production showed an excellent

goodness of fit, and corroborates the model (Figure 6). The model parameters could be further tuned to assimilate remotely sensed pigments to predict production over local spatial scales (~ 100 km, Prasad *et al.*, 1992).

7.4 The annual picture from ship and satellite

A sequence of surface pigment images of the 1980 phytoplankton spring bloom on the Grand Bank of Newfoundland was derived from the Nimbus-7 CZCS. This data set was augmented with *in situ* shipboard observations of physical and biological data to examine spatial and temporal variability of the surface pigment fields. Ship-to-satellite data comparisons were performed along a transect at 47°N (Figures 1 & 7) and a regression model has been presented for estimating satellite chlorophyll (Equation 3.6).

The satellite imagery suggests considerable temporal and spatial variability in surface chlorophyll concentrations across the period of investigation (Figures 8, 11 & 15). Patterns in near-surface pigment concentration are associated with the evolution of the spring bloom. First indications of the bloom were inshore, but the bloom was ultimately stronger offshore. Diatoms were the dominant species in the spring; dinoflagellates dominated an early fall bloom (Figure 15). As the season progressed, water column stratification and stability (associated with the sea surface temperature) increased (Figure 14). There was also a fairly abrupt increase in the production-to-biomass ratio (Figure 17), perhaps attributable to a change in phytoplankton species composition.

7.5 A semi-empirical model based on secondary variables

Most primary production models developed for satellite data have relied on knowledge of pigment concentration, light absorption, and incident light in the water column. All three of these variables are closely related, and focus on the light harvesting capacity of phytoplankton. However, seasonal variability in these variables has resulted in considerable scatter in predictions of annual primary production, leading to a search for other inputs which might be used. Secondary variables such as sea surface temperature, for example, account for much of the variability in the predicted production when used in some models (Balch *et al.*, 1989c).

The challenge lies in utilizing parameters other than pigment concentration that can be derived *via* satellite and that provide new information about primary production. Therefore the use of other remotely-sensed variables to improve primary productivity prediction constituted a new avenue worth investigating on the Grand Banks.

A preliminary assessment of the relationship between sea-surface temperature, water column stability, integral chlorophyll, and remote sensing optical depth (1/K490) was made over the Grand Banks with the aim of predicting integral production. Sea-surface temperature was highly correlated with water column stability (Figure 19). Further, 96% of the variance in integral chlorophyll was explained by combining three variables (water column stability, sea-surface temperature, and 1/K490) in a multiple regression (Equation 4.3). Temporal variations in 1/K490 coincide with changes in integral chlorophyll and satellite detectable chlorophyll, and hence optical depth

parameters, such as the quantum yield for photosynthesis, on the Grand Banks in connection with production algorithm development.

Seasonal estimates of water column quantum yield (ϕ_C) for carbon fixation have been computed. Mean values of ϕ_C showed a twofold to sixfold variation from spring through summer. A shift in distribution of normalized quantum yield (ϕ_C/ϕ_{max}) towards lower values in the upper 20m suggested frequent light saturation (Figure 22). The estimated specific absorption coefficient for phytoplankton ($a_{ph}.Chl^{-1}$) also varied seasonally. Net plankton had a lower specific absorption in spring than the nanoplankton which dominate the post-bloom season (summer-fall) on the Grand Banks. A good correlation between surface incident radiation and ϕ_C/ϕ_{max} allows a reasonable prediction of water column quantum yield (Figure 24). Seasonal estimates of ϕ_C and $a_{ph}.Chl^{-1}$ (Table 4 a to g), which essentially parameterize the light-harvesting and photosynthetic capabilities of phytoplankton, could be used to refine satellite-remote sensing-based production models.

7.7 Calculating primary production on the Grand Banks

Calculating the primary production on the Grand Banks has involved a series of interrelated steps. To convert ocean color to integral production has required calibration with synoptic shipboard data, the use of secondary variables, and the determination and parameterization of factors reflecting phytoplankton physiology.

Chlorophyll detected by Nimbus-7 CZCS satellite imagery was used to calculate

decreased with increase in chlorophyll (Figure 21). Integral chlorophyll along with ρ, the ratio of chl*a* to (chl*a* + phaeo*a*), ψ^* (cross-section of photosynthesis per unit of areal chlorophyll), photosynthetically available radiation, and quantum yield have been used to compute integral production over the Grand Banks (Equations 4.4 & 4.5). Total and mean pigment values agree well with the values based on trophic categories proposed by Morel and Berthon (1989).

The model developed permits prediction of integral chlorophyll using sea-surface temperature and optical data initially, and later incorporates a combination of parameters and variables to predict water column production. A good estimate of integral chlorophyll allows prediction of primary production with greater degree of precision than has been possible with other semi-empirical models. Simultaneous assimilation of sea surface temperature and optical depth into one model for predicting integral chlorophyll (Equation 4.3) demonstrates the usefulness and need for a thermal channel in future ocean color sensors. Thermal data can be considered a key to both the physical and biological structure of the water column.

7.6 Variability in physiological state

There is a need to parameterize adequately various physiological processes which control the light-harvesting and photosynthetic capabilities of phytoplankton. Although it has been possible to parameterize the physical factors accurately, the physiological factors remain elusive (Morel 1991). This has prompted a study of physiological

the depth-integrated pigment content of the euphotic zone on the Grand Banks. This value was used along with a computed value of chlorophyll-specific cross section (Equations 6.2 & 6.3) and computed values of quantum yield in an algorithm to predict the annual production. This site-specific adjustment of the physiological parameters was necessary to take seasonal variation into account. Mean primary production computed from the algorithm was 194 g C m^{-2} yr^{-1}, which compared well with the mean shipboard measured value of 186 g C m^{-2} yr^{-1}. Integral chlorophyll and production profiles by month for the Northern and Tail region, differ somewhat, suggesting that the Grand Banks are heterogenous seasonally and spatially (Figures 26 & 27).

The results from the Grand Banks suggest that photoadaptive parameters are important and must be taken account of in the estimation of primary production. Remote estimation of photoadaptive parameters from space still remains a major challenge, especially if the "$P_m{}^b/_K$" models (section 6.4) are to be applied to large data sets.

To get some idea of how this study of the Grand Banks fits into a global context, I compared my estimates of primary production using CZCS with determinations made by other investigators. There have been only very few studies of this type, and Table 6 provides a comparison of the CZCS-derived primary production estimates from the Pacific and from other regions of the Atlantic ocean. The highest value of primary production from CZCS is reported by Feldman (1986). His estimates were made for one of the most productive regions in the equatorial Pacific Ocean, the Peru Upwelling.

Table 6. Comparison of primary production estimates for different areas using CZCS data.

Investigator	Study area	Primary production (g C m^{-2} d^{-1})
Brown *et al.* (1985)	N. Atlantic Shelf Slope water Gulf Stream	0.92 0.91 0.42
Feldman (1986)	Peru Upwelling Open ocean	2.77 0.29
Kuring *et al.* (1990)	Georges Bank Slope water	1.13 0.80
This study	Grand Banks	0.53

However, the open ocean production values he reports are comparatively speaking very low but probably typical of the open ocean generally. The Brown *et al.* (1985) estimate of primary production for the Slope Waters is somewhat higher than that of Kuring *et al.* (1990), although they used the same CZCS data from the North Atlantic ocean. This shows how choice and parameterization of algorithm may affect production estimates. The Grand Banks, which belong to the productive part of the western north Atlantic, has rather low values, but not as low as Feldman's open ocean ones. None of the production values reported in Table 6 seem out of line, and the Grand Banks values I have determined fall within the range.

Table 7. Comparison of CZCS derived primary production estimates from Georges Bank, Grand Banks and Slope waters. Values for Georges Bank and Slope water from Kuring *et al.* 1990.

Month	Georges Bank	Slope water	Grand Banks
April	1.00	0.85	0.73
May	1.10	1.05	1.58
June	1.25	0.78	0.37
July	1.17	0.53	0.08

Only one other study provides monthly estimates of production from CZCS, that of Kuring *et al.* (1990). This makes for an interesting comparison in that Kuring *et al.* (1990) cover the period of the spring bloom on another important fishing bank in the western North Atlantic, Georges Bank. Table 7 provides a comparison of the mean integral production estimates from Georges Bank, Grand Banks, and the Slope waters during April, May, June and July. The values of production from Georges Bank are somewhat higher than those for the Grand Banks. It also seems that a peak in the spring bloom is more fully-developed on the Grand Banks, and this occurs during May. The production values on Georges Bank are rather uniform from April through July, without a distinct peak in production during the spring bloom although there is a slight peak in June. The Slope waters show an intermediate situation with a peak in May, but not so pronounced as on the Grand Banks.

REFERENCES CITED

Abbott, M.R. and B. Barksdale. 1991. Phytoplankton pigment patterns and wind forcing off central California. *Journal of Geophysical Research*, **96**: 14,649-14,667.

Abbott, M.R. and D.B. Chelton. 1991. Advances in passive remote sensing of the ocean. Reviews of Geophysics, Supplement, *U.S. National report to International Union of Geodesy and Geophysics*. 571-589.

Abbott, M.R. and P.M. Zion. 1987. Spatial and temporal variability of phytoplankton pigment off northern California during Coastal Ocean Dynamics Experiment 1. *Journal of Geophysical Research*, **92**: 1745-1756.

Anderson, J.T. and G.A. Gardner. 1986. Plankton communities and physical oceanography observed on the southeast shoal region, Grand Bank of Newfoundland *Journal of Plankton Research*, **8**: 1111-1135.

André, J.M. and A. Morel. 1989. Simulated effects of barometric pressure and ozone content upon the estimate of marine phytoplankton from space. *Journal of Geophysical Research*, **94**: 1029-1037.

Arnone, R.A. and P.E. La Violette. 1986. Satellite definition of the Bio-optical and thermal variation of coastal eddies associated with the African current. *Journal of Geophysical Research*, **91**: 2351-2364.

Bainbridge, V. 1961. Warm-water species in the plankton of Newfoundland during winter months. *Nature*, **191**: 1216-1217.

Balch, W.M., R.W. Eppley, M.R. Abbott, and F.M.H. Reid. 1989a. Bias in satellite-derived pigment measurements due to coccolithophores and dinoflagellates. *Journal of Plankton Research*, **11**: 575-581.

Balch, W.M., M.R. Abbott, and R.W. Eppley. 1989b. Remote sensing of primary production - I. A comparison of empirical and semi-analytical algorithms. *Deep-Sea Research*, **36**: 281-295.

Balch, W.M., R.W. Eppley and M.R. Abbott. 1989c. Remote sensing of primary production - II. A semi-analytical algorithm based on pigments, temperature, and light. *Deep-Sea Research*, **36**: 1201-1217.

Balch, W.M., P.M. Holligan, S.G. Ackleson, and K.J. Voss. 1991. Biological and optical properties of mesoscale coccolithophore blooms in the Gulf of Maine. *Limnology and Oceanography*, **36**: 629-643.

Balch, W.M., R. Evans, J. Brown, G. Feldman, C. McClain and W. Esais. 1992. The remote sensing of ocean primary productivity: Use of a new data compilation to test satellite algorithms. *Journal of Geophysical Research*, **97**: 2279-2293.

Bannister, T.T. 1974. Production equations in terms of chlorophyll concentration, quantum yield, and upper limit of production. *Limnology and Oceanography*, **19**: 1-12.

Barale, V., P. Malanotte Rizzoli, and M.C. Hendershott. 1984. Remotely sensed dynamics of the Adriatic Sea. *Deep-Sea Research*, **31**: 1433-1459.

Barale, V., C.R. McClain, and P. Malanotte-Rizzoli. 1986. Space and time variability of the surface color field in the North Adriatic sea. *Journal of Geophysical Research*, **91**: 12,957- 12,974.

Barale, V., and C.C. Trees. 1987. Spatial variability of the ocean color field in CZCS imagery. *Advances in Space Research*, **7**: 95-100.

Barale, V., and R. Wittenburg Fay. 1986. Variability of the ocean surface color field in central California near-coastal waters as observed in a seasonal analysis of CZCS imagery. *Journal of Marine Research*, **44**: 291-316.

Berner, T., K. Wyman, and P.G. Falkowski. 1989. Photoadaptation and the package effect in *Dunaliella tertiolecta* (Chlorophyceae). *Journal of Phycology*, **25**: 70-78.

Berthon, J.F. and A. Morel. 1992. Validation of a spectral light-photosynthesis model and use of the model in conjunction with remotely-sensed pigment observations. *Limnology and Oceanography*, **37**: 781-796.

Bidigare, R.R., R.C. Smith, K.S. Baker, and J. Marra. 1987. Oceanic primary production estimates from measurements of spectral irradiance and pigment concentrations. *Global Biogeochemical Cycles* **1**: 171-186.

Bricaud, A., A.L. Bedhomme, and A. Morel. 1988. Optical properties of diverse phytoplankton species: Experimental results and theoretical interpretation. *Journal of Plankton Research*, **10**: 851-873.

Bricaud, A., and A. Morel. 1986. Light attenuation and scattering by phytoplanktonic cells: A theoretical model. *Applied Optics*. **25**: 571-580.

Brown, O.B., R.H. Evans, J.W. Brown, H.R. Gordon, R.C. Smith, K.S. Baker. 1985. Phytoplankton blooming off the U.S. East Coast: A satellite description. *Science*, **229**: 163-167.

Buzdalin, Y.I. and A.A. Elizarov. 1962. Hydrological conditions in the Newfoundland Banks and Labrador areas in 1960. Pp. 152-168 in Y.Y. Marti (ed.) *Soviet Fisheries Investigations in the Northwest Atlantic* (Israel programme for scientific Translations, Jerusalem 1963).

Campbell J.W. and J.E. O'Reilly 1988. Role of satellites in estimating primary production on the northwest Atlantic continental shelf. *Continental Shelf Research*, **8**: 179-204.

Campbell, J.W. 1989. Temporal patterns of phytoplankton abundance in the North Atlantic. *Advances in Space Research*, **9**: 455-460.

Carder, K.L., R.G. Steward, J.H. Paul, and G.A. Vargo. 1986. Relationships between chlorophyll and ocean color constituents as they affect remote-sensing reflectance models. *Limnology and Oceanography*, **31**: 403-413.

Carder, K.L., R.G. Steward, G.R. Harvey, and P.B. Ortner. 1989. Marine humic and fulvic acids: Their effects on remote sensing of ocean chlorophyll. *Limnology and Oceanography*, **34**: 68-81.

Clark, D.K., 1981. Phytoplankton algorithms for the Nimbus-7 CZCS. Pp. 227-238 *in* J.F.R. Gower (ed.), *Oceanography from space*, Plenum, New York.

Clarke, G.K., Ewing, G.C. and Lorenzen, C.J. 1970. Spectra of backscattered light from the sea obtained from aircraft as a measure of chlorophyll concentration. *Science*. **167**: 1119-1121.

Clarke, R.A., H.W. Hill, R.F. Reiniger, and B.A. Warren. 1980. Current system south and east of the Grand Bank of Newfoundland. *Journal of Physical Oceanography*, **10**: 25-65.

Cleveland, J.S., M.J. Perry, D.A. Kiefer, and M.C. Talbot. 1989. Maximal quantum yield of photosynthesis in the northwestern sargasso sea. *Journal of Marine Research*, **47**: 869-886.

Collins, D.J., D.A. Kiefer, J.B. SooHoo, C. Stallings, and W.L. Yang. 1986. A model for the use of satellite remote sensing for the measurement of primary production in the ocean, *Ocean Optics* 8:335-348 (Proc. SPIE 637).

Deuser, W.G., F.E. Muller-Karger, and C. Hemleben. 1988. Temporal variations of particle fluxes in the deep subtropical and tropical North Atlantic: Eulerian *versus* Lagrangian effects. *Journal of Geophysical Research*, **93**: 6857-6862.

Draper, N.R., and H. Smith. 1981. *Applied regression analysis*. John Wiley and Sons.

Dubinsky Z., P.G.Falkowski and K.Wyman 1986. Light harvesting and utilization by phytoplankton. *Plant and Cell Physiology*, **27**: 1335-1349.

Eppley, R.W. 1972. Temperature and Phytoplankton growth in the sea. *Fisheries Bulletin, US*, 70: 1063-1085.

Eppley R.W., E. Steward, M.R. Abbott and U. Heyman. 1985. Estimating ocean primary production from satellite chlorophyll: Introduction to regional differences and statistics for the southern California Bight. *Journal of Plankton Research*, **7**: 57-70.

Esaias, W.E., 1980. Remote sensing of oceanic phytoplankton: Present capabilities and future goals. Pp. 321-337 *In*: , P.G. Falkowski, editor, *Primary productivity in the sea* Environmental Science Research, Vol. **19**, Plenum Press, New York, pp. 321-337.

Esaias, W.E., G.C. Feldman, C.R. McClain and J.A. Elrod. 1986. Monthly satellite-derived phytoplankton pigment distribution for the north Atlantic ocean basin. *EOS*, **67**: 835-837.

Falkowski P.G. 1981. Light-shade adaptation and assimilation numbers. *Journal of Plankton Research*, **3**: 203-216.

Feldman, G.C. 1986. Variability of the productive habitat in the eastern equatorial Pacific, *EOS*, **67**: 106-108.

Feldman, G.C., D.K. Clark, and D. Halpern. 1984. Satellite color observations of the phytoplankton distribution in the eastern equatorial Pacific during the 1982-83 El Nino. *Science*, **226**: 1069-1071.

Feldman, G.C., N. Kuring, C. Ng, W. Esaias, C.R. McClain, J. Elrod, N. Maynard, D. Endres, R. Evans, J. Brown, S. Walsh, M. Carle, and G. Podesta. 1989. Ocean color: Availability of the global data set. *EOS*, **70**: 634-641.

Gardner, G.A. and Howell, E.T. 1983. Zooplankton distribution across the shelf break on the southeast shoal of the Newfoundland Grand Banks in May, 1981. *Canadian*

Fisheries Aquatic Sciences Rep. **1724**: 61pp.

GOFS. 1984. Global Ocean Flux Study. *U.S. National Academy.*

Gomes, M.C. 1991. *Predictions under uncertainty: Fish assemblages and food webs on the Grand Banks of Newfoundland.* Ph.D. thesis. Memorial University of Newfoundland, St. John's, Newfoundland, August, 230pp.

Gomes, M.C., Haedrich, R.L. and Rice, J.L., 1992. Biogeography of groundfish assemblages on the Grand Bank of Newfoundland. *Journal of Northwest Atlantic Fisheries Science*, (in press)

Gordon, H.R., and Clark, D.K. 1980. Remote sensing optical properties of a stratified ocean: an improved interpretation. *Applied Optics*, **19**: 3428-3430.

Gordon, H.R., D.K. Clark, J.L. Mueller, and W.A. Hovis. 1980. Phytoplankton pigments derived from the Nimbus-7 CZCS: initial comparisons with surface measurements. *Science*, **210**: 63-66.

Gordon, H.R. and A.Y. Morel. 1983. *Remote Assessment of Ocean Color for Interpretation of satellite visible imagery.* Springer-Verlag, New York. p. 113.

Gordon, H.R., D.K. Clark, J.W. Brown, D.B. Brown, R.H. Evans. 1982. Satellite measurement of the phytoplankton pigment concentration in the surface waters of a warm core Gulf Stream ring. *Journal of Marine Research*, **40**: 491-502.

Gordon, H.R., Clark, D.K., Brown, J.W., Brown, O.B., Evans, R.H., and Broenkow, W.W., 1983a. Phytoplankton pigment concentrations in the Middle Atlantic Bight:

Comparisons of ship determinations and CZCS estimates. *Applied Optics*, **22**: 20-36.

Gordon, H.R., J.W. Brown, O.B. Brown, R.H. Evans, and D.K. Clark. 1983b. Nimbus 7 CZCS: reduction of its radiometric sensitivity with time. *Applied Optics*, **22**: 3929-3931.

Gordon, H.R. 1987. Calibration requirements and methodology for remote sensors viewing the ocean in the visible. *Remote Sensing of the Environment*, **22**: 103-126.

Gordon, H.R. and D.J. Castano. 1987. Coastal Zone Color Scanner atmospheric correction algorithm: multiple scattering effects. *Applied Optics*. **26**: 2111-2122.

Gordon, H.R., O.B. Brown, R.H. Evans, J.W. Brown, R.C. Smith, K.S. Baker, and D.K. Clark. 1988. A semianalytical radiance model of the ocean color. *Journal of Geophysical Research*, **93**: 10,909-10,924.

Greenberg, D. A. and B.D. Petrie. 1988. The mean barotropic circulation on the Newfoundland Shelf and slope. *Journal of Geophysical Research*, **37**: 15,541-15,550.

Hallagraeff, G.M. 1981. Seasonal study of phytoplankton pigments and species at a coastal station off Sidney: Importance of the diatoms and the nanoplankton. *Mar. Biol.*, **61**: 107-118.

Harrison W.G. and T. Platt. 1980. Variations in assimilation number of coastal marine phytoplankton: effects of environmental covariates. *Journal of Plankton Research*, **2**: 249-260.

Harrison, W.G. and Platt, T. 1986. Photosynthesis-irradiance relationships in polar and

temperate phytoplankton populations. *Polar Biology*, **5**: 153-164.

Hayes, R.M. and R.Q. Robe. 1978. Oceanography of the Grand Banks of Newfoundland in 1973. No. CG 373-73. United States Coast Guard, Oceanographic Unit, Washington D.C., 436pp.

Helbig, J., G. Mertz, and P. Pepin. 1992. Environmental influences on the recruitment of Newfoundland/Labrador Cod. *Fisheries Oceanography*, **1**: 39-56.

Hollibaugh, J.T., and J.A. Booth. 1981. Observations on the dynamics and distribution of phytoplankton and primary production on the Grand Banks in the 1980 season. Pp. 4-1 - 4-65 in *Grand Banks Oceanographic Studies*, Vol. 1 Mobil Oil Canada., Ltd.

Holligan, P.M., M. Viollier, D.S. Harbour, P. Camus, and M. Champagne-Philippe. 1983. Satellite and ship studies of coccolithophore production along a continental shelf edge. *Nature*, **304**: 339-342.

Hovis, W.A., D.K. Clark, F. Anderson, R.W. Austin, W.H. Wilson, E.T. Baker, D. Ball, H.R. Gordon, J.L. Mueller, S.Y. El-Sayed, B. Sturm, R.C. Wrigley, and C.S. Yentsch. 1980. Nimbus-7 Coastal Zone Color Scanner: system description and initial imagery. *Science*, **210**: 60-63.

IGBP. 1988. The International Geosphere-Biosphere Programme: A study of global change. *IGBP Rep.* **4**. 200 p.

JGOFS. 1988. Report of the first session of the SCOR committee for JGOFS. *Scientific Committee Oceanic Research*, 50 p.

Kiefer, D.A. and B.G. Mitchell. 1983. A simple, steady state description of phytoplankton growth based on absorption cross section and quantum efficiency. *Limnology and Oceanography*, **27**: 492-499.

Kirk J.T.O. 1983. *Light and photosynthesis in aquatic ecosystems*, Cambridge University Press, Cambridge, 401 pp.

Kishino, M., N. Okami, M. Takahashi, and S. Ichimura. 1985. Light utilization efficiency and quantum yield of phytoplankton in a thermally stratified sea. *Limnology and Oceanography*, **31**: 557-566.

Kitchen, J.C. and J.R.V. Zaneveld. 1990. On the noncorrelation of the vertical structure of light scattering and chlorophyll *a* in Case I waters. *Journal of Geophysical Research*, **95**: 20,237-20,246.

Kuring, N., M.R. Lewis, T. Platt, and J.E. O'Reilly. 1990. Satellite-derived estimates of primary production on the northwest Atlantic continental shelf. *Continental Shelf Research*. **10**: 461-484.

Laurs, R.M., P.C. Fiedler, and D.R. Montgomery. 1984. Albacore tuna catch distributions relative to environmental features observed form satellites. *Deep-Sea Research*, **31**: 1085-1099.

Ley, A.C., and D.C. Mauzerall. 1982. Absolute absorption cross-section for photosystem II and the minimum quantum requirement for photosynthesis in *Chlorella vulgaris*. *Biochimica et Biophysica Acta*, **680**: 95-106.

Li, W.K.W. 1986. Experimental approaches to field measurements: methods and

interpretation. Pp. 251-286. In: Trevor Platt, and W.K.W. Li (ed.) Photosynthetic picoplankton. *Canadian Bulletin Fisheries Aquatic Sciences*. **214.**

Malone, T.C. 1987. Primary production of the ocean water column as a function of surface light intensity. *Deep-Sea Research*, **34**: 139.

Malone, T.C., M.B. Chervin, D.C. Boardman. 1979. Effects of 22μm screens on size-frequency distributions of suspended particles and biomass estimates of phytoplankton size fractions. *Limnology and Oceanography*, **24**, 956-960.

Malone, T.C., T.S. Hopkins, P.G. Falkowski, and T.E. Whitledge. 1983. Production and transport of phytoplankton biomass over the continental shelf of the New York Bight. *Continental Shelf Research*, **1**: 305-337.

Margalef, R. 1978. Life-forms of phytoplankton as survival alternatives in an unstable environment. *Oceanologica Acta*, **1**: 493-509.

McClain, C.R., W.E. Esaias, G.C. Feldman, J. Elrod, D. Endres, J. Firestone, M. Darzi, R. Evans, and J. Brown. 1990. Physical and Biological processes in the North Atlantic during the first GARP global experiment. *Journal of Geophysical Research*, **95**: 18,027-18,048.

McClain, C.R., L.J. Pietrafesa, and J.A. Yoder. 1984. Observations of the Gulf Stream-induced and wind-driven upwelling in the Georgia Bight using ocean color and infrared imagery. *Journal of Geophysical Research*, **89**: 3705-3723.

Mitchell, B.G., and O. Holm-Hansen. 1991. Bio-optical properties of Antarctic waters: Differentiation from temperate ocean models. *Deep-Sea Research*, **38**: 1009-1028.

Mobil Oil Canada Limited. 1981. Grand Banks Oceanographic Studies. Final Report. Vol. 1:Pp 4-65.

Morel, A., and L. Prieur. 1977. Analysis of variations in ocean color. *Limnology and Oceanography*, **22**: 709-722.

Morel, A. 1978. Available, usable, and stored radiant energy in relation to marine photosynthesis. *Deep-Sea Research*, **25**: 673-688.

Morel, A. L. Lazzara, and J. Gostan. 1987. Growth rate and quantum yield time response for a diatom to changing irradiances (energy and color). *Limnology and Oceanography*, **32**: 1066-1084.

Morel, A. 1988. Optical modelling of the upper ocean in relation to its biogenous matter content (Case 1 waters). *Journal of Geophysical Research*, **93**: 10,749-10,768.

Morel, André and J.F. Berthon. 1989. Surface pigments, algal biomass profiles, and potential production of the euphotic layer: Relationships reinvestigated in view of remote sensing applications. *Limnology and Oceanography*, **34**: 1545-1562.

Morel, André. 1991. Light and marine photosynthesis: a spectral model with geochemical and climatological implications. *Progress in Oceanography*, **26**: 263-306.

Morel, A. and J-M. André. 1991. Pigment distribution and primary production in the western Mediterranean as derived and modeled from coastal zone color scanner observation. *Journal of Geophysical Research*, **96**: 12,685-12,698.

Mortimer, C.H. 1988. Discoveries and testable hypotheses arising form Coastal Zone

Color Scanner imagery of the southern Lake Michigan. *Limnology and Oceanography*, **33**: 203-226.

Mueller, J.L. 1985. Nimbus-7 CZCS: Confirmation of its radiometric sensitivity decay rate through 1982. *Applied Optics*, **24**: 1043-1047.

Mueller, J.L. 1988. Nimbus-7 CZCS: electronic overshoot due to cloud reflectance. *Applied Optics*, 27: 438-440.

Mueller, J.L. and E.R. Lange. 1989. Bio-optical provinces of the Northeast Pacific Ocean: A provisional analysis. *Limnology and Oceanography*, **34**: 1572-1586.

Muller-Karger, F.E., C.R. McClain, and P.L. Richardson. 1988. The dispersal of the Amazon's water. *Nature*, **333**: 56-59.

Muller-Karger, F.E., C.R. McClain, R.N. Sambrotto, and G.C. Ray. 1990. A comparison of ship and coastal zone color scanner mapped distribution of phytoplankton in the south-eastern Bering sea. *Journal of Geophysical Research*, **95**: 11,483-11,499.

Osborne B.A. and R.J. Geider. 1986. Effect of nitrate-nitrogen limitation on photosynthesis of diatom *Phaeodactylum tricornutum* Bohlin (Bacillariophyceae). *Plant, Cell and Environment*, **9**, 617-625.

Pelaez, J. and J.A. McGowan. 1986. Phytoplankton pigment patterns in the California current as determined by satellite. *Limnology and Oceanography*, **31**, 927-950.

Perry, M.J. 1986. Assessing marine primary production from space. *BioScience*, **36**: 461-467.

Peterson, R. B., M.N. Sivak, and D.A. Walker. 1988. Relationship between steady-state fluorescence yield and photosynthetic efficiency in spinach leaf tissue. *Plant Physiology*, **88**: 158-163.

Petrie, B. and C. Anderson. 1983. Circulation on the Newfoundland continental shelf. *Atmosphere and Ocean*, **21**: 207-226.

Platt, T. 1986. Primary production of the ocean water column as a function of surface light intensity: Algorithms for remote sensing. *Deep-Sea Research*, **33**: 1-15.

Platt, T. and S. Sathyendranath. 1988. Oceanic primary production estimation by remote sensing at local and regional scales. *Science*, **241**: 1613-1620.

Platt, T., S. Sathyendranath, C.M. Caverhill, and M.R. Lewis. 1988. Ocean primary production and available light : further algorithms for remote sensing *Deep-Sea Research*, **35**: 855-879.

Pomeroy, L.R., W.J. Wiebe, D. Deibel, R.J. Thompson, G.T. Rowe, and J.D. Pakulski. 1991. Bacterial responses to temperature and substrate concentration during the Newfoundland spring bloom. *Marine Ecology Progress Series*, **75**:143-159.

Prasad, K.S. and J.T. Hollibaugh. 1992. Quantum yield estimates of phytoplankton on the Grand Banks of Newfoundland for use in production models. *Limnology and Oceanography*, **37**: 1271-1279.

Prasad, K.S., J.T. Hollibaugh, D.C. Schneider, and R.L. Haedrich. 1992. A model for determining primary production on the Grand Banks. *Continental Shelf Research*, **12**: 563-575.

Prasad, K.S. and R.L. Haedrich. 1992. Satellite observations of phytoplankton variability on the Grand Banks of Newfoundland during a spring bloom. *International Journal of Remote Sensing*, (in press).

Preisendorfer, R.W. 1986. Secchi disk science: Visual optics of natural waters. *Limnology and Oceanography*, **31**: 909-926.

Quenzel, H. 1983. Scattering, absorption, emission and radiative transfer in the atmosphere, Pp. 1-25. In: *P. Camagni and S. Sandroni. (eds.). Optical Remote Sensing of Air Pollution*, Elsevier, Amsterdam.

Ridout, P.S. and R.J. Morris. 1988. Further studies of short-term variation in the pigment composition of a spring phytoplankton bloom. *Marine Biology*, **97**: 597-602.

Robinson, I.S. 1985. *Satellite Oceanography*, Ellis Horwood Limited, Chichester.

Ryther, J.H. and C.S. Yentsch. 1957. The estimation of phytoplankton production in the ocean from chlorophyll and light data. *Limnology and Oceanography*, **2**: 281-285.

SAS. 1985. *Statistical Analysis System. User's Guide: Basics.* SAS Institute Inc., North Carolina 27511, USA.

Sathyendranath, S., and T. Platt. 1989. Remote sensing of ocean chlorophyll: consequence of nonuniform pigment profiles. *Applied Optics*, **28**: 490-495.

Sathyendranath, S., L. Lazzara, and L. Prieur. 1987. Variations in the spectral values of specific absorption of phytoplankton. *Limnology and Oceanography*, **32**: 403-415.

Sathyendranath, S., T. Platt, C.M. Caverhill, R.E. Warnock, and M.R. Lewis. 1989. Remote sensing of ocean primary production: Computations using a spectral model. *Deep-Sea Research*, **36**: 431-453.

SeaWiFS. 1987. *Report of the joint EOSAT/NASA SeaWiFS working group.* NASA-EOSC, Washington DC. 91 p.

Schneider, D.C., and D.A. Methven. 1988. Response of capelin to wind-induced thermal events in the southern labrador current. *Journal of Marine Research*, **46**: 105-118.

Smith, R.C., and K.S. Baker. 1978. The bio-optical state of ocean waters and remote sensing. *Limnology and Oceanography*, **23**: 247-259.

Smith, R.C. and K.S. Baker. 1982. Oceanic chlorophyll concentrations as determined by satellite (Nimbus-7) Coastal Zone Color Scanner. *Marine Biology*, **66**: 269-279.

Smith, R.C., R.W. Eppley, and K.S. Baker. 1982. Correlation of primary production as measured aboard ship in southern California coastal waters and as estimated from satellite chlorophyll images. *Marine Biology*, **6**: 281-288.

Smith, R.C., B.B. Prezelin, R.R. Bidigare and K.S. Baker. 1989. Bio-optical modeling of photosynthetic production in coastal waters. *Limnology and Oceanography*, **34**: 1524-1544.

Sokal, R. R. and F.J. Rohlf. 1981. *Biometry.* W.H. Freeman and Company. New York. 859 Pp.

Sosik, H. M., and B.G. Mitchell. 1991. Absorption, fluorescence, and quantum yield

for growth in nitrogen-limited *Dunaliella tertiolecta*. *Limnology and Oceanography*, **36**: 910-921.

Soule, F.M., P.S. Branson, and R.P. Dinsmore. 1951. Physical oceanography of the Grand Banks region and the Labrador Seas in 1951. *U.S. Coast Guard Bulletin*, 37.

Strickland, J.D.H. 1958. Solar radiation penetrating the ocean. a review of requirements, data and methods of measurements, with particular reference to photosynthetic productivity. *Journal of the Fisheries Research Board of Canada*, **15**: 453-493.

Tanada, T. 1951. The photosynthetic efficiency of carotenoid pigments in *Navicula minima*. *Americal Journal of Botany*, **38**: 276-283.

Thomas, A.C., and P.T. Strub. 1989. Interannual variability in phytoplankton pigment distributions during the spring transition along the west coast of North America. *Journal of Geophysical Research*, **94**: 18,095-18,117.

Walsh, J.J. and D.A. Dieterle. 1988. Use of satellite ocean colour observations to refine understanding of global geochemical cycles. Pp. 287-318. *In*: T.Rosswall, R.G. Woodmanse, and P.G. Risser. (eds.), *Scales and Global change*. John Wiley.

Westbroek, P., E.W. De Vrind-De Jong, P. Van derwal, A.H. Borman, and J.P.M. De Vrind. 1985. Biopolymer-mediated calcium and manganese accumulation and biomineralization. *Geological Minjbouw*, **64**: 5-15.

Wroblewski, J.S. 1989. A model of the spring bloom in the North Atlantic and its impact on ocean optics. *Limnology and Oceanography*, **34**: 1563-1571.

Yoder, J.A., L.P. Atkinson, S.S. Bishop., J.H. Blanton, T.N. Lee and L.J. Pietrafesa. 1985. Phytoplankton dynamics with Gulf Stream intrusions on the Southeastern United States continental shelf during summer 1981. *Continental Shelf Research*, **4**: 611-635.

Yoder, J.A., C.R. McClain, J.O. Blanton, L.-Y. Oey. 1987. Spatial scales in CZCS-chlorophyll imagery of the southeastern U.S. Continental shelf. *Limnology and Oceanography*, **32**: 929-941.

Appendix Table A. Raw CZCS satellite data from NASA examined during the course of this research on remote sensing on the Grand Banks. CZCS images not fully processed for pigment had cloud cover >50%.

NASA Scene Number	Date	Comments
Volume 1		Label = 000103
79038144456.N17;1	07 FEB 1979	
79083143028.N17;1	24 MAR 1979	
79112144706.N17;1	22 APR 1979	
79117143516.N17;1	27 APR 1979	
79140144720.N17;1	20 MAY 1979	
79143140100.N17;1	23 MAY 1979	
79150142720.N17;1	30 MAY 1979	
79163150256.N17;1	12 JUN 1979	
79197151733.N17;1	16 JUL 1979	
79214152543.N17;1	02 AUG 1979	
Volume 2		Label = 000104
79230151654.N17;1	18 AUG 1979	
79241151705.N17;1	29 AUG 1979	
79257150525.N17;1	14 SEP 1979	
79257150725.N17;1	14 SEP 1979	
79267144826.N17;1	24 SEP 1979	
80051145328.N17;1	**20 FEB 1980**	Fully processed
80074151104.N17;1	15 MAR 1980	
80099142305.N17;1	09 APR 1980	

80106145100.N17;1	**16 APR 1980**	Fully processed
80120140326.N17;1	30 APR 1980	
Volume 3		Label = 000105
80121142126.N17;1	01 MAY 1980	
80123145808.N17;1	**03 MAY 1980**	Fully processed
80138142757.N17;1	18 MAY 1980	
80132141929.N17;1	12 MAY 1980	
80139144747.N17;1	19 MAY 1980	
80177143329.N17;1	26 JUN 1980	
80169153140.N17;1	18 JUN 1980	
80182142421.N17;1	01 JUL 1980	
80137141421.N17;1	05 JUL 1980	
80232142823.N17;1	19 AUG 1980	
Volume 4		Label = 000106
80249143554.N17;1	**05 SEP 1980**	Fully processed
80251151304.N17;1	07 SEP 1980	
80256150154.N17;1	12 SEP 1980	
80260143349.N17;1	16 SEP 1980	
80268151935.N17;1	24 SEP 1980	
80261145144.N17;1	**17 SEP 1980**	Fully processed
80261145344.N17;1	17 SEP 1980	
80284150816.N17;1	10 OCT 1980	
81104141350.N17;1	14 APR 1980	
81142135507.N17;1	22 MAY 1981	
Volume 5		Label = 000107
81134145346.N17;1	14 MAY 1981	

81183143208.N17;1	**02 JUL 1981**	Fully processed
81184144948.N17;1	03 JUL 1981	
78310145920.N17;1	06 NOV 1978	
78315144215.N17;1	10 NOV 1978	

Appendix Table B. Daily values during 1980 for incident radiation and PAR'. TIR values are from AES (Canada) and PAR' values calculated from equation 2.6.

OBS = observation #; Y = year; M = month; D = day;

TIR = Total incident radiation (Ein m^{-2} day^{-1});

PAR' = photosynthetically available radiation (Ein m^{-2} day^{-1})

OBS	Y	M	D	TIR	PAR'
1	80	1	1	17.9644	6.4309
2	80	1	2	19.1202	6.8732
3	80	1	3	3.8793	1.0412
4	80	1	4	17.3701	6.2035
5	80	1	5	32.2976	11.9154
6	80	1	6	13.6265	4.7710
7	80	1	7	32.9246	12.1553
8	80	1	8	6.1862	1.9240
9	80	1	9	22.7047	8.2447
10	80	1	10	7.7071	2.5059
11	80	1	11	28.1937	10.3450
12	80	1	12	16.9489	6.0423
13	80	1	13	17.0613	6.0853
14	80	1	15	28.2311	10.3594
15	80	1	16	9.4291	3.1649
16	80	1	17	31.2447	11.5125
17	80	1	18	26.6261	9.7453
18	80	1	19	8.1610	2.6796
19	80	1	20	6.4389	2.0207
20	80	1	21	21.7594	7.8830
21	80	1	22	29.3495	10.7873
22	80	1	23	35.8072	13.2583
23	80	1	24	6.5419	2.0601
24	80	1	25	29.8549	10.9807
25	80	1	26	19.7192	7.1023
26	80	1	27	18.1469	6.5007
27	80	1	28	29.4759	10.8357
28	80	1	29	26.4857	9.6915
29	80	1	30	17.2063	6.1408
30	80	1	31	33.4487	12.3559
31	80	2	1	20.9592	7.5769
32	80	2	2	36.0411	13.3479

OBS	Y	M	D	TIR	PAR'
33	80	2	3	34.4735	12.7480
34	80	2	4	39.8175	14.7929
35	80	2	5	32.3631	11.9405
36	80	2	6	15.9756	5.6699
37	80	2	7	28.8956	10.6136
38	80	2	8	15.3439	5.4282
39	80	2	9	25.8961	9.4659
40	80	2	10	49.2091	18.3866
41	80	2	11	8.0767	2.6474
42	80	2	13	24.0102	8.7443
43	80	2	14	35.8118	13.2601
44	80	2	15	40.2480	14.9576
45	80	2	16	46.4482	17.3301
46	80	2	17	9.2466	3.0950
47	80	2	18	42.7234	15.9048
48	80	2	19	35.2550	13.0470
49	80	2	20	56.3968	21.1369
50	80	2	21	15.1146	5.3404
51	80	2	22	65.1520	24.4871
52	80	2	23	43.6359	16.2540
53	80	2	24	35.9522	13.3138
54	80	2	25	21.6799	7.8526
55	80	2	26	10.8656	3.7146
56	80	2	27	20.379	7.3548
57	80	2	28	50.870	19.0222
58	80	2	29	23.917	8.7085
59	80	3	1	55.957	20.9686
60	80	3	2	63.762	23.9553
61	80	3	3	34.539	12.7731
62	80	3	4	21.652	7.8419
63	80	3	5	73.706	27.7603
64	80	3	6	29.410	10.8106
65	80	3	7	67.590	25.4200
66	80	3	8	37.197	13.7901
67	80	3	9	18.947	6.8069
68	80	3	10	31.409	11.5752
69	80	3	11	35.817	13.2619
70	80	3	12	66.907	25.1586
71	80	3	13	56.191	21.0581
72	80	3	14	84.899	32.0434
73	80	3	15	22.892	8.3164
74	80	3	16	67.015	25.1997
75	80	3	17	57.230	21.4556
76	80	3	18	54.399	20.3723
77	80	3	19	15.555	5.5087
78	80	3	20	39.144	14.5350

OBS	Y	M	D	TIR	PAR'
125	80	5	10	30.243	11.1293
126	80	5	11	119.447	45.2632
127	80	5	12	102.363	38.7258
128	80	5	13	118.427	44.8729
129	80	5	14	18.582	6.6672
130	80	5	15	38.690	14.3613
131	80	5	16	125.072	47.4155
132	80	5	17	124.740	47.2884
133	80	5	18	129.396	49.0700
134	80	5	19	106.813	40.4287
135	80	5	20	48.283	18.0320
136	80	5	21	134.347	50.9645
137	80	5	22	109.082	41.2971
138	80	5	23	34.825	12.8823
139	80	5	24	57.464	21.5452
140	80	5	25	67.075	25.2230
141	80	5	26	81.956	30.9171
142	80	5	27	72.480	27.2911
143	80	5	30	59.686	22.3957
144	80	5	31	130.973	49.6735
145	80	6	1	97.267	36.7759
146	80	6	2	23.421	8.5187
147	80	6	3	70.388	26.4908
148	80	6	4	39.429	14.6442
149	80	6	5	22.396	8.1266
150	80	6	6	51.862	19.4018
151	80	6	7	44.474	16.5745
152	80	6	8	119.541	45.2991
153	80	6	9	46.912	17.5074
154	80	6	10	129.756	49.2079
155	80	6	11	82.270	31.0370
156	80	6	12	54.726	20.4977
157	80	6	13	137.543	52.1874
158	80	6	14	133.897	50.7926
159	80	6	15	34.137	12.6191
160	80	6	16	64.310	24.1648
161	80	6	17	134.300	50.9466
162	80	6	18	44.853	16.7195
163	80	6	19	79.963	30.1543
164	80	6	20	57.548	21.5774
165	80	6	21	94.202	35.6030
166	80	6	23	91.554	34.5896
167	80	6	24	29.162	10.7157
168	80	6	25	126.008	47.7736
169	80	6	26	108.432	41.0482
170	80	6	27	113.921	43.1486

OBS	Y	M	D	TIR	PAR'
79	80	3	21	79.373	29.9287
80	80	3	22	25.784	9.4229
81	80	3	23	10.178	3.4513
82	80	3	24	16.827	5.9958
83	80	3	25	16.565	5.8955
84	80	3	26	63.701	23.9320
85	80	3	27	40.164	14.9254
86	80	3	28	35.058	12.9718
87	80	3	29	28.713	10.5438
88	80	3	30	98.610	37.2898
89	80	3	31	46.926	17.5128
90	80	4	1	68.741	25.8605
91	80	4	2	96.626	36.5306
92	80	4	3	98.718	37.3310
93	80	4	4	103.724	39.2469
94	80	4	5	47.234	17.6309
95	80	4	6	78.283	29.5115
96	80	4	7	111.366	42.1709
97	80	4	8	110.697	41.9149
98	80	4	9	84.998	32.0810
99	80	4	10	66.991	25.1908
100	80	4	11	42.752	15.9156
101	80	4	12	29.289	10.7640
102	80	4	13	49.738	18.5889
103	80	4	14	60.791	22.8183
104	80	4	15	110.790	41.9507
105	80	4	16	29.167	10.7175
106	80	4	17	42.387	15.7759
107	80	4	18	68.844	25.8999
108	80	4	19	81.423	30.7130
109	80	4	20	31.352	11.5537
110	80	4	21	101.829	38.5217
111	80	4	22	107.234	40.5898
112	80	4	23	24.338	8.8697
113	80	4	26	17.749	6.3485
114	80	4	29	120.322	45.5981
115	80	4	30	126.953	48.1353
116	80	5	1	44.146	16.4492
117	80	5	2	123.266	46.7244
118	80	5	3	106.672	40.3749
119	80	5	4	27.220	9.9727
120	80	5	5	17.099	6.0996
121	80	5	6	49.354	18.4421
122	80	5	7	17.501	6.2536
123	80	5	8	54.988	20.5979
124	80	5	9	128.717	48.8104

OBS	Y	M	D	TIR	PAR'
171	80	6	28	116.223	44.0295
172	80	6	29	109.124	41.3132
173	80	6	30	111.417	42.1906
174	80	7	1	36.205	13.4105
175	80	7	2	30.098	11.0738
176	80	7	3	46.378	17.3033
177	80	7	4	41.240	15.3372
178	80	7	5	143.879	54.6119
179	80	7	6	69.719	26.2347
180	80	7	7	102.569	38.8046
181	80	7	8	55.672	20.8594
182	80	7	9	81.582	30.7738
183	80	7	10	40.346	14.9952
184	80	7	11	68.568	25.7942
185	80	7	12	23.196	8.4328
186	80	7	13	55.690	20.8665
187	80	7	14	92.241	34.8528
188	80	7	15	113.018	42.8030
189	80	7	16	44.174	16.4599
190	80	7	17	109.026	41.2756
191	80	7	18	81.774	30.8472
192	80	7	19	48.971	18.2952
193	80	7	20	42.312	15.7472
194	80	7	21	39.588	14.7051
195	80	7	22	28.896	10.6136
196	80	7	23	19.747	7.1131
197	80	7	24	50.402	18.8432
198	80	7	25	81.362	30.6897
199	80	7	26	50.168	18.7536
200	80	7	27	99.102	37.4778
201	80	7	28	103.996	39.3507
202	80	7	29	116.270	44.0474
203	80	7	30	81.596	30.7792
204	80	7	31	63.135	23.7153
205	80	8	1	120.065	45.4996
206	80	8	2	122.938	46.5990
207	80	8	3	12.129	4.1980
208	80	8	4	40.468	15.0418
209	80	8	5	28.634	10.5134
210	80	8	6	63.725	23.9410
211	80	8	7	77.927	29.3754
212	80	8	8	55.962	20.9704
213	80	8	9	76.472	28.8185
214	80	8	10	87.496	33.0371
215	80	8	11	65.896	24.7718
216	80	8	12	41.502	15.4375

OBS	Y	M	D	TIR	PAR'
217	80	8	13	17.010	6.0656
218	80	8	14	27.141	9.9422
219	80	8	15	48.517	18.1216
220	80	8	16	10.992	3.7629
221	80	8	17	39.518	14.6783
222	80	8	18	71.942	27.0852
223	80	8	19	90.959	34.3622
224	80	8	21	69.860	26.2884
225	80	8	22	94.277	35.6317
226	80	8	23	107.225	40.5862
227	80	8	24	30.098	11.0738
228	80	8	25	32.672	12.0586
229	80	8	26	70.346	26.4746
230	80	8	27	54.445	20.3902
231	80	8	28	17.454	6.2357
232	80	8	29	82.195	31.0084
233	80	8	31	63.561	23.8783
234	80	9	1	73.744	27.7746
235	80	9	2	15.653	5.5463
236	80	9	3	43.847	16.3346
237	80	9	4	83.912	31.6655
238	80	9	6	65.952	24.7933
239	80	9	7	83.542	31.5241
240	80	9	8	61.015	22.9042
241	80	9	9	46.476	17.3409
242	80	9	10	71.586	26.9491
243	80	9	11	68.535	25.7817
244	80	9	12	72.288	27.2177
245	80	9	13	53.599	20.0661
246	80	9	14	81.886	30.8902
247	80	9	15	19.331	6.9537
248	80	9	16	69.836	26.2795
249	80	9	17	92.372	34.9029
250	80	9	18	43.374	16.1537
251	80	9	19	31.282	11.5268
252	80	9	20	52.293	19.5666
253	80	9	21	11.989	4.1443
254	80	9	22	29.729	10.9324
255	80	9	23	20.987	7.5876
256	80	9	26	34.300	12.6318
257	80	9	27	51.469	19.2514
258	80	9	28	80.098	30.2062
259	80	9	29	71.619	26.9617
260	80	9	30	77.253	29.1175
261	80	10	1	31.919	11.7704
262	80	10	2	54.675	20.4780

OBS	Y	M	D	TIR	PAR'
263	80	10	3	31.015	11.4248
264	80	10	4	35.288	13.0596
265	80	10	5	57.164	21.4306
266	80	10	6	9.569	3.2186
267	80	10	7	7.380	2.3806
268	80	10	8	17.141	6.1157
269	80	10	9	14.240	5.0056
270	80	10	10	56.172	21.0510
271	80	10	11	66.533	25.0153
272	80	10	12	51.020	19.0795
273	80	10	13	8.404	2.7727
274	80	10	14	29.827	10.9700
275	80	10	15	31.371	11.5609
276	80	10	16	26.4108	9.6629
277	80	10	17	25.8212	9.4373
278	80	10	18	35.2831	13.0578
279	80	10	19	13.2709	4.6349
280	80	10	20	26.1956	9.5805
281	80	10	21	40.0561	14.8842
282	80	10	22	42.2461	15.7222
283	80	10	23	10.5662	3.6000
284	80	10	24	19.6958	7.0934
285	80	10	25	28.8535	10.5975
286	80	10	26	31.7922	11.7220
287	80	10	27	36.9583	13.6988
288	80	10	28	27.2016	9.9655
289	80	10	29	17.1408	6.1157
290	80	10	30	30.0374	11.0505
291	80	10	31	26.1160	9.5501
292	80	11	1	20.2901	7.3208
293	80	11	2	31.8811	11.7560
294	80	11	3	38.9284	14.4526
295	80	11	4	34.8525	12.8930
296	80	11	5	25.2082	9.2027
297	80	11	6	27.7678	10.1821
298	80	11	7	29.7519	10.9413
299	80	11	8	29.2840	10.7623
300	80	11	9	5.0585	1.4924
301	80	11	10	12.0917	4.1837
302	80	11	11	5.3346	1.5981
303	80	11	12	7.0145	2.2409
304	80	11	13	9.4665	3.1792
305	80	11	14	9.4572	3.1756
306	80	11	15	16.5746	5.8991
307	80	11	16	22.9246	8.3289
308	80	11	17	32.3444	11.9333

Appendix Table B

OBS	Y	M	D	TIR	PAR'
309	80	11	18	11.0014	3.7665
310	80	11	19	7.9364	2.5937
311	80	11	20	7.0332	2.2481
312	80	11	21	22.3444	8.1069
313	80	11	23	18.7833	6.7442
314	80	11	24	38.7412	14.3810
315	80	11	25	12.7281	4.4272
316	80	11	26	8.7553	2.9070
317	80	11	27	33.7342	12.4651
318	80	11	28	5.6481	1.7181
319	80	11	29	9.2139	3.0825
320	80	11	30	3.7716	1.0000
321	80	12	1	23.5938	8.5850
322	80	12	2	27.2531	9.9852
323	80	12	3	26.7384	9.7882
324	80	12	4	19.9157	7.1776
325	80	12	5	5.1474	1.5265
326	80	12	6	6.6121	2.0869
327	80	12	7	4.6748	1.3456
328	80	12	8	9.8035	3.3081
329	80	12	9	5.9148	1.8201
330	80	12	10	7.4216	2.3967
331	80	12	11	27.5386	10.0944
332	80	12	12	33.1773	12.2520
333	80	12	13	21.5535	7.8043
334	80	12	14	3.4581	0.8801
335	80	12	15	13.8699	4.8641
336	80	12	16	18.2498	6.5401
337	80	12	17	6.4015	2.0063
338	80	12	18	22.7515	8.2626
339	80	12	19	17.6836	6.3234
340	80	12	20	26.0505	9.5250
341	80	12	21	20.1450	7.2653
342	80	12	22	29.6116	10.8876
343	80	12	23	29.8642	10.9843
344	80	12	24	4.1413	1.1415
345	80	12	25	9.7146	3.2741
346	80	12	26	13.2522	4.6278
347	80	12	27	17.0800	6.0925
348	80	12	29	8.1610	2.6796
349	80	12	30	7.1221	2.2821
350	80	12	31	7.1923	2.3090

Appendix Table C. Values for $\log_{10}$ integral chlorophyll and $\log_{10}$ satellite detectable chlorophyll.

OBS = observation #; CR = cruise; ST = station;

LNCHL = $\log_{10}$ integral chlorophyll;

LNSDC = $\log_{10}$ satellite detectable chlorophyll;

OBS	CR	ST	LNCHL	LNSDC
1	80M01	14	2.03797	-1.62964
2	80M01	33	2.53568	-1.35868
3	80M03	21	4.23700	0.25774
4	80M03	27	5.65957	1.85081
5	80M03	33	3.22883	-0.69315
6	80M03	38	3.16863	-0.60514
7	80M03	49	1.90954	-1.80789
8	80M03	50	3.37673	-0.59059
9	80M05	14	5.59712	1.86625
10	80M05	38	3.66740	-0.17554
11	80M05	39	5.66452	1.93543
12	80M05	40	5.19559	1.66903
13	80M05	42	5.86611	1.88843
14	80M05	45	5.28928	1.42983
15	80M07	1	1.21640	-2.68825
16	80M07	14	3.14415	-0.93649
17	80M07	19	2.20827	-1.50508
18	80M07	21	3.44362	-0.12670
19	80M07	33	3.39367	-1.70926
20	80M07	42	2.94575	-0.96758
21	80M07	45	3.01185	-0.50916
22	80M07	49	4.32744	0.59884
23	80M07	7	1.87564	-1.73161
24	80M09	1	2.21375	-1.76026
25	80M09	14	2.06051	-2.19823
26	80M09	18	2.04769	-1.98050
27	80M09	19	2.55334	-1.24133
28	80M09	27	3.34990	-1.79577
29	80M09	39	2.30757	-1.26585
30	80M09	7	1.73607	-2.44185
31	80M11	41	2.08256	-2.50104
32	80M11	45	2.50960	-1.22078

OBS	CR	ST	LNCHL	LNSDC
33	80M11	49	2.83174	-2.44185
34	80M13	1	2.51163	-1.37437
35	80M13	14	1.58412	-1.93102
36	80M13	18	2.90279	-0.87467
37	80M13	19	4.02446	0.04879
38	80M13	21	2.37491	-1.96611
39	80M13	27	2.49321	-1.50508
40	80M13	33	1.67241	-2.05573
41	80M13	38	1.34807	-2.37516
42	80M13	39	2.43580	-1.78976
43	80M13	40	2.36790	-1.66073
44	80M13	41	2.17475	-2.81341
45	80M13	42	1.89837	-2.76462
46	80M13	45	1.33500	-3.10109
47	80M13	49	2.96527	-1.28374
48	80M13	50	2.39790	-2.56395
49	80M13	8	2.36556	-1.87080
50	80M14	14	4.44118	0.49042
51	80M14	18	3.47661	-0.24335
52	80M14	19	3.84481	-0.13467
53	80M14	27	3.17805	-0.55687
54	80M14	38	3.24649	-0.51249
55	80M14	39	2.29757	-1.08176
56	80M14	4	2.79728	-0.98350
57	80M14	40	3.43237	-0.50253
58	80M14	42	3.00815	-0.94161
59	80M14	45	3.10571	-0.70522
60	80M14	48	3.35864	-0.26007
61	80M14	49	3.38608	-0.26657
62	80M14	8	2.91099	-0.61990

Appendix Table D. Values for production measured on shipboard and production for the same station determined from Eqn. 2.15.

OBS = observation #; CR = cruise; ST = station;
P = calculated production; Prod = observed production

OBS	CR	ST	P	PROD
1	80M01	14	107.27	132.0
2	80M03	21	902.66	923.7
3	80M03	27	4680.01	3684.6
4	80M03	33	336.31	393.3
5	80M03	38	346.45	609.3
6	80M03	42	327.27	478.5
7	80M03	45	277.79	543.0
8	80M03	48	1510.19	870.0
9	80M03	49	86.62	99.0
10	80M03	50	314.02	181.2
11	80M03	8	2224.36	971.1
12	80M05	1	901.48	834.9
13	80M05	14	2778.09	2427.0
14	80M05	18	2118.47	2807.7
15	80M05	33	274.32	424.4
16	80M05	38	403.35	373.5
17	80M05	39	2971.78	3165.3
18	80M05	40	1859.36	2591.1
19	80M05	41	1576.55	1102.8
20	80M05	42	3635.52	4089.9
21	80M05	45	2041.97	2668.5
22	80M05	48	796.80	2500.8
23	80M05	49	321.71	930.6
24	80M05	50	260.61	622.5
25	80M07	1	71.65	134.4
26	80M07	19	127.73	198.3
27	80M07	21	311.46	786.0
28	80M07	33	417.94	643.8
29	80M07	41	629.85	485.1
30	80M07	42	267.04	406.8
31	80M07	45	285.29	350.7
32	80M07	49	1063.26	1537.2
33	80M07	50	528.47	829.5
34	80M09	1	145.89	17.7
35	80M09	14	125.16	9.6

Appendix Table D

OBS	CR	ST	P	PROD
36	80M09	18	123.57	11.1
37	80M09	19	204.88	27.9
38	80M09	27	454.41	21.3
39	80M09	49	106.43	399.3
40	80M11	39	361.57	208.2
41	80M11	40	662.45	404.7
42	80M11	41	75.22	392.1
43	80M11	49	159.11	187.5
44	80M13	18	170.83	475.8
45	80M13	19	524.43	729.9
46	80M13	21	100.76	396.6
47	80M13	27	113.42	422.4
48	80M13	33	49.91	181.5
49	80M13	38	36.09	252.0
50	80M13	39	107.09	303.3
51	80M13	40	100.06	354.0
52	80M13	41	82.48	155.1
53	80M13	42	62.57	261.6
54	80M13	45	35.62	119.1
55	80M13	49	181.84	225.6
56	80M13	50	103.105	136.5
57	80M14	18	303.222	352.2
58	80M14	19	438.196	191.4
59	80M14	27	224.956	83.7
60	80M14	38	240.891	140.1
61	80M14	39	93.263	293.1
62	80M14	4	153.720	102.3
63	80M14	40	290.100	333.0
64	80M14	42	189.807	232.2
65	80M14	45	209.256	374.1
66	80M14	48	269.479	237.0
67	80M14	49	276.978	54.0

Appendix Table E. Values for satellite detectable chlorophyll and for diffuse attentuation at 490 nm (calculated from equation 2.7).

OBS = observation #; CR = cruise; ST = station;

SDC = satellite detectable chlorophyll;

ATTEN = Diffuse attenuation coefficient at 490 nm.

OBS	CR	ST	SDC	ATTEN
1	80M01	14	0.196	0.03147
2	80M01	33	0.257	0.03969
3	80M03	21	1.294	0.16644
4	80M03	27	6.365	0.84934
5	80M03	33	0.500	0.06377
6	80M03	38	0.546	0.06077
7	80M03	49	0.164	0.03005
8	80M03	50	0.554	0.07213
9	80M05	14	6.464	0.78836
10	80M05	38	0.839	0.09371
11	80M05	39	6.927	0.85438
12	80M05	40	5.307	0.49036
13	80M05	42	6.609	1.08778
14	80M05	45	4.178	0.54739
15	80M07	1	0.068	0.02527
16	80M07	14	0.392	0.05962
17	80M07	19	0.222	0.03374
18	80M07	21	0.881	0.07644
19	80M07	33	0.181	0.07318
20	80M07	42	0.380	0.05143
21	80M07	45	0.601	0.05394
22	80M07	49	1.820	0.18341
23	80M07	7	0.177	0.02971
24	80M09	1	0.172	0.03382
25	80M09	14	0.111	0.03175
26	80M09	18	0.138	0.03159
27	80M09	19	0.289	0.04008
28	80M09	27	0.166	0.07050
29	80M09	39	0.282	0.03530

Appendix Table E

OBS	CR	ST	SDC	ATTEN
30	80M09	7	0.087	0.02845
31	80M11	39	0.119	0.09242
32	80M11	40	0.129	0.17023
33	80M11	41	0.082	0.03202
34	80M11	45	0.295	0.03912
35	80M11	49	0.087	0.04756
36	80M13	1	0.253	0.03916
37	80M13	14	0.145	0.02730
38	80M13	18	0.417	0.04991
39	80M13	19	1.050	0.13325
40	80M13	21	0.140	0.03647
41	80M13	27	0.222	0.03877
42	80M13	33	0.128	0.02794
43	80M13	38	0.093	0.02590
44	80M13	39	0.167	0.03761
45	80M13	40	0.190	0.03634
46	80M13	41	0.060	0.03326
47	80M13	42	0.063	0.02994
48	80M13	45	0.045	0.02583
49	80M13	49	0.277	0.05215
50	80M13	50	0.077	0.03689
51	80M13	8	0.154	0.03630
52	80M14	14	1.633	0.20760
53	80M14	18	0.784	0.07869
54	80M14	19	0.874	0.11120
55	80M14	27	0.573	0.06123
56	80M14	38	0.599	0.064687
57	80M14	39	0.339	0.035134
58	80M14	4	0.374	0.046486
59	80M14	40	0.605	0.075686
60	80M14	42	0.390	0.053797
61	80M14	45	0.494	0.057874
62	80M14	48	0.771	0.071021
63	80M14	49	0.766	0.072708
64	80M14	8	0.538	0.050193

Appendix Table F. Values for sea surface temperature measured on shipboard and vertical stability (calculated from equation 4.1) for the same station determined from CTD profiles.

OBS = observation #; CR = cruise; ST = station;
TEMP = sea surface temperature; VS = vertical stability

OBS	CR	ST	TEMP	VS
1	80M05	10	2.3	4.62
2	80M05	12	3.2	6.30
3	80M05	14	2.6	3.15
4	80M05	16	2.1	4.20
5	80M05	18	1.6	6.30
6	80M05	21	2.3	1.26
7	80M05	22	2.6	2.73
8	80M05	26	2.6	8.40
9	80M05	27	2.7	5.88
10	80M05	29	3.2	2.10
11	80M05	30	3.4	3.15
12	80M05	32	2.5	3.99
13	80M05	33	3.5	2.11
14	80M05	34	2.3	2.10
15	80M05	35	2.9	1.47
16	80M05	36	2.3	1.68
17	80M05	37	2.0	1.68
18	80M05	38	1.7	3.78
19	80M05	39	2.0	4.20
20	80M05	40	2.2	4.41
21	80M05	41	4.3	2.52
22	80M05	42	3.5	4.20
23	80M05	43	4.2	5.25
24	80M05	44	4.5	3.78
25	80M05	45	3.7	3.99
26	80M05	46	4.4	8.19
27	80M05	47	3.5	4.20
28	80M05	48	3.2	3.78
29	80M05	49	1.5	5.04
30	80M05	50	5.5	5.88
31	80M05	8	2.3	9.60

OBS	CR	ST	TEMP	VS
32	80M07	10	6.0	11.13
33	80M07	11	4.2	10.50
34	80M07	12	6.5	5.04
35	80M07	13	4.2	4.20
36	80M07	14	5.8	4.62
37	80M07	16	5.4	6.30
38	80M07	17	4.8	5.67
39	80M07	18	3.5	6.72
40	80M07	19	5.0	24.15
41	80M07	21	5.5	14.07
42	80M07	24	5.8	9.45
43	80M07	25	5.2	13.44
44	80M07	26	4.8	12.18
45	80M07	27	4.3	12.60
46	80M07	28	4.8	11.55
47	80M07	29	5.0	2.73
48	*80M07*	*30*	*4.8*	*6.30*
49	80M07	32	4.7	7.35
50	80M07	33	5.2	8.61
51	80M07	34	5.8	8.61
52	80M07	35	5.4	6.30
53	80M07	36	4.5	6.30
54	80M07	37	4.8	8.40
55	80M07	38	1.2	9.87
56	80M07	39	3.5	14.70
57	80M07	40	5.0	12.60
58	80M07	43	7.2	19.11
59	80M07	44	6.0	13.02
60	80M07	45	6.0	7.14
61	80M07	46	6.1	10.50
62	80M07	47	6.2	7.98
63	80M07	49	4.0	10.29
64	80M07	50	4.8	7.98
65	80M07	8	4.7	11.76
66	80M07	9	5.9	11.55
67	80M09	10	9.4	28.98
68	80M09	11	9.0	26.88
69	80M09	15	8.6	21.21
70	80M09	17	7.7	23.10
71	80M09	18	7.7	28.14
72	80M09	19	8.6	31.50
73	80M09	8	8.7	27.30
74	80M11	10	11.3	35.91
75	80M11	11	11.5	38.64
76	80M11	12	11.6	40.95
77	80M11	13	11.8	38.22

OBS	CR	ST	TEMP	VS
78	80M11	14	11.6	37.80
79	80M11	15	11.0	33.18
80	80M11	16	11.0	37.38
81	80M11	17	10.9	37.17
82	80M11	18	10.6	37.38
83	80M11	19	10.4	42.42
84	80M11	20	15.1	63.00
85	80M11	21	14.3	57.12
86	80M11	22	13.7	42.84
87	80M11	23	13.0	43.89
88	80M11	24	12.5	43.68
89	80M11	25	12.7	39.48
90	80M11	26	11.9	40.32
91	80M11	27	11.5	45.78
92	80M11	28	11.5	41.58
93	80M11	29	11.4	41.58
94	80M11	30	11.6	40.95
95	80M11	31	12.0	39.99
96	80M11	32	11.0	39.99
97	80M11	33	12.0	39.06
98	80M11	34	12.0	39.27
99	80M11	35	12.2	39.27
100	80M11	36	12.4	38.64
101	80M11	37	12.1	40.32
102	80M11	38	11.2	39.48
103	80M11	39	10.5	44.73
104	80M11	40	10.4	46.20
105	80M11	8	12.1	40.95
106	80M11	9	11.1	42.42
107	80M13	10	9.5	37.17
108	80M13	11	10.5	39.27
109	80M13	12	9.6	33.60
110	80M13	16	7.5	26.04
111	80M13	21	15.3	55.23
112	80M13	22	14.6	54.39
113	80M13	23	14.3	52.50
114	80M13	24	14.5	52.50
115	80M13	25	13.5	52.50
116	80M13	26	14.2	54.39
117	80M13	27	13.5	52.50
118	80M13	28	13.3	48.93
119	80M13	29	13.0	45.99
120	80M13	30	12.0	42.00
121	80M13	31	12.3	39.27
122	80M13	32	12.0	42.84
123	80M13	33	12.3	43.05

OBS	CR	ST	TEMP	VS
124	80M13	37	12.6	42.42
125	80M13	38	10.5	38.22
126	80M13	39	8.5	34.02
127	80M13	40	9.4	31.50
128	80M13	41	17.0	57.12
129	80M13	43	14.6	56.70
130	80M13	44	15.4	50.82
131	80M13	45	15.0	51.87
132	80M13	46	15.6	52.08
133	80M13	47	14.9	48.51
134	80M13	48	13.8	48.30
135	80M13	49	11.9	47.46
136	80M13	50	11.9	44.56
137	80M13	8	10.8	42.00
138	80M14	10	5.9	29.19
139	80M14	11	6.1	27.30
140	80M14	12	5.9	24.99
141	80M14	13	6.1	24.15
142	80M14	14	6.6	18.90
143	80M14	15	6.8	18.69
144	80M14	16	6.1	5.25
145	80M14	17	4.6	10.08
146	80M14	18	4.4	17.43
147	80M14	19	6.7	4.20
148	80M14	24	7.6	28.98
149	80M14	25	7.4	30.24
150	80M14	26	7.0	30.45
151	80M14	28	6.8	34.02
152	80M14	29	6.3	30.87
153	80M14	30	6.6	29.40
154	80M14	31	6.9	28.35
155	80M14	32	6.3	24.99
156	80M14	33	6.2	24.78
157	80M14	34	6.4	23.73
158	80M14	35	7.9	25.20
159	80M14	36	8.0	26.25
160	80M14	37	6.9	16.80
161	80M14	38	5.1	17.85
162	80M14	39	3.2	8.82
163	80M14	40	8.0	10.50
164	80M14	41	12.2	27.30
165	80M14	42	10.5	22.05
166	80M14	43	11.7	21.00
167	80M14	44	11.9	21.00
168	80M14	45	11.2	25.20
169	80M14	46	10.0	22.05

OBS	CR	ST	TEMP	VS
170	80M14	47	7.6	12.81
171	80M14	48	7.4	9.03
172	80M14	49	4.6	10.50
173	80M14	8	6.4	19.32
174	80M14	9	6.1	32.55

Appendix Table G. Values for normalized quantum yield (calculated from equation 5.3) and measured incident radiation.

OBS = observation #; CR = cruise; ST = station;
NMQE = normalized quantum yield, $\bar{\phi}_C/\bar{\phi}_{max}$; LNMQE = $\log_{10}(\bar{\phi}_C/\bar{\phi}_{max})$;
TIR = incident radiation, I_o; LNTIR = $\log_{10}(I_o)$

OBS	CR	ST	NMQE	LNMQE	TIR	LNTIR
1	80M03	21	0.05927	-2.82562	109.613	4.69696
2	80M03	27	0.12687	-2.06456	89.248	3.89686
3	80M03	33	0.06436	-2.74327	117.798	4.76897
4	80M03	38	0.10655	-2.23916	117.071	4.76278
5	80M03	41	0.10132	-2.28949	48.410	3.87970
6	80M03	42	0.12851	-2.05178	72.237	4.27996
7	80M03	45	0.07200	-2.63116	102.043	4.62539
8	80M03	48	0.03508	-3.35026	104.278	4.64706
9	80M03	49	0.06846	-2.68153	104.278	4.64706
10	80M03	50	0.02889	-3.54424	104.278	4.64706
11	80M05	14	0.14103	-1.95877	31.063	3.43600
12	80M05	18	0.06145	-2.78960	108.160	4.68362
13	80M05	33	0.09408	-2.36362	57.516	4.05207
14	80M05	38	0.03406	-3.37973	136.346	4.91519
15	80M05	39	0.03917	-3.23976	136.346	4.91519
16	80M05	40	0.05125	-2.97100	136.346	4.91519
17	80M05	41	0.12595	-2.07188	27.850	3.32684
18	80M05	42	0.20256	-1.59673	27.850	3.32684
19	80M05	45	0.38521	-0.95396	17.012	2.83391
20	80M05	48	0.21380	-1.54271	51.510	3.94178
21	80M05	49	0.19705	-1.62429	51.510	3.94178
22	80M05	50	0.16271	-1.81576	51.510	3.94178
23	80M07	19	0.12236	-2.10076	86.679	4.46221
24	80M07	21	0.16518	-1.80074	73.997	4.30403
25	80M07	33	0.19420	-1.63386	54.192	3.99253
26	80M07	38	0.06679	-2.70622	46.287	3.83485
27	80M07	39	0.11973	-2.12256	46.287	3.83485
28	80M07	40	0.24559	-1.40408	46.287	3.83485
29	80M07	41	0.03703	-3.29598	102.713	4.63194
30	80M07	42	0.10132	-2.28942	102.713	4.63194
31	80M07	45	0.35329	-1.04047	23.772	3.16850

OBS	CR	ST	NMQE	LNMQE	TIR	LNTIR
32	80M07	49	0.13348	-2.01380	73.997	4.30403
33	80M07	50	0.14492	-1.93158	73.997	4.30403
34	80M11	39	0.03928	-3.23696	66.874	4.20281
35	80M11	40	0.04168	-3.17780	66.874	4.20281
36	80M13	8	0.08803	-2.43011	76.008	4.33084
37	80M13	18	0.65452	-0.42385	19.414	2.96600
38	80M13	19	0.08653	-2.44729	73.383	4.29569
39	80M13	21	0.20394	-1.58991	88.048	4.47788
40	80M13	27	0.26562	-1.32570	63.969	4.15840
41	80M13	33	0.34250	-1.07148	48.438	3.88028
42	80M13	38	0.42335	-0.85956	75.254	4.32087
43	80M13	39	0.17170	-1.76200	75.254	4.32087
44	80M13	40	0.21448	-1.53953	75.254	4.32087
45	80M13	41	0.10882	-2.21802	78.830	4.36729
46	80M13	42	0.24198	-1.41889	78.830	4.36729
47	80M13	45	0.22030	-1.51279	69.248	4.23770
48	80M13	49	0.06428	-2.74444	88.048	4.47788
49	80M13	50	0.06860	-2.67950	88.048	4.47788
50	80M14	8	0.48768	-0.71810	6.257	1.83374
51	80M14	14	0.29881	-1.20795	8.855	2.18099
52	80M14	18	0.32207	-1.13298	16.453	2.80052
53	80M14	19	0.12112	-2.11101	16.453	2.80052
54	80M14	38	0.63749	-0.45022	4.162	1.42604
55	80M14	39	3.44477	1.23686	4.162	1.42604
56	80M14	40	1.25820	0.22969	4.1622	1.42604
57	80M14	42	0.15500	-1.86432	36.0069	3.58371
58	80M14	45	0.22652	-1.48494	36.0069	3.58371
59	80M14	48	0.15613	-1.85709	25.6993	3.24646